045

STRAIN HARDENING AND STABLE TEARING EFFECTS IN FITNESS-FOR-SERVICE ASSESSMENT: Progress Report

D. T. Read

National Bureau of Standards
U.S. Department of Commerce
Boulder, Colorado 80303

May 1987

NBSIR 86-3045

STRAIN HARDENING AND STABLE TEARING EFFECTS IN FITNESS-FOR-SERVICE ASSESSMENT: Progress Report

D. T. Read

Fracture and Deformation Division
Institute for Materials Science and Engineering
National Bureau of Standards
Boulder, Colorado 80303

May 1987

Sponsored by
David Taylor Naval Ship Research and Development Center
Annapolis, Maryland 21402

U.S. DEPARTMENT OF COMMERCE, Malcolm Baldrige, Secretary

NATIONAL BUREAU OF STANDARDS, Ernest Ambler, Director

CONTENTS

STRAIN HARDENING AND STABLE TEARING EFFECTS IN FITNESS-FOR-SERVICE ASSESSMENT: PROGRESS REPORT

D.T. Read

Fracture and Deformation Division
National Bureau of Standards
Boulder, Colorado 80303

This report describes studies done to provide information on how to account for material strain-hardening and tearing in fitness-for-service assessment. Included are a literature review, a study of the strength and ductility of cracked tensile panels under compliant loading, a report on applied J-integral measurements in an HSLA steel, a study of the relationship of the essential work of fracture to the J-integral, and a description of potential drop techniques for crack length measurement in double-edge-notched tensile panels.

Key words: assessment curve; ductility; fracture; J-integral; R-curve; toughness.

1. INTRODUCTION

The fitness-for-service concept implies that geometrical flaws in structural materials are acceptable as long as such flaws do not reduce structural strength, ductility, or functional capability below tolerable limits. Accordingly, with regard to tearing, a slight amount of slow stable ductile tearing at a crack tip does not in itself threaten structural integrity any more than did the initial existence of the crack. Modern tough metals prevent catastrophic flaw growth under overstrains, first by blunting, and then, for severe overstrains, by slow, stable, ductile tearing. As test techniques improve, ever smaller amounts of tearing are detected at ever lower toughness levels. Sometimes materials that are known to have excellent toughness in practice show detectable tearing at very low toughness levels. Fitness-for-service analysis of slow stable ductile tearing can extend the demonstrable margin of safety of a structure above the initiation of subcritical tearing, to allow fuller use of real material toughness and avoid artificial problems from improved test methods that

detect very small amounts of tearing. Because unstable tearing is, by definition, out of control, it must always be avoided. Further, the extent of stable tearing must be restricted to safe levels that do not threaten structural fitness for service. Tearing considerations influence the choice of critical J level, J_c, for use in material evaluation, and they can provide guidance on how material tearing resistance should be weighted against other desirable material properties in material selection.

Tearing and tearing instability in elastic-plastic and ductile fracture in thick specimens (as opposed to thin sheet) has been an active research area since the mid-1970s. Instability in thin sheets was studied even earlier, for aerospace applications. Paris, Hutchinson, and Rice are among the eminent names in fracture associated with the early studies of stable and unstable ductile tearing. Their research sought to extend the use of the J-integral, J, as a fracture parameter beyond the initiation of tearing at J_{Ic}, to finite values of crack extension, Δa. Material resistance to tearing was expressed as a resistance curve, called the J-R curve, in which J was plotted against Δa. The slope of the material J-R curve was converted to a dimensionless tearing modulus $T_{mat} = (E/\sigma_y^2)(dJ/da)$, where E is Young's modulus and σ_y is material flow stress. Once material resistance to tearing had been characterized, this resistance could be compared to the driving force for tearing, as produced by specially designed compliant test fixtures. Quantitative characterization of the driving force for fracture in terms of the applied tearing modulus, T_{app}, was developed as the natural complement to material resistance to tearing, T_{mat}. Tearing becomes unstable when T_{app} exceeds T_{mat}.

This report describes studies done to provide information on how to account for material strain-hardening and tearing in fitness-for-service assessment. Included are a literature review, a study of the strength and ductility of cracked tensile panels under compliant loading, a report on applied J-integral measurements in an HSLA steel, a study of the relationship of the essential work of fracture to the J-integral, and a description of potential drop techniques for crack length measurement in double-edge-notched tensile panels. References and figures are listed at the end of each chapter.

2. LITERATURE REVIEW ON DUCTILE TEARING AND TEARING INSTABILITY

2.1 Introduction

A literature search was carried out to find reports of previous studies relevant to the present goal of developing a procedure for applying the tearing modulus-tearing instability concept to failure prediction and failure avoidance in naval materials and structures. Such a procedure must be based on the fundamentals of tearing behavior, must account for dependence of J-R curves on structural, as well as specimen, geometry and size, and must be adaptable to new materials.

Two indices were searched, the Metals Abstracts Index and the NASA Index. The key words used were tearing modulus, R-curve, and stability. A total of 276 references were found after discarding several that were clearly extraneous. For present purposes, methods applicable to thin sheets, properties of specific materials measured using only one specimen geometry, and test methods themselves are not directly relevant. One hundred and forty references on aspects of fracture not specifically relevant to the goals of the present study, including sixteen entries on tearing of thin sheets, were excluded from further consideration here.

Thin sheets tend to behave in a more ductile manner than thick plates of the same material because thin sheets experience less through-thickness constraint. Treatment of ductile tearing and instability in thin sheets was developed in the 1950's and 1960's for aerospace applications. Although the thin-sheet technology cannot be simply adapted for use in thick plates, it has served as a guide and a precedent for studies of tearing in thick plates.

The other excluded studies were largely measurements or estimates of the J-R curve for a given material using a single specimen size.

The remaining entries included eighteen on fundamentals, thirty-seven on geometry dependence, and fourteen on modeling of material tearing modulus based on more basic material properties. After eliminating duplicates, eighteen remained on fundamentals [1-18], twenty-seven remained on geometry dependence [19-45], and eleven remained on modeling [46-56]. Several key papers introducing the current concept of tearing instability are found in

the book entitled Elastic-Plastic Fracture--Special Technical Publication 668, edited by J. D. Landes, J. A. Begley, and G. A. Clarke, published by the American Society for Testing and Materials.

2.2 Basic Concepts of Tearing Instability

This report is not intended to be an introduction to the subject, but, for completeness, some of the fundamental concepts of tearing instability theory will be reviewed here. Then, the well-established aspects of the theory will be summarized.

2.2.1 Fundamentals

Recent attempts to understand, describe, and predict the fracture process of unstable ductile rupture have utilized the well-known R-curve approach [57-59]. An R-curve is a plot of some fracture resistance parameter against crack growth. Fracture parameters used have included the derivative with respect to crack length of energy absorbed (reversibly and/or irreversibly) by the specimen, stress intensity factor, K, J-integral, J,crack tip opening displacement, CTOD, and so on. Just as applied stress on a tensile specimen can take on any value up to the maximum capability of the specimen material, an applied fracture parameter can also take on any value up to the capability of the specimen material. The denotation "applied fracture parameter" or "fracture driving force" indicates that the fracture parameter is to be understood in this sense. On the other hand, certain stress levels are correlated with specific material responses, such as the yield stress and the ultimate stress. These stress levels are understood as material properties. Likewise, certain fracture parameter levels are associated with specific material responses, such as brittle fracture, crack blunting, crack initiation, and ductile tearing. When a fracture parameter is used to measure the fracture driving force associated with a certain specific material response, it is called a material fracture resistance parameter, or a toughness. The classic example of a fracture parameter is G, the derivative with respect to crack length of elastic potential energy contained in the specimen.

The relevance of fracture resistance and fracture driving parameters to tearing can be clarified by an analysis of the tearing process as follows. Each increment of crack length can change the fracture driving parameter. If, for a small increment of crack length, the fracture driving parameter increases more than the fracture resistance parameter, then another, larger increment of crack length is predicted. If the driving force parameter continues to increase faster than the material fracture resistance parameter, the process accelerates and catastrophic ductile rupture occurs. By plotting fracture driving force curves on the same graph with a material R-curve, the conditions for instability can be identified.

The R-curve concept has been demonstrated to apply when the J-integral is used as the fracture driving and fracture resistance parameters [8, 14, 60]. It is not surprising that the R-curve approach using the J-integral (J-R-curve) works when the method is applied to predict instability in the very same specimen geometry as the material R-curve is measured. Indeed, this success would be expected from the principles of the mechanics of linear systems with one nonlinear element for any parameter which increased monotonically with crack length, as long as it was consistently calculated and applied [61].

2.2.2 Well-Established Aspects

There is general agreement in the literature that a material tearing modulus, T_{mat}, that characterizes material resistance to ductile tearing under elastic-plastic or fully plastic strain in terms of the J-integral, can be at least operationally defined. The material tearing modulus is calculated directly from the measured J-R curve. A standard method for measuring J-R curves has been written, and verified by a round-robin test series. It is recognized that the material tearing modulus may depend on specimen size and geometry. It is recognized that the J-R curve is, in general, curved, so that T_{mat} depends on J. It has been found convenient to use plots known as J-T plots, which have J on the y-axis and T on the x-axis, to determine the conditions for equality of T_{mat} and T_{app} (Fig. 1). On such plots the material property is represented by a J_{mat}-T_{mat} curve and the applied conditions are represented by a J_{app}-T_{app} curve. Where these

T_{app}, so that the necessary and sufficient conditions for fracture are satisfied. The various curves on such a plot can be used to identify safe and unsafe conditions with respect to fracture by ductile tearing.

2.3 Problems with Tearing Instability Theory

Because the mechanics of elastic-plastic solids has proved to be a difficult field, with analytic solutions rarely available for problems of interest, especially those involving varying through-thickness stress, a complete solution to the general problem of propagating cracks in elastic plastic media is not expected to be available soon. Several specific problems with tearing instability theory have been encountered.

The present obstacles to use of the J-R-curve approach can be contrasted with the current understanding of static cracks. Methods are currently available for calculating the fracture driving parameter in terms of the J-integral for all relevant types of geometries [62]. A standard for measurement of J_{Ic} has been established [63]. It appears that J_{Ic} values obtained in standard tests are conservative, that is, lower than or equal to values obtained for other geometries. On the other hand, the ranges of applicability of present methods of calculating applied J-integrals for cases of growing cracks have not been verified, and the conservatism of standard-specimen J-R curves is open to question, especially for thin specimens of ductile material.

2.3.1 Definition and Meaning of the J-Integral During Tearing

The most fundamental of these problems is that the J-integral, as formally defined [64], applies to non-linear elasticity but not to plasticity as found in real metals. Once stable tearing occurs, the original J-integral no longer gives the amplitude of the strain singularity at the crack tip, because of the unloading of the plastically strained region formed at the original crack tip. This implies some ambiguity in the meaning of the pseudo J-integrals used for tearing instability. Extensions and modifications of the J-integral are discussed in the literature. A correction procedure [65] for J for use in J-R curve measurements has gained

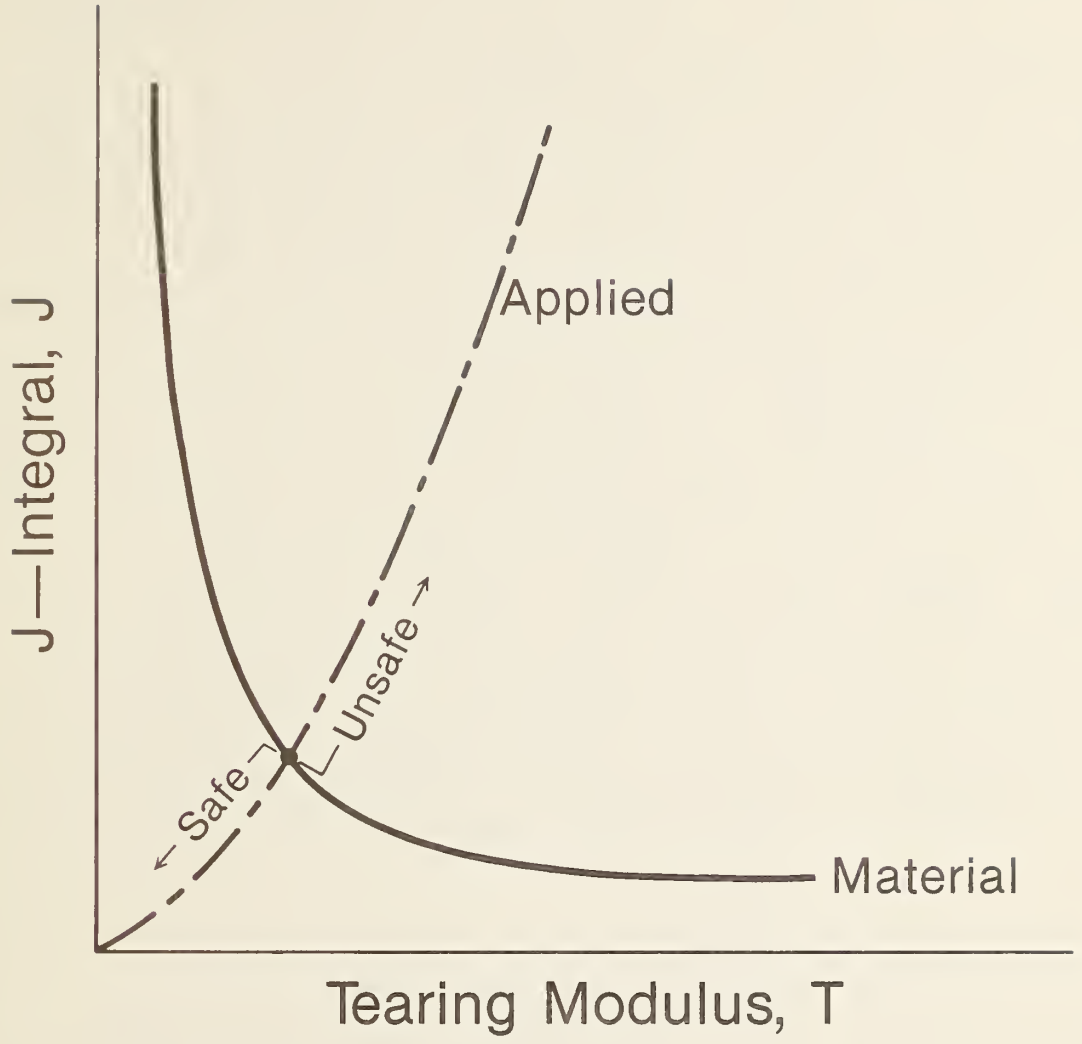

Figure 1. Schematic J-T diagram.

acceptance, but the final significance of the corrected J produced by this correction is still unclear, although it satisfies the Rice criterion for a valid expression for the J-integral during tearing.

Because the J-integral no longer specifically characterizes the strain field at the crack tip after tearing has occurred, the geometry-independence of J-R curves is open to serious question. The question of geometry-dependence of R-curves is discussed in a separate section below.

The amount of tearing permissible before J may become inapplicable has been estimated to be rather small [14]. This problem is avoided in K-R curves for ultra-high-strength thin sheet materials, because the deformation is generally linear elastic, and the stress intensity factor K appears to adequately characterize the stress distribution around the crack tip. This results in K-R curves which are sufficiently geometry-independent, as long as the sheet thickness remains constant. However, many modern structural materials possess so much ductility that the strain fields are no longer generally linear elastic. These materials, of course, have higher toughness than those described by K-R curves. But the analytical framework needed to exploit the toughness of these materials in cases of growing cracks does not yet exist.

2.3.2 Local and Global Instability

Tearing instability theory can be applied to prediction of global instability or local instability. Laboratory tests typically involve global instability, while structures pose problems of local instability.

In ductile fracture, instability has been defined as "a sudden increase in crack size and deformation of the test specimen" [17]. In J-R curve measurements or in studies of tearing instability using standard test-pieces, tearing typically starts after the maximum load is reached. The first part of a test is always stable. The rate of specimen deformation is controlled directly by the testing machine. Instability manifests itself when the deformation rate increases and the load decreases with no change in the testing machine's rate of travel. The rapid, unstable tearing is typically clearly distinguishable from the slow stable tearing preceeding it. This is a global instability, because the limit load of the specimen as

a whole is reached and subsequent tearing directly and immediately reduces the load carrying capacity of the specimen as a whole.

Because of the complexity of most structures, local instability can occur and must be considered. By definition, such a local instability can sever only a small part of the structure, at least at first. For instance, if a part through surface flaw pops through and then arrests, the event would be a local instability. The damage caused by a local instability may be acceptable, or, it may be unacceptable in itself, such as a leak in a pressure vessel. Or, the local damage may form a larger crack which threatens to escalate into a global instability. Local instability can occur below the limit load of the full structure, for example, at a severe stress concentrator. In such a case, the structure itself controls T_{app}. The situation here is more complex than those covered by the simple theory where the testing machine compliance controls T_{app} up to global instability. An example was given by Paris et al. in an early paper on tearing instability [14], the example of a deep surface flaw. The compliance of the testing machine and the overall length of the flawed plate are irrevelant in this case. The local compliance of the flawed plate controls T_{app}

The key features of local and global instabilities are emphasized on the following table:

Instability type	Local	Global
Typical example:	Complicated structure	Simple specimen
T_{app} controlled by:	local compliance	full specimen and testing machine compliance
Load level relative to global limit load:	below	identical

This table implies that a flaw should be evaluated for stability using local compliance if the structure as a whole is below its limit load. If the structure as a whole is at its limit load the full global compliance must be considered. Of course, a local instability can extend the tearing far enough to reduce the limit load of the whole structure, causing a potential global instability. This is exactly what consideration of local instability seeks to avoid.

Development and testing of tearing instability theory is needed to show how to use concepts proven and data obtained on global instability, the usual case for material testing, to analyze and predict the occurrence of local instability in complex structures.

2.3.3 Specimen/Structure Size Effect

Use of the J-R curve in design must include by consideration of the size effect which occurs in the temperature range of the ductile/brittle transition in steels. In this temperature range, large and small specimens can have qualitatively different behavior. At a given temperature, cleavage can terminate R-curve behavior at significantly lower values in large specimens than in small ones. Therefore, one must be assured that the material is out of the transition range before applying a J-R curve from small specimens to predictions of the behavior of thick structural sections.

2.3.4 Treatment of Flaw Size

In the first papers describing the fundamentals of tearing instability theory, simple versions were presented. In these papers, the specimen stability was independent of flaw size. That is, the flaw size simply cancelled out. This means that the simple tearing instability theory does not provide an answer to the question, "How large a flaw can be tolerated?" The theory must developed further to investigate questions of flaw size.

2.3.5 Flaw Assessment Procedures

Tearing instability theory offers a means of assessing structural stability for J values in excess of J_{Ic} Therefore it can be used in selecting appropriate values of J for use in J-based flaw assessment procedures such as that embodied in the J-integral estimation curve. One criterion proposed is that the J value at which $T_{mat} = 50$, called J_{50}, is appropriate as a critical J value. Further study of this area is needed. Such studies are in progress, both in the present program and elsewhere.

2.4 Material Tearing Properties

2.4.1 Geometry Dependence

It has been widely recognized that the geometry-dependence of the material J-R curve must be understood if tearing instability theory is to become useful [19-45]. The incentive for using tearing analysis is that a material R-curve measured by standard test procedures can be applied to predictions of structural instability for geometries different from the test geometry. The requirements are that the material R-curve must be unique, that is, the measured curve must actually apply to the other geometries in question, and that fracture driving parameters can be calculated accurately as functions of applied stress or strain and crack size for all geometries of interest, even in the presence of growing cracks.

A precedent for successful treatment of this problem exists. The R-curve approach has been applied successfully in the aircraft and aerospace industries for thin sheets of high-strength material of a given thickness. The fracture driving parameter used is K_1, and its applicability is restricted to materials where failure occurs at stresses below net section yielding. The stress intensity factor K_1 has been found to adequately characterize the stress distribution around the crack tip, resulting in K-R curves which are sufficiently geometry-independent, as long as the sheet thickness remains constant.

A crucial test of the method would be the application of an R-curve measured for one geometry to different geometries. Interesting geometrical differences would include changes of scale of in-plane dimensions, changes of loading mode fracture type (for example, predominantly tensile vs predominantly bending), and changes of thickness. Any method which could handle these three types of geometrical changes, using a single material R-curve, would have to be judged eminently successful.

The physical causes of R-curve behavior are qualitatively appreciated at present; however, quantitative methods of calculating material R-curves from specimen geometry and physical, mechanical, and metallurgical properties are not available at present and are unlikely to be available in the near future. Recent studies generally agree that J-R curves for a given material at a given temperature are independent of in-plane specimen size and ligament length for compact tensile (CT) specimens of sufficient size [42]. However, thickness effects have sometimes been found. Changing from surface-flawed plates to compact tensile specimens was found to have a large effect on the J-R curve [32]. A round-robin study revealed that J-R curves in CT specimens differed from those for three-point-bend specimens. On the other hand, the J-R curve for a pipe in bending agreed with that for CT specimens when the appropriate equations for J for the pipe were used [62].

Willoughby, Pratt, and Turner [40] have reported that rising R-curves, that is, J values increasing with crack length, occur because of "an increase in remote plastic work," rather than changing behavior at the crack tip. They noted that this work is, in general, geometry-dependent.

The present status is that the dependence of J-R curves on specimen size and geometry is a subject of current research. It is not yet known how to establish conservative limits on R-curves. Therefore empirical checks on the actual J-R curve for various geometries of interest are needed. Again, studies are in progress, both within the current program and elsewhere.

2.4.2 Tearing Properties Modeling

Several papers have appeared in the literature in which the J-R curve is calculated from more fundamental properties [46-56]. The situation is some what analogous to the relationship between an engineering stress-strain

curve and a true stress-strain curve. The true curve is the material property. Different engineering curves are appropriate for different specimen geometries such as tension, torsion, and shear.

Analogously, the measured J-R curves are taken as specimen-specific manifestations of more fundamental properties, such as critical strain or critical crack stretch. Such models usually can fit observed J-R curves quite well. They indicate that J-R curves are probably geometry-dependent. But no clear candidate for the fundamental fracture parameter has emerged.

2.5 Conclusions of Literature Review

Based on a literature review on the subject of ductile tearing, the following conclusions can be drawn: The J-R curve has been established as a measurement of material resistance to tearing. Tearing instability theory is well-established as a potential means of analyzing the possibility of unstable ductile tearing, in which the J-R curve quantifies material tearing resistance. The major obstacles to application of tearing instability theory are lack of information about T_{mat} and T_{app} for specific situations.

In order to develop the treatment of tearing to a state where it can be conveniently and generally used in the evaluation of structural materials, the following issues must be addressed further:

1. Identification of appropriate qualitative use of T_{mat} for predicting material performance in the presence of cracks and estimating tolerable crack sizes;
2. Procedures for quantitative use of tearing instability theory for predicting material performance in the presence of cracks and calculating tolerable crack size and required toughness levels. This issue can be broken down as follows:
   a. Proper and workable procedures for determination of T_{app} from stress-strain state and configuration, accounting for the procedure used to determine T_{mat} and considering other material properties.
   b. Extension of existing J-integral calculations, especially the J-integral estimation curve, to calculation of T_{app}.

c. Specimen-structure geometry and size dependence of J-R curves, accounting for the definition of J used.

2.6 References

[1] M. G. Vassilaros and J. A. Joyce, "An Experimental Evaluation of Tearing Instability Using the Compact Specimen," Report Number AD-A107633 DTNSRDC-81/029, November, 1981.

[2] P. C. Paris and G. I. Zahalak, "Progress in Elastic-Plastic Fracture Mechanics and Its Applications," Nonlinear and Dynamic Fracture Mechanics, American Society of Mechanical Engineers, New York, 1979, pp. 125-134.

[3] H. W. Liu, "On the Fundamental Basis of Fracture Mechanics," Engineering Fracture Mechanics 17, 424-438, 1983.

[4] S. Aihara, S. Machida, and T. Kanazawa, "A Study on Unstable Ductile Fracture," Advances in Fracture Research, Vol.5, Pergamon Press, Oxford, 1982, pp. 2329-2336.

[5] H. Tada, P. C. Paris, and R. M. Gamble, "A Stability Analysis of Circumferential Cracks for Reactor Piping Systems," Fracture Mechanics: Twelfth Conference, ASTM STP 700, American Society for Testing and Materials, Philadelphia, 1980, pp. 296-313.

[6] D. Rhodes, J. C. Radon, L. E. Culver, "Analysis of Combined Static and Fatigue Crack Growth Data," Fatigue of Engineering Materials and Structures 4, 1981, pp. 49-63.

[7] C. E. Turner, "Fracture Mechanics Assessments and Design. Elastic-Plastic Aspects of Fracture Stress Analysis: Methods for Other Than Standardized Test Conditions," Fracture Mechanics in Design and Service, Royal Society, London, 1981, pp. 73-92.

[8] J. A. Joyce and M. G. Vassilaros, "An Experimental Evaluation of Tearing Instability Using the Compact Specimen," Fracture Mechanics: Thirteenth Conference, ASTM STP 743, American Society for Testing and Materials, Philadelphia, 1981, pp. 525-542.

[9] C. E. Turner, "Use of the R-Curve for Design with Contained Yield--In Relation to Stable and Unstable Crack Growth," in Fracture and Fatigue: Elasto-Plasticity, Thin Sheet, and Micromechanisms Problems:

Proceedings of the Third European Colloquium on Fracture, Pergamon Press, Oxford, 1980, pp. 315-328.

[10] A. A. Willoughby, P. L. Pratt, and C. E. Turner, "The Meaning of Elastic-Plastic Fracture Criteria During Slow Crack Growth, Growth," International Journal of Fracture 17, 1981, pp. 449-466.

[11] C. E. Turner, "Stable Crack Growth and Resistance Curves," in Developments in Fracture Mechanics - 1, Applied Science Publishers, London, 1979, pp. 107-144.

[12] B. A.Bilby, "Fracture--Energy Conditions in Macroscopic Cracking," in Advances in Research on the Strength and Fracture of Materials: Proceedings of the Fourth International Conference on Fracture, Pergamon Press, New York, 1978, pp. 1-18.

[13] S. Kaiser, "On the Relation Between Stable Crack Growth and Fatigue," Report Number TRITA-HFL-0035 PUBL-215 ISSN-0349-1234, Royal Institute of Technology, Stockholm, 1983.

[14] P. C. Paris, H. Tada, A. Zahoor, and H. Ernst, "The Theory of Instability of the Tearing Mode of Elastic-Plastic Crack Growth," Elastic-Plastic Fracture, ASTM STP 668, American Society for Testing and Materials, Philadelphia 1979, pp. 5-36.

[15] J. W. Hutchinson and P. C. Paris, "Stabilty Analysis of J-Controlled Crack Growth," Elastic-Plastic Fracture, ASTM STP 668, American Society for Testing and Materials, Philadelphia 1979, pp. 37-64.

[16] M. F. Kanninen, E. F. Rybicki, R. B. Stonesifer, D. Broek, A. R. Rosenfield, C. W. Marshall, and G. T. Hahn, "Elastic-Plastic Fracture Mechanics for Two-Dimensional Stable Crack Growth and Instability Problems," Elastic Plastic Fracture, ASTM STP 668, American Society for Testing and Materials, Philadelphia, 1979, pp. 121-150.

[17] P. C. Paris, H. Tada, H. Ernst, and A. Zahoor, "Initial Experimental Investigation of Tearing Instability Theory," Elastic-Plastic Fracture, ASTM STP 668, American Society for Testing and Materials, Philadelphia, 1979, pp. 251-265.

[18] C. E. Turner, "Description of Stable and Unstable Crack Growth in the Elastic Plastic Regime in Terms of Jr Resistance Curves," Fracture Mechanics, ASTM STP 677, American Society for Testing and Materials, Philadelphia, 1979, pp. 614-628.

[19] C. E. Turner, "Stable Crack Growth and Resistance Curves," in Developments in Fracture Mechanics, Vol.1, editededited by L. G. Chell, Applied Science Publishers, London 1979, pp. 107-144.

[20] L. A. Simpson and B.J.S. Wilkins, "Prediction of Fast Fracture in Zr-2.5 Percent Nb Pressure Tubes Using Elastic-Plastic Fracture Mechanics," in Proceedings of the Third International Conference on Mechanical Behavior of Materials, Pergamon Press, Oxford, 1979, pp. 563-572.

[21] J. D. Landes and D. E. McCabe, "Effect of Specimen Size and Geometry on Ductile Fracture Characterization," Proceedings of the Third International Conference on Mechanical Behavior of Materials, Pergamon Press, Oxford, 1979, pp. 539-547.

[22] J. P. Gudas, J. A. Joyce, and D. A. Davis, "Investigation of Specimen Geometry Modification of Determine the Conservative J_I-R Curve Tearing Modulus Using the HY-130 Steel System," Fracture Mechanics, ASTM STP 677, American Society for Testing and Materials, Philadelphia, 1979, pp. 474-485.

[23] L. A. Simpson and C. F. Clarke, "An Elastic-Plastic R-Curve Description of Fracture in Zr--2.5Nb Pressure Tube Alloy," Elastic-Plastic Fracture, ASTM STP 668, American Society for Testing and Materials, Philadelphia, 1979, pp. 643-662.

[24] D. E. McCabe and J. D. Landes, "Elastic-Plastic R-Curves--For Fracture Toughness Estimation in Steel Plates," Journal of Engineering Materials and Technology 100, 1978, pp. 258-265.

[25] D. E. McCabe and J. D. Landes, "An Evaluation of Elastic-Plastic Methods Applied to Crack Growth Resistance Measurements," Elastic-Plastic Fracture, ASTM STP 668, American Society for Testing and Materials, Philadelphia, 1979, pp. 288-306.

[26] N. J. Adams, H. G. Munro, B. K. Neale, "The Influence of Specimen Configuration on Yield Zone Formation and Fracture Resistance," in Advances in Research on the Strength and Fracture of Materials: Proceedings of the Fourth International Conference on Fracture, Volume 3B, Pergamon Press, New York, 1978, pp.593-600.

[27] G. R. Irwin and P. C. Paris, "Elasto-Plastic Crack Tip Characterization in Relation to R-Curves, in Advances in Research on the Strength

and Fracture of Materials: Proceedings of the Fourth International Conference on Fracture, Volume 1, Pergamon Press, New York, 1978, pp. 93-100.

[28] S. Kaiser, "Experimental Studies of Different Instability Criteria Based on the J-R Curve," Report Number TRITA-HFL-0034 PUBL-214 ISSN-0349-1234, 1983.

[29] H. L. Bernstein, "A Study of the J-Integral Method Using Polycarbonate," Report Number AD-A121170 AFWAL-TR-82-4080, 1982.

[30] W. J. Mills, "Effect of Specimen Size on the Fracture Toughness of Type 304 Stainless steel," Report Number DE82-012517 HEDL-TME-81-52, Hanford Engineering Development Laboratory, Richland, Washington, 1981.

[31] S. Banerjee, "A New Basis for the Determination of Fracture Toughness," Report Number NASA-TM-78592 A-7837, National Aeronautics and Space Administration, Ames Research Center, California, 1979.

[32] S. J. Garwood, "Ductile Crack Instability in Pressurized Components," Pressure Vessel Technology, Vol.1, Institution of Mechanical Engineers, Bury St. Edmunds, England, 1980, pp. 93-101.

[33] J. P. Gudas and D. A. Davis, "Evaluation of the Tentative J_I-R Curve Testing Procedure by Round Robin Tests of HY130 Steel," ASTM Journal of Testing and Evaluation 10, 1982, pp. 252-262.

[34] H. -J. Kaiser and K. E. Hagedorn, "Prediction of Maximum Load Values of Different Sized CT-Specimens Using the J-R Curve Concept," Fracture and the Role of Microstructure, Vol.1, Fracture and Fracture Toughness, Engineering Materials Advisory Services Ltd., Cradley Heath, England, 1982, pp. 76-83.

[35] T. Kodaira, M. Matsumoto, and N. Nakajima, "Application of D. C. Electrical Potential Method for Measurement of J-R Curve by a Single Specimen," Journal of the Iron and Steel Institute of Japan 68, 1982, pp. 1040-1045.

[36] J. Carlsson, S. Kaiser, K. Markstron, C. Wuthrich, and H. Oberg, "Experimental Studies of Stable Crack Growth," Advances in Fracture Research, Volume 2, Pergamon Press, Oxford, 1982, pp. 863-869.

[37] H. -J. Kaiser and K. E. Hagedorn, "The Influence of Specimen Geometry on Stable Crack Growth for a High-Strength Steel", Advances in Fracture Research, Volume 2, Pergamon Press, Oxford, 1982, pp.855-862.

[38] L. A. Simpson, "Effects of Specimen Geometry on Elastic-Plastic R-Curves for Zr-2.5 Percent Nb," Advances in Fracture Research, Volume 2, Pergamon Press, Oxford, 1982, pp. 833-841.

[39] M. A. Khan, T. Shoji, and H. Takahashi, "Characterization of the Crack Toughness Behavior of Structural Steels by the Tearing Modulus Parameter and Acoustic Emission," Journal of Testing and Evaluation 10, 1982, pp. 3-11.

[40] A. A. Willoughby, P. L. Pratt, and C. E. Turner, "The Meaning of Elastic-Plastic Fracture Criteria During Slow Crack Growth," International Journal of Fracture 17, 1981, pp.449-465.

[41] M. G. Vassilaros, J. A. Joyce, and J. P. Gudas, "Effects of Specimen Geometry on the J-R Curve for ASTM A533B Steel," Fracture Mechanics: Twelfth Conference, ASTM STP 700, American Society for Testing and Materials, Philadelphia, 1980, pp. 251-270.

[42] J. P. Gudas, M. G. Vassilaros, J. A. Joyce, D. A. Davis, and D. R. Anderson, "A Summary of Recent Investigations of Compact Specimen Geometry Effects on the JI-R Curve of High-Strength Steels," Report Number NUREG/ CR-1813, David W.Taylor Naval Ship Research and Development Center, Annapolis, 1980.

[43] H. Takahashi, M. A. Khan, and M. Suzuki, "A Simple Test Method for the Evaluation of Tearing Modulus," Journal of Testing and Evaluation 9, 1981, pp. 14-23.

[44] K. W. Carlson and J.A. Williams, "The Effect of Crack Length and Side Grooves on the Ductile Fracture Properties of ASTM A533 Steel," Report Number NUREG/CR-1171, Hanford Engineering Development Laboratory, Richland, 1980.

[45] K. W. Carlson and J. A. Williams, "A More Basic Approach to the Analysis of Multiple-Specimen R-Curves for Determination of J_c--Critical J-Integral Values at Onset of Crack Extension," Fracture Mechanics: Thirteenth Conference, ASTM STP 743, American Society for Testing and Materials, Philadelphia, 1981, pp. 503-524.

[46] I. M. Bernstein, "The Role of Microstructure and Environment on the Fracture of Iron--Carbon Alloys," Mechanical Properties of B.C.C. Metals, Metallurgical Society/AIME, Warrendale, Pennsylvania, 1981, pp. 173-179.

[47] E. Smith, "Plane Strain Crack Instability Under Small-Scale Yielding Conditions," International Journal of Engineering Science 20, 1982, pp. 15-18.

[48] D. Wagner, J. J. Charrier, and D. Francois, "Observations of Ductile Mechanisms of Stable Crack Growth in Two Phase Alloys," Analytical and Experimental Fracture Mechanics, Sijthoff and Noordhoff, Alphen Ann den Rijn, Netherlands, 1981, pp. 199-210.

[49] D. A. Curry, "Estimating a J Resistance Curve for a Perfectly Plastic Material," International Journal of Fracture 15, R59-R62, 1979.

[50] M. P. Wnuk, "Occurrence of Catastrophic Fracture in Fully Yielded Components Stability Analysis," International Journal of Fracture 15, 1979, pp. 553-581.

[51] H. W. Liu and A. S. Kuo, "Fracture Toughness of Thin and Tough Plates," International Journal of Fracture 14, 1978, pp. R109-R112.

[52] M. P. Wnuk and S. Sedmak, "Final Stretch Model of Ductile Fracture," Fracture Mechanics: Thirteenth Symposium, ASTM STP 743, American Society for Testing and Materials, Philadelphia, 1981, pp. 236-249.

[53] M. Piszczek and M. P. Wnuk, "Subcritical and Fatigue Crack Growth in Anti-Plane Strain State," International Journal of Solids and Structures 16, 1980, pp. 1135-1146.

[54] H. Ernst, P. C. Paris, and M. Rossow, "Analysis of Load-Displacement Relationship to Determine J-R Curve and Tearing Instability Material Properties," Fracture Mechanics, ASTM STP 677, American Society for Testing and Materials, Philadelphia, 1979, pp. 581-599.

[55] W.P.A. Belchar and S. G. Druce, "Micromechanisms of Ductile, Stable Crack Growth in Nuclear Pressure Vessel Steels," Atomic Energy Research Establishment, Harwell, England, 1981.

[56] J. A. Blind, "Micromechanisms of Crack Extension in Alloys," Air Force Institute of Technology, Wright-Patterson AFB, Ohio, Available from NTIS: SAP: HC A13/MF A01.

[57] D. E. McCabe and H. A. Ernst, "A Perspective on R-Curves and Instability Theory," Fracture Mechanics: Fourteenth Symposium--Volume I: Theory and Analysis, ASTM STP 791, J. C. Lewis and G. Sines, Eds., American Society for Testing and Materials, Philadelphia, 1983, pp. I-561-I-584.

[58] David Broek, Elementary Engineering Fracture Mechanics, Third Edition, Martinus Nijhoff, The Netherlands, 1983, pp. 185-215.

[59] "Standard Practice for R-Curve Determination," 1982 Annual Book of ASTM Standards, Part 10, Metals--Mechanical, Fracture, and Corrosion Testing; Fatigue; Erosion and Wear; Effect of Temperature, American Society for Testing and Materials, Philadelphia, 1982, pp. 680-699.

[60] P. C. Paris, H. Tada, A. Zahoor, and H. Ernst, "The Theory of Instability of the Tearing Mode of Elastic-Plastic Crack Growth," Elastic-Plastic Fracture, ASTM STP 668, J. D. Landes, J. A. Begley, and G. A. Clarke, Eds., American Society for Testing and Materials, Philadelphia, 1979, pp. 5-36.

[61] J. A. Joyce and M. G. Vassilaros, "An Experimental Evaluation of Tearing Instability Using the Compact Specimen," Fracture Mechanics: Thirteenth Conference, ASTM STP 743, Richard Roberts, Ed., American Society for Testing and Materials, Philadelphia, 1981, pp.525-542.

[62] M. G. Vassilaros, J. P. Gudas, and J. A. Joyce, "J-Integral Fracture Toughness and Tearing Instability Behavior of ASTM A106 Steel Pipes" in, Circumferential Cracks in Pressure Vessels and Piping Vol. II, edited by G.M. Wilkowski, PVP - Vol. 95, American Society of Mechanical Engineers, New York, 1984, pp. 295-307.

[63] "Standard Test for J_{Ic}, a Measure of Fracture Toughness," 1986 Annual Book of ASTM Standards, Section 3, Metals Test Methods and Analytical Proceudres, American Society for Testing and Materials, Philadelphia, 1986, pp. 768-786.

[64] J. R. Rice, "A Path Independent Integral and Approximate Analysis of Strain Concentration by Notches and Cracks," Journal of Applied Mechanics 35, 1968, pp.379-386.

[65] H. A. Ernst, P. C. Paris, and J. D. Landes, "Estimations on J-Integral and Tearing Modulus T from a Single Specimen Test Record," Fracture Mechanics: Thirteenth Conference, ASTM STP 743, Richard Robert, Ed., American Society for Testing and Materials, Philadelphia, 1981, pps.476-502.

3. STRENGTH AND DUCTILITY OF CRACKED TENSILE PANELS

Measurements of the strength and ductility of cracked tensile panels of aluminum 5052-H32 at room temperature were performed to study the effect of the applied tearing modulus. Very small cracks significantly reduced tensile panel ductility. Larger cracks were needed to produce comparable relative reductions in panel strength. The ductility and strength of cracked tensile panels were independent of the applied tearing modulus. Applied tearing modulus appeared to control material ability to withstand artificially produced growing cracks while under compliant loading, implying that high material tearing modulus would be beneficial in this situation.

3.1 Introduction

The experiments described below were performed in order to clarify the qualitative aspects of stable and unstable tearing in a strain-hardening material and to relate this tearing behavior to tearing instability theory [1]. Because in tearing instability theory a steeply-rising J-R curve indicates high resistance to tearing, one might naively assume that a material with a steep J-R curve is superior in every situation to one with a shallower J-R curve. This assumption could be checked by testing a series of materials with a systematic gradation of J-R curves. However it would be difficult to vary the J-R curve without varying other material properties as well.

In tearing instability theory, the slope of the material J-R curve is normalized to become the material tearing modulus, T_{mat}. The complementary driving force for tearing is the applied tearing modulus, T_{app}. T_{app} is controllable by varying testing machine compliance. Therefore one can investigate some aspects of the contribution of T_{mat} to material performance in the presence of cracks by varying T_{app}. Sensitivity to T_{app} in a certain situation would indicate that T_{mat} is probably important in that situation.

The key performance variables for a cracked specimen are strength and elongation. Although structures are rarely designed to elongate beyond yield, fracture mechanics theory and experience show that large structures

require a certain degree of material ductility in order to achieve their design strength. Fracture toughness specimens of acceptably ductile materials nearly always reach their full strength level. The degree of material toughness is indicated by specimen deformability, not strength. Low toughness specimens fracture after only slight plastic deformation, while high toughness specimens can withstand considerable amount.

Therefore, the relationship between strength, elongation, and crack size in tensile panels under varying T_{app} is explored in this study, by forcibly elongating to failure specimens prepared with cracks of various sizes.

The complement of a measurement of strain-to-failure for a given initial crack size is a measurement where the specimen is loaded under displacement control to some initial strain value, and the crack is then extended until the specimen fails. Such a process is plausible in practical applications, through stress-corrosion-cracking, or fatigue crack growth from pulsating loads superposed on large constant loads, for example. Furthermore, tearing instability theory considers, as a thought experiment, the response of a specimen under compliant loading to a small increase in crack length. This consideration of a spontaneous small increment of crack length is central to the tearing instability theory developed by Paris et al., as noted above in Chapter 2. An experimental interpretation of the occurrence of a small increment of crack growth in a specimen under compliant load was realized as part of this study. Specimens were compliantly loaded to various elongation levels, and then cracks were extended by saw cutting until specimen failure. Surprisingly, the effect of machine compliance in this case turned out to be different than in the case of constant crack size with increasing imposed total elongation.

3.1.1 Material and Specimens

The specimen material, chosen for its strain-hardening characteristics, availability and machinability, was aluminum alloy 5052-H32. This alloy contains 2.5 percent magnesium and 0.25 percent chromium by weight; it is designed to have good workability, very good resistance to corrosion, high fatigue strength, and moderate static strength. Among other applications,

it is said to be suitable for "miscellaneous marine and transport applications." [2] Its tensile properties, determined from a test of a large flat coupon as described below, are listed in Table 1. The measured properties are in good agreement with the typical values found in [2].

Two specimen types were used in this study: large flat coupons, referred to from now on as tensile panels; and compact tensile specimens. The dimensions of the specimens are shown in Figure 1. The ends of the tensile panels were suitable for clamping in wedge grips, described below. In most of the tests, double edge notches (DEN) were cut in the tensile panels at the center of the specimen's length. Except as specifically noted below, all notches were started with a hacksaw and finished with a jeweler's saw 0.25 mm in width. Notches of various lengths were used. The compact tensile specimens had in-plane dimensions standard for 25-mm-thick specimens, but the actual thickness was only 3.2 mm.

About 35 tensile panels and 10 compact tensile (CT) specimens were used in the course of this investigation.

Table 1. Tensile properties of the aluminum 5052-H32 alloy used in the present study, as measured with a large coupon specimen.

Yield strength, 0.2 percent offset	179 MPa	25.9 ksi
Ultimate strength	245 MPa	35.6 ksi
Uniform elongation	10 percent	
Reduction of area	57 percent	

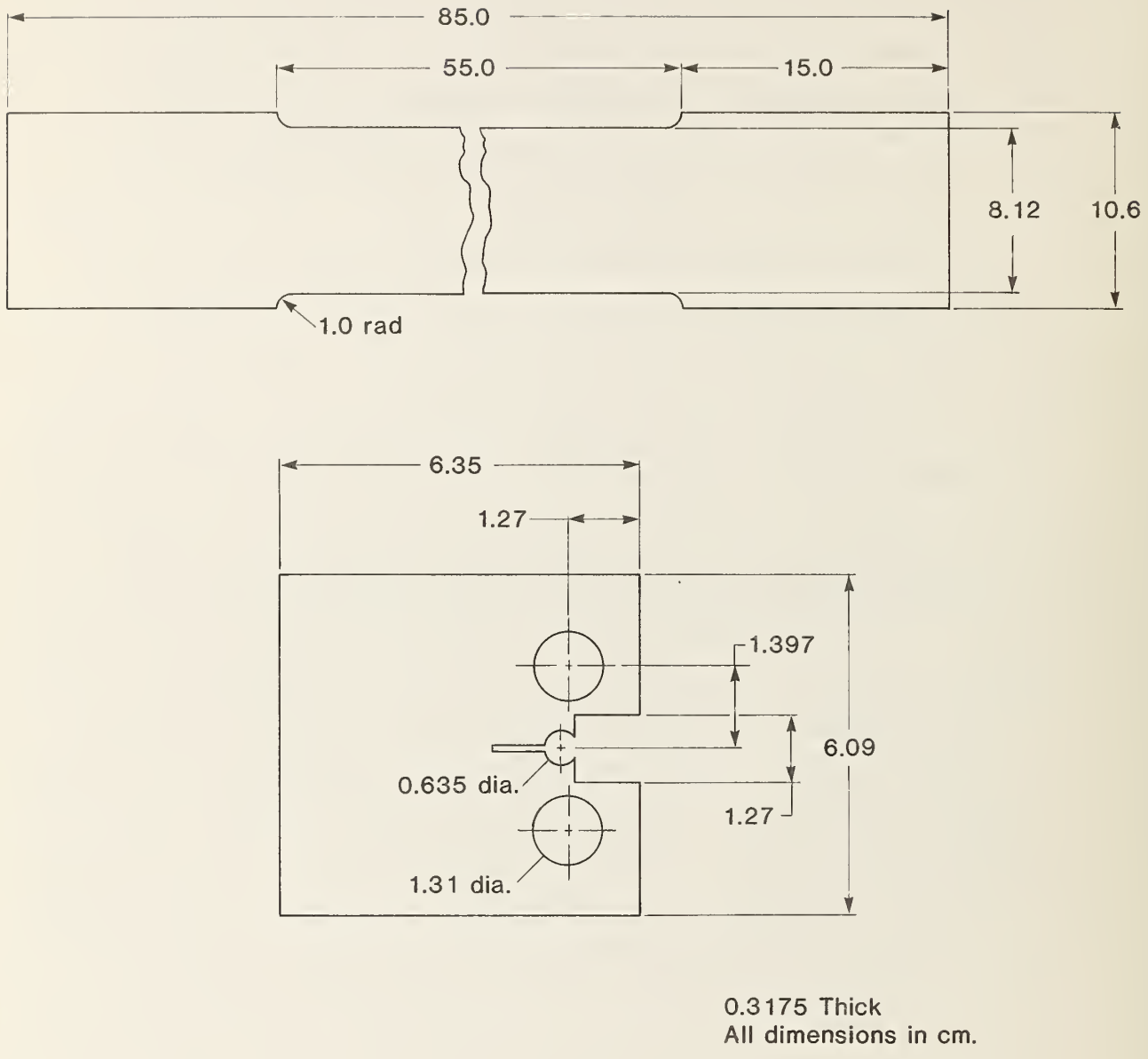

Figure 1. Tensile panels (a) and compact (b) specimens used in the present study.

3.1.2 Measurements, Apparatus, and Procedures

Measurements made in the course of this investigation were:

- o J-R curve on CT specimens;
- o Strain to failure as a function of crack length and load-train compliance;
- o Residual strength as a function ofr notch length and load-train compliance;
- o Artificially-grown crack length at failure as a function of initial strain and compliance;
- o CMOD, load, imposed displacement, and crack length during a constant-extension-rate test to failure, for five crack tip radii.

All tests were performed using servohydraulic test stands with automatic computer-controlled data acquisition and storage. Applied load was measured using load cells, instrumented with electrical resistance strain gages as usual, built into the test stands. Crack mouth opening displacement (CMOD) was measured using the double-cantilever-beam gages (clip gages) conventionally used for fracture testing [3]. Overall specimen displacement was measured using the linear variable differential transformer (LVDT) built into the test stand.

Wedge grips were used to hold the ends of the tensile panels. One end had insulated micarta or PTFE sheets between the wedge blocks and the wedge block holder, to provide electrical insulation. The usual fracture mechanics clevises were used in the tests of the compact specimens.

In the J-R curve measurements, the initiated cracks were finished with a jeweler's saw, instead of fatigue cracking, in order to reproduce the crack tip condition used in the tensile panel tests. Single-specimen, unloading-compliance techniques were used for conducting the tests and calculating J-integrals.

In the strain-to-failure tests, the remote failure strain was obtained by measuring the separation of marks scribed on the specimen surface away from the notch before and after pulling the specimen. Crack mouth opening displacement was recorded continuously during the test.

Variable effective load-train compliance was obtained for these tests by electronically simulating the presence of a spring in the load train. The artificial spring circuit adjusted the servohydraulically-imposed specimen displacement in response to load changes. Load decreases produced proportional increases in the imposed displacement, just as would be the case if an actual mechanical spring were included in the load train. The response time of the artificial spring was slower than that of a real spring, because it was limited by the response time of the testing machine, a few tenths of a second. This was not a liability for the material tested, because it is not subject to cleavage and its behavior is practically rate-independent. In fact, it had the advantage that the unstable fracture process was slowed somewhat, allowing easier qualitative observation.

"Artificial" crack growth in specimens under load was obtained by sawing with a hacksaw. The simulated spring was used during these tests to provide a variable load-train compliance. The initial imposed strain was not held constant, but was allowed to evolve during the test, controlled by the load train compliance and the artificially growing crack. Because the specimens were thin and the loading was displacement controlled, only small amounts of energy were released when the specimens failed, so that the procedure was not hazardous. For thicker or larger specimens, however, the safety aspects of such a procedure would require careful consideration. Tests involving artificial crack growth have been conducted previously, as described by Broek [4].

Because most of the DEN specimens of the present study had saw-cut crack tips, a check of the effect of the tip shape was performed. Notches with tips of various widths were obtained by drilling holes of selected diameters at the notch tips. The notch tip width was taken to be equal to the hole diameter. Two of the notches were finished with saws, one with a jeweler's saw and the other with a hacksaw. These notch widths were measured with feeler gages. A fatigue-sharpened notch was also used in this series; its width was taken to be zero. Notch widths of 0.0, 0.4, 0.8, 1.6, and 3.2 mm were obtained. Potential drop across the plane of crack propagation was measured at four locations in these specimens. Applied load and crack mouth opening displacement (CMOD) were recorded throughout each test.

Because none of the specimens in this study failed before general yielding, measurements providing information on the material ductility were of interest. Two displacement measurements, total specimen displacement (at the load point) and crack mouth opening displacement, were recorded continuously during most of the tests. Displacements near maximum load were of interest as indicators of the material fracture resistance. For specificity, the lower limit of near-maximum loads was chosen as 0.9 times P_{max}, the maximum load. The points corresponding to P_{max}, 0.9 P_{max} before maximum load, and 0.9 P_{max} after maximum load were easily identifiable on plots of load against displacement. From such plots, crack mouth opening or total specimen displacement from the 0.9 P_{max} to P_{max}, P to 0.9 P_{max} (after maximum), or 0.9 P_{max} (before maximum) to 0.9 P_{max} (after maximum) points could be obtained. These displacements, especially the displacement from 0.9 P_{max} to P_{max}, were used as indicators of specimen ductility.

3.1.3 Results

The experimental results are shown in Figures 2 to 10. The J-R curves obtained for three specimens of the A15052-H32 are shown in Figure 2. The specimen thickness used was not large enough to produce formally valid results according to the standard procedure.

Strain-to-failure as a function of crack length is shown in Figure 3. The relative crack length on the abcissa is the total specimen cross section intercepted by the crack. If the full width of the double-edge-cracked specimen is taken as 2W, and each crack has length a, the relative crack size would be given by a/W. No effect of compliance was found in these tests. The strain used in Figure 3 is the remote strain. The decrease in specimen ductility produced by the cracks is confirmed by the plot of extension near maximum load against crack size, Figure 4. Specimens with shorter cracks have considerably larger capacity for extension.

Crack length at failure during artificial crack growth is plotted as a function of compliance in Figure 5 for two initial strain values. Ideal displacement control corresponds to zero compliance, while load control corresponds to infinite compliance. In contrast, strain-to-failure measurements of tensile panels with cracks of various sizes (Fig. 6),

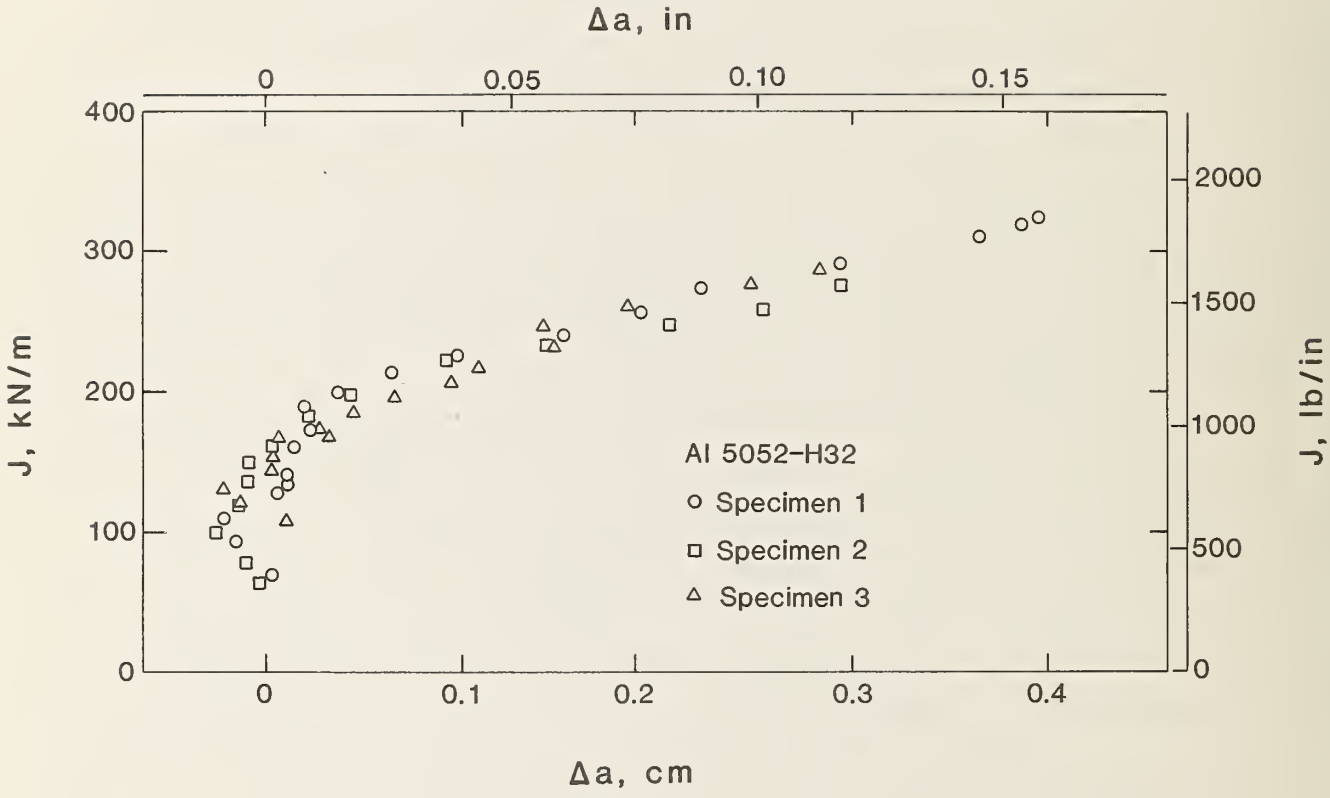

Figure 2. J-R curves for three compact tensile specimens of aluminum 5052-H32.

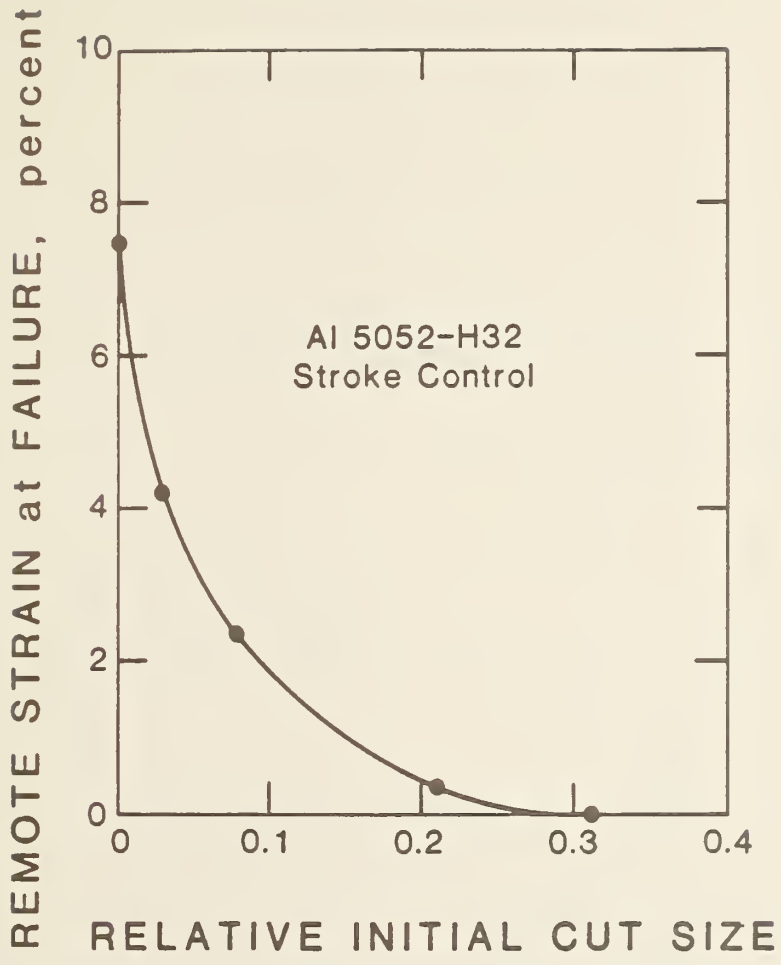

Figure 3. Remote strain to failure plotted against relative initial crack size for tensile panels of aluminum 5052-H32, tested under stroke control for low compliance.

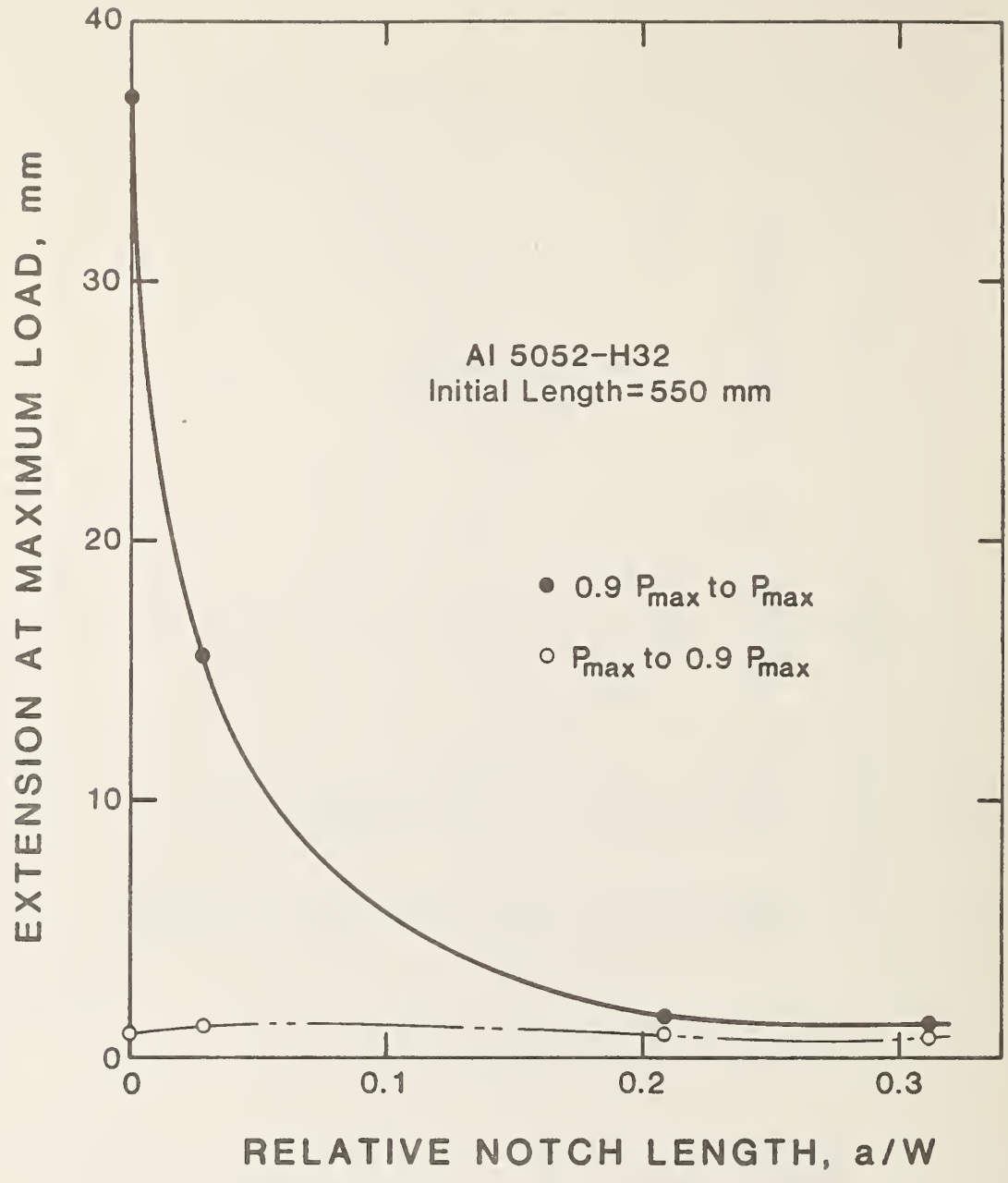

Figure 4. Extension near maximum load plotted against relative crack size. Extensions during the load increase from 0.9 to 1.0 times maximum load P_{max} and extensions during the following load decrease from 1.0 to 0.9 P_{max} are shown.

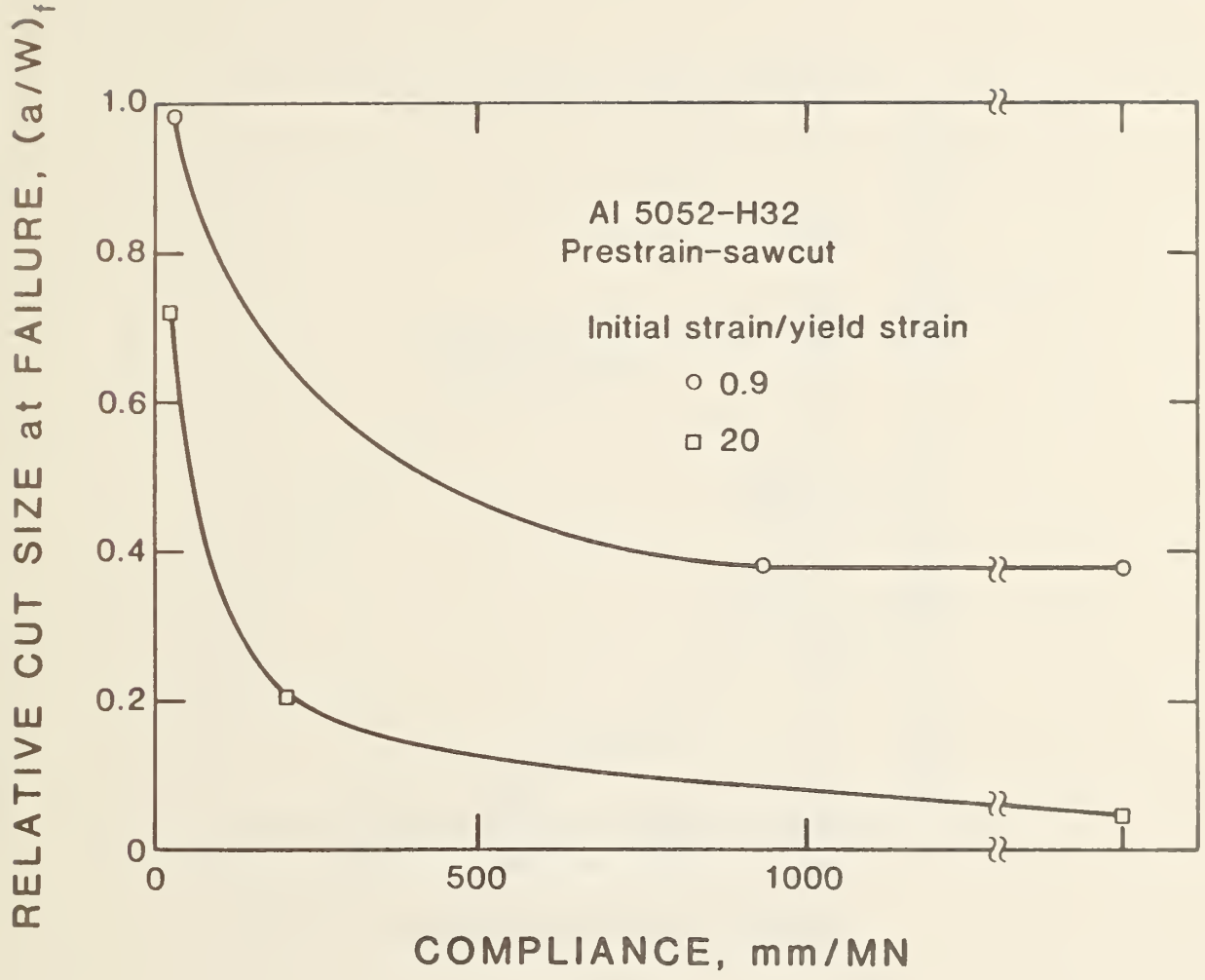

Figure 5. Crack length at failure during artificial crack growth plotted against compliance imposed by electronically simulated spring, for two initial strains, in aluminum 5052-H32.

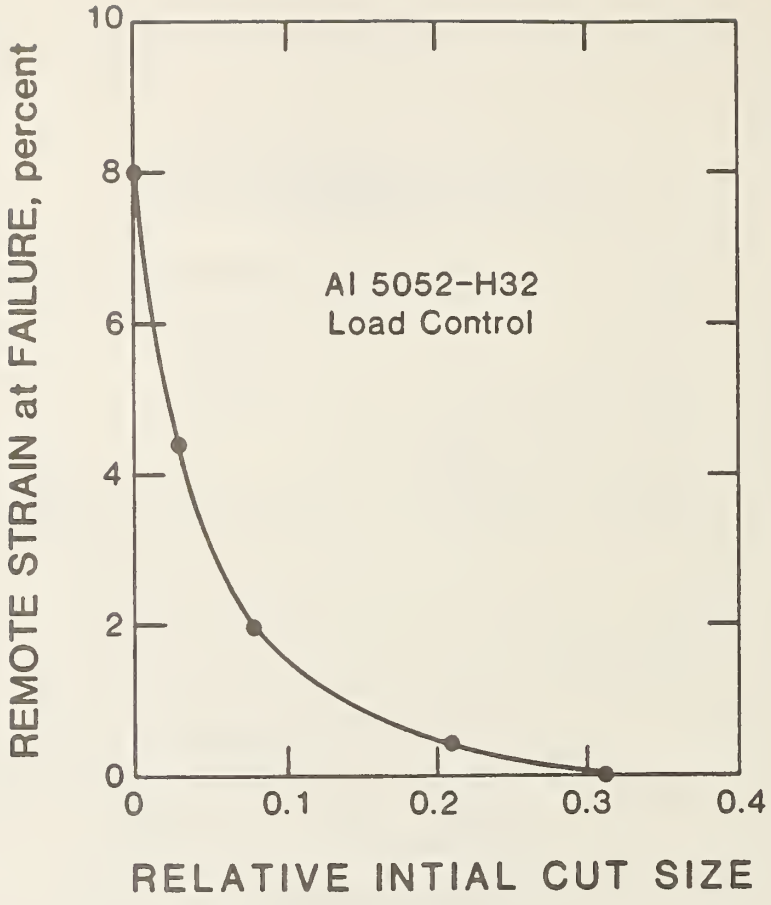

Figure 6. Remote strain to failure plotted against relative initial crack size for tensile panels of aluminum 5052-H32, tested under load control for high compliance.

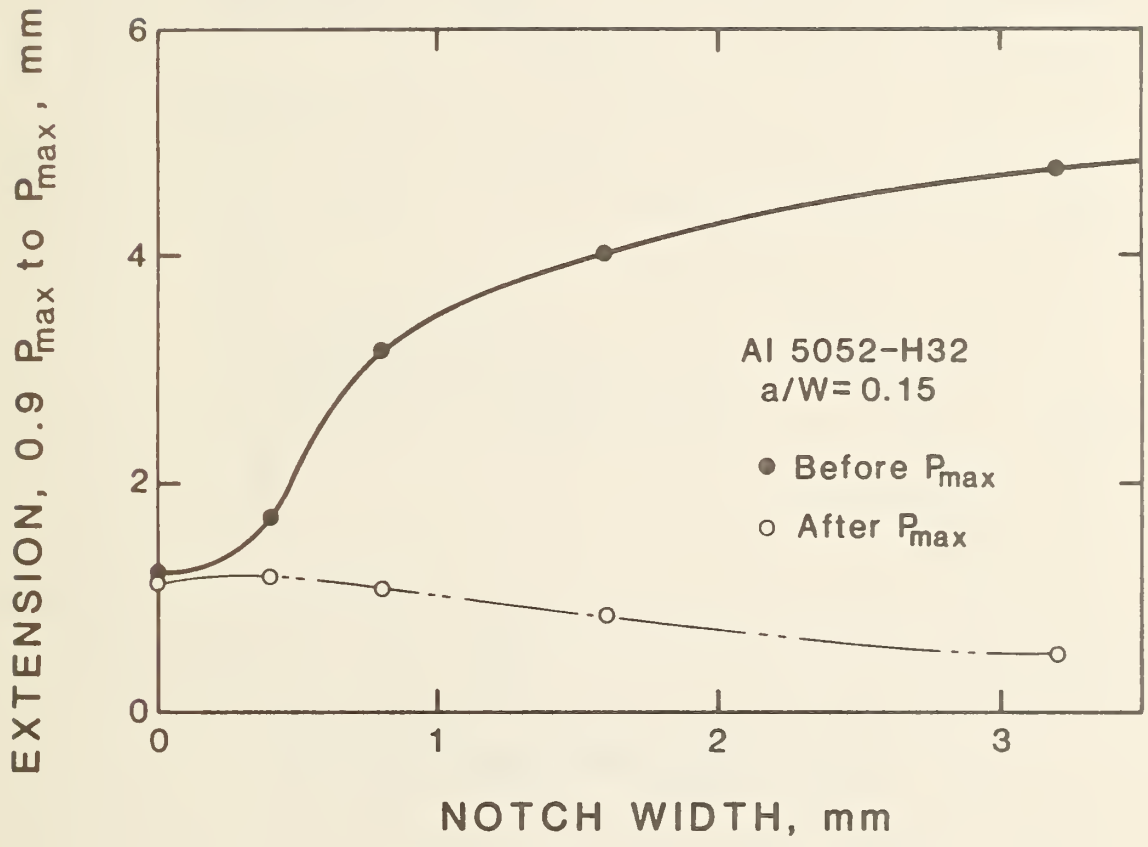

Figure 7. Plot of total specimen extension near maximum load against notch tip width.

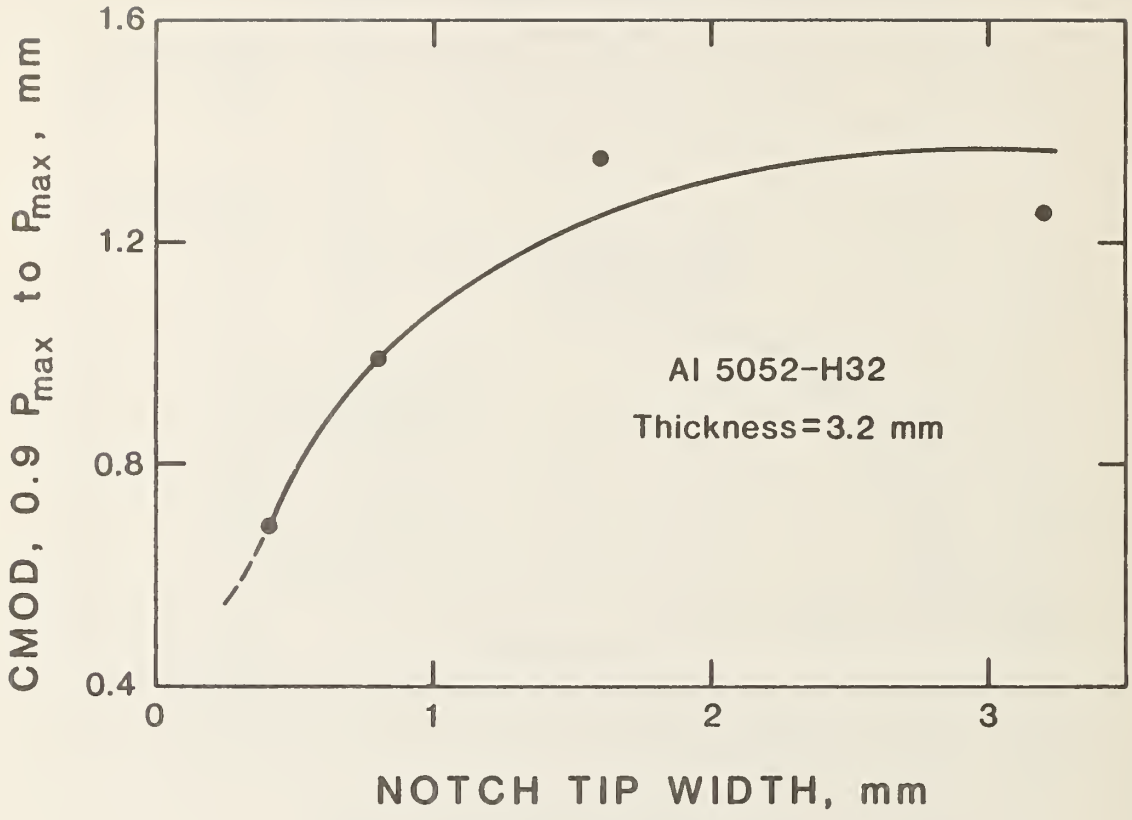

Figure 8. Plot of crack mouth opening displacement (CMOD) near maximum load against notch tip width.

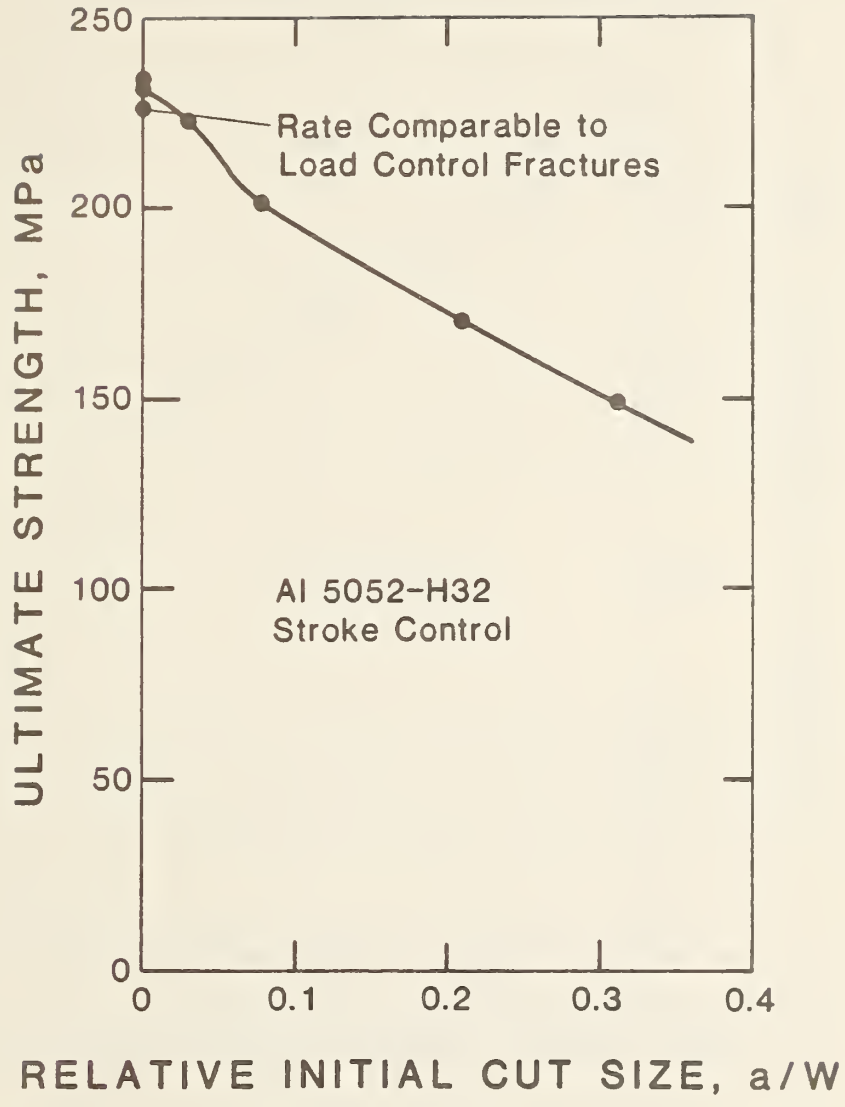

Figure 9. Ultimate strength of notched tensile panel plotted against initial notch size, under stroke control.

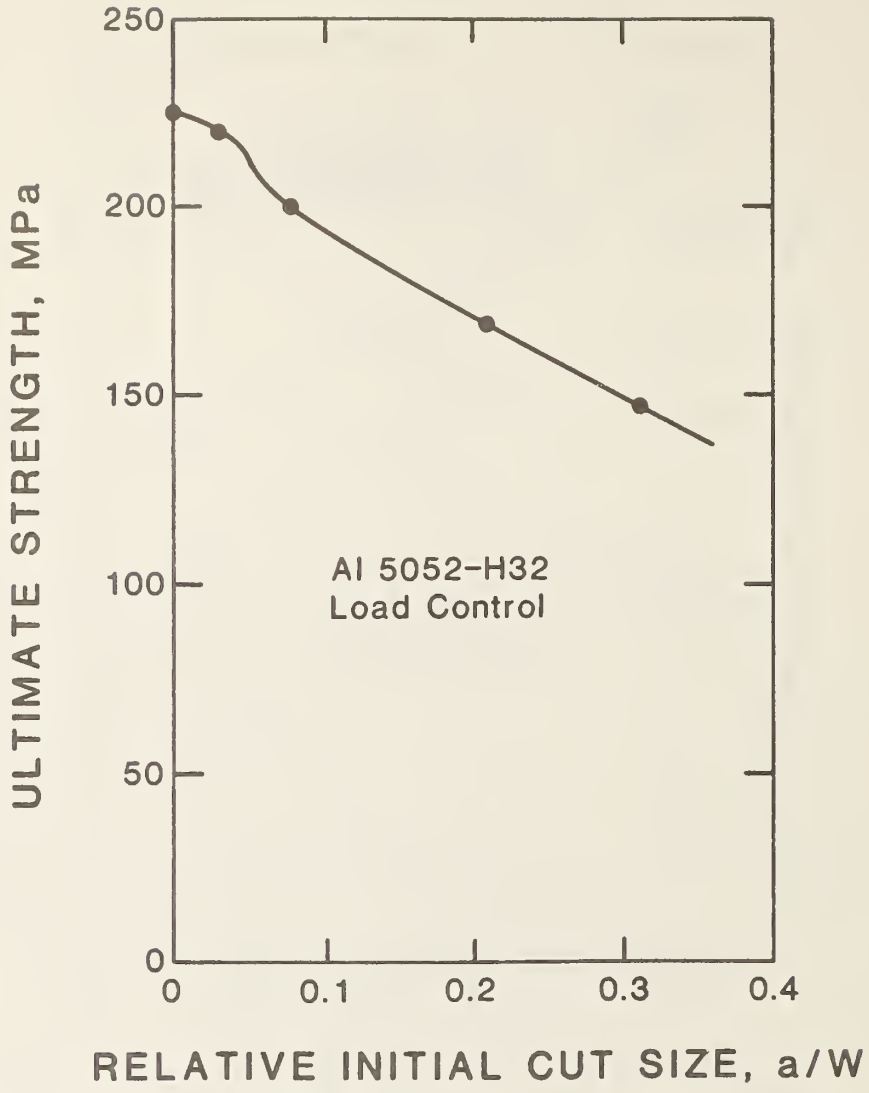

Figure 10. Ultimate strength of notched tensile panel plotted against initial notch size, under load control.

obtained with the testing machine in load control, agree with those of Figure 3, in stroke control.

The measurements on the specimens with varying notch widths yielded a large family of test records. Analysis of these showed that the clearest effect of notch width occurs in extension between 90 percent of maximum specimen load and maximum load P_{max} The specimens with very narrow notches possessed the capacity for some extension with near-maximum loads, but the specimens with wide notches clearly had more. Figure 7 shows specimen extension between 0.9 P_{max} and P_{max} plotted against notch width. The same trend for CMOD is evident in Figure 8. The double-edge-notched specimen with the fatigue-sharpened notches was omitted from this figure because its notch was longer than those ot the other specimens on the side where CMOD was measured, although the total notch length for both notches was the same as for the other specimens.

3.1.4 Discussion

The specimen material chosen for these studies was quite ductile with substantial strain hardening, as shown by its tensile properties. Its high ductility was confirmed by the measured J-R curve. Saw-cut crack tips were used for this curve, for consistency with the crack-tip preparation used in the tensile panel tests.

The strain-to-failure measurements were suggested by the previously reported strong effect of crack size on the driving force for fracture [5]. As anticipated, strain-to-failure decreased rapidly with increasing crack size, Figure 3. The decrease of failure strain with crack size was much more rapid than that of ultimate strength, Figure 9. The strength declined in proportion to the remaining net cross-sectional area, as expected for a tough material. These results suggest that even small cracks can compromise structural ductility, but larger cracks must be present before structural strength is affected. This result shows the strong detrimental effect on specimen ductility of net section yielding, which increased in this material as relative crack size increased from 0.0 to 0.3.

If tearing modulus always controls material performance, loading specimens under high T_{app} must produce failure more readily than loading

under low T_{app}. This hypothesis was checked by measuring strain to failure as a function of crack size for two similar sets of specimens, one with the testing machine in displacement control and one in load control, Figures 3 and 7. In load control, ideally, a very large change in specimen length produces no change in applied load. Actually, of course, the testing machine applies loads over finite time spans, and so the effective compliance is a function of frequency of loading. The testing machine response time was of the order of half a second. The tests were conducted at low loading rates (many seconds), so in load control the effective compliance was infinite, in the time scale of the test. The total compliance available in displacement control was 41mm/MN.

The result, shown above in Figures 3 and 6, and 9 and 10, was that compliance had no effect on remote strain to failure or maximum remote stress.

Load-train compliance proved to be more relevant in the next experiment. In tests on artificial crack growth, compliance had a significant effect on crack growth to failure. As shown in Figure 5, for initial strains below yield, compliant loading reduced the crack size at failure by nearly a factor of two. The remaining ligament at failure for the lowest compliance value was only about one-fortieth of the value at infinite compliance. This striking effect was repeated for specimens prestrained to twenty times yield strain. The final crack length in the low compliance test was fifteen times the final length in the infinite-compliance test. This result indicates that high material tearing modulus is likely to contribute to material durability under artificial crack growth.

The two results discussed above indicate that structural designers should consider using high-tearing-modulus material especially in situations where progressive crack growth from causes other than the main structural load is possible. This conclusion is drawn directly from the observation that high T_{app} produced fracture at lesser notch lengths than low T_{app} under artificial notch growth, Figure 5. It is assumed that where a high T_{app} promotes fracture, a high T_{mat} will enhance fracture resistance.

The experiments on crack tip radius were consistent with expectations. Sharp cracks reduced ductility more than blunt cracks, because they introduced a larger degree of strain concentration.

3.2 Conclusions

The conclusions of the work reported here can be summarized as follows:
1) Very small cracks can significantly reduce tensile panel ductility. Larger cracks must be present before panel strength is significantly reduced. A crack so large that only net section yielding occurs reduces the ductility, measured by post-yield strain remote from the crack, to nil.
2) The relative magnitudes of material and applied tearing modulus do not control ductility or strength of cracked tensile panels.
3) The value of material tearing modulus relative to applied tearing modulus does affect resistance to failure at cracks produced artificially while the main load on the specimen evolves in time as dictated by the combined compliance of the specimen and load train. Low load train compliance, and therefore, presumably, high material tearing modulus, increases the crack size at failure.

3.3 Acknowledgments

The technical support of J. D. McColskey and D. P. Vigliotti in conducting the tests reported here is appreciated. This report was prepared as part of the Fracture Control Technology Program, under the sponsorship of Dr. H. H. Vanderveldt, Naval Sea Systems Command (SEA 05R25). The effort was directed by Dr. John P. Gudas, David Taylor Naval Ship Research and Development Center, under Program Element 62761N, Task Area SF-61-544-504.

3.4 References

[1] Section 2, this report.
[2] American Society for Metals, Metals Handbook Ninth Edition, Volume 2, Properties and Selection: Nonferrous Alloys and Pure Metals, American

Society for Metals, 1979, p. 101.

[3] American Society for Testing and Materials, "Standard Test Method E399-81 for Plane-Strain Fracture Toughness of Metallic Materials," in 1982 Annual Book of ASTM Standards, Part 10, American Society for Testing and Materials, Philadelphia, 1982, pp. 592-622.

[4] David Broek, Elementary Engineering Fracture Mechanics, Third Edition, Martinus Nijhoff, The Netherlands, 1983, pp. 185-215.

[5] D. T. Read, "Applied J-Integral Values in Tensile Panels," Ductile Fracture Test Methods, Proceedings of a CSNI Workshop, Nuclear Energy Agency, Organization for Economic Cooperation and Development, Paris, 1983, pp. 273-291.

4. APPLIED J-INTEGRAL VALUES FOR ASTM A-710 STEEL PANELS

4.1 Abstract

In a test program motivated by the need for a quantitative relationship among fracture toughness, flaw size, and applied loading for small flaws, to be used for fitness-for-service assessment, applied J-integral was measured as a function of applied strain in eight 14-mm-thick specimens of A710 Gr A Cℓ 3 steel plate. All the edge cracks had lengths less than 3 percent of the specimen width of 82 mm. Six specimens were tested in tension; two were loaded by four-point-bending in the plane of the plate. One single-edge-cracked, transverse-oriented specimen was tested at -30°C. Electrical resistance strain gauge and clip-gauge crack mouth opening displacement measurements were used to obtain quantities inside the J-integral. The J-integral was calculated by trapezoidal rule integration. Unloading crack-mouth compliance measurements were used to obtain crack length values so that tearing effects could be observed.

Lüders strains occurring right after yield caused rapid increases in the applied J-integral values for the tensile specimens. Except for the Lüders strain effect, the behavior of the applied J-integral in bending was similar to that in tension. The extra J-integral produced by tearing was ascribed to two causes: loading of a longer crack in gross-section-yielding, and net section yielding accompanying the tearing. The initiation toughness and tearing resistance of the panels with short cracks were greater than those of conventional three-point-bend specimens of the same thickness. No effect of temperature on applied J-integral was found from the specimen tested at -30°C. The present data support Wilson's prediction of the dependence of J on strain for a material with a bilinear stress/strain curve.

4.2 Introduction

This paper describes experimental results of direct evaluations of the J-integral as a function of applied strain in tensile and bending panels with

small cracks. This test program was motivated by the need for a general, experimentally verified, quantitative relationship among fracture toughness, flaw size, and applied loading for small flaws, to be used for fitness-for-service assessment. The cracks used here intercept only up to 3.4 per cent of the specimen cross-sectional area. This is small enough that attainable loads are sufficient to cause considerable specimen yielding in locations remote from the crack plane. Equations that relate J-integral to area under the specimen's load-displacement curve for deeply cracked specimens are not applicable to the small cracks used here. The J-integral values for these small cracks are of interest for studies of fracture at cracks within elastic-plastic and fully plastic strain fields.

The experimental techniques used have been described in detail previously [1]. Including the present results, sufficient data now exist on the small-crack behavior of the J-integral as a function of applied strain for comparison to theoretical predictions, comparisons of the behavior of different alloys, comparison of tensile and bending results, and identification of the effect of ductile tearing.

4.3 Theoretical Background

The J-integral has been defined as a path-independent line integral on a contour surrounding a crack tip [2]; it has also appeared as the amplitude of the Hutchinson-Rice-Rosengren (HRR) stress/strain singularity [3,4]. A modified J-integral has been used in tearing studies [5]. The integral used in this paper is asserted to be the path-independent line integral J [1], taken on a contour lying far from the crack tip. No claim is intended regarding the existence or amplitudes of HRR stress-strain fields in the present specimens, or about any unique correspondence between the J-integral measured here and the initiation or extent of tearing.

Several theoretical predictions of the behavior of the J-integral in specimens with small cracks are available [6-10]. Figure 1 displays three of these, two for cracks in infinite plates calculated from an analysis by Wilson and one by calculated from an analysis given by Shih, German, and Kumar [11]. The conversions used in this figure for the normalized J-integral, j, and the normalized remote strain, e, are

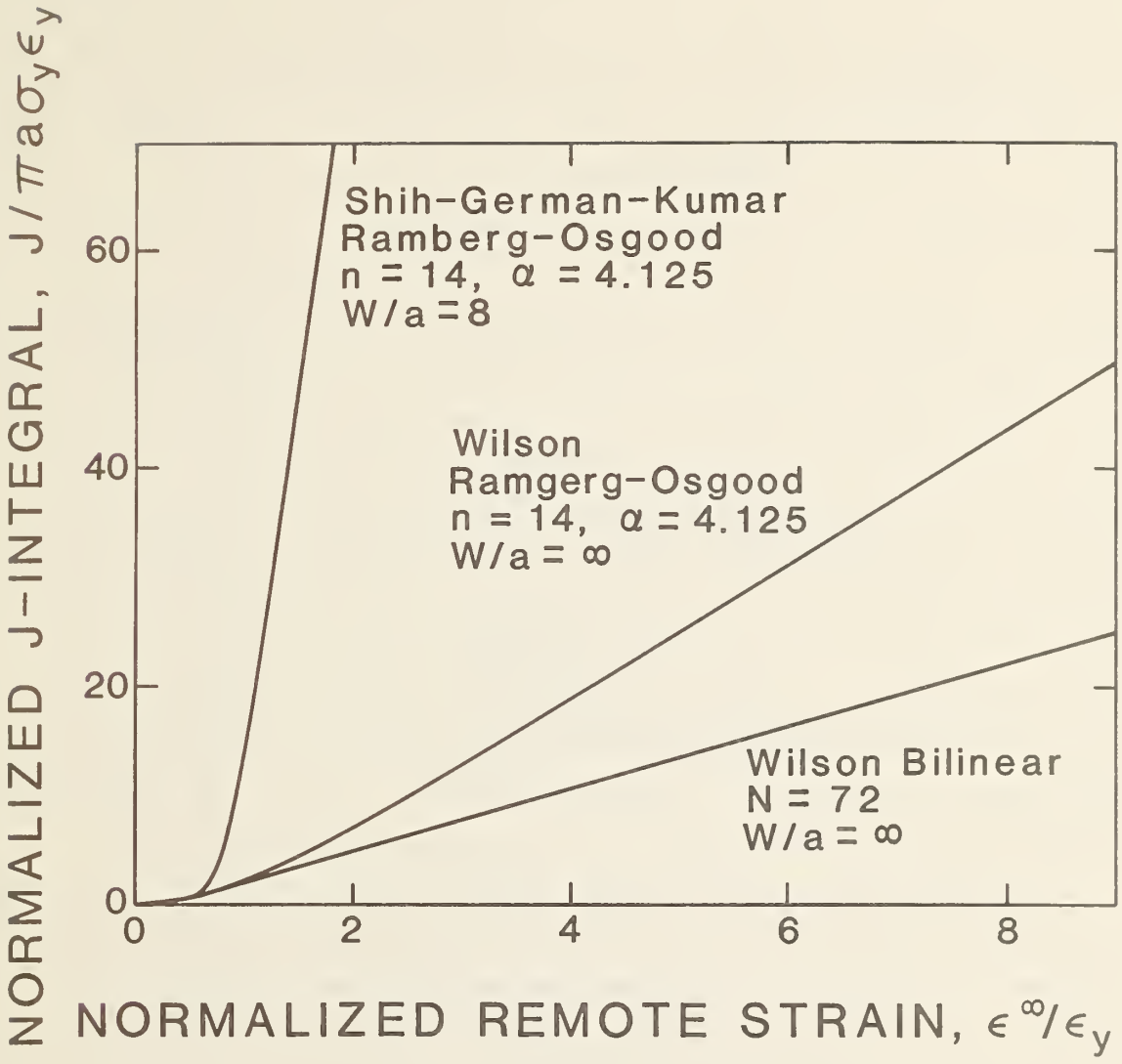

Figure 1. Three theoretical predictions of the behavior of the J-integral as a function of remote strain in specimens with small, W/a = 8, and infinitesinal, W/a = ∞, cracks.

$$j = JE/(\pi a \sigma_y^2) \quad (1)$$

and

$$e = \epsilon/\epsilon_y, \quad (2)$$

where J is J-integral, E is Young's modulus, a is crack size, σ_{ys} is material flow strength, σ_u is material ultimate strength, σ_y is material flow strength $(\sigma_{ys} + \sigma_u)/2$, and ϵ_y is nominal material flow strain, given by σ_y/E. The two curves labelled Wilson Bilinear and Wilson Ramberg-Osgood are different predictions constructed using, respectively, bilinear and Ramberg-Osgood representations of the stress-strain curve of the specimen material. The Ramberg-Osgood constants n and α were obtained by fitting the specimen material true stress-strain curve, which was calculated from the engineering stress-strain curve. Figure 2 compares the specimen material true stress-strain curve its Ramberg-Osgood and bilinear representations. The Ramberg-Osgood parameters used were n = 14 and α = 4.125. A slope of E/N = E/72 was used for the upper part of the bilinear representation.

The Ramberg-Osgood curve (Figure 1) for J as a function of strain makes use of upper-bound plane stress h factors calculated by He and Hutchinson [12] to relate J to strain. To apply this approach to the present specimen material, the h factors given for a series of work hardening exponents n were plotted against 1/n for extrapolation to n = 14. The Ramberg-Osgood curve plotted in Fig. 1 is thus an extrapolated upper bound. It differs by a factor of $h/(2\pi) = 2.5$ from the curve labelled Wilson Bilinear. The Bilinear curve is an analytical continuation of the linear elastic relationship for J as a function of strain. Similar curves were given previously by Merkle [7] and by Begley, Landes, and Wilson [6]. Turner [8] has reported curves derived from finite element analyses that lie generally between Wilson's two curves in Figure 1. In addition, the relationship between crack tip opening displacement (CTOD) and strain given originally by Burdekin and described by Dawes [9] can be converted to give J if the constraint factor m is known. For m values in the range 1 to 2 the CTOD curve also falls generally between the two curves given by Wilson's analysis.

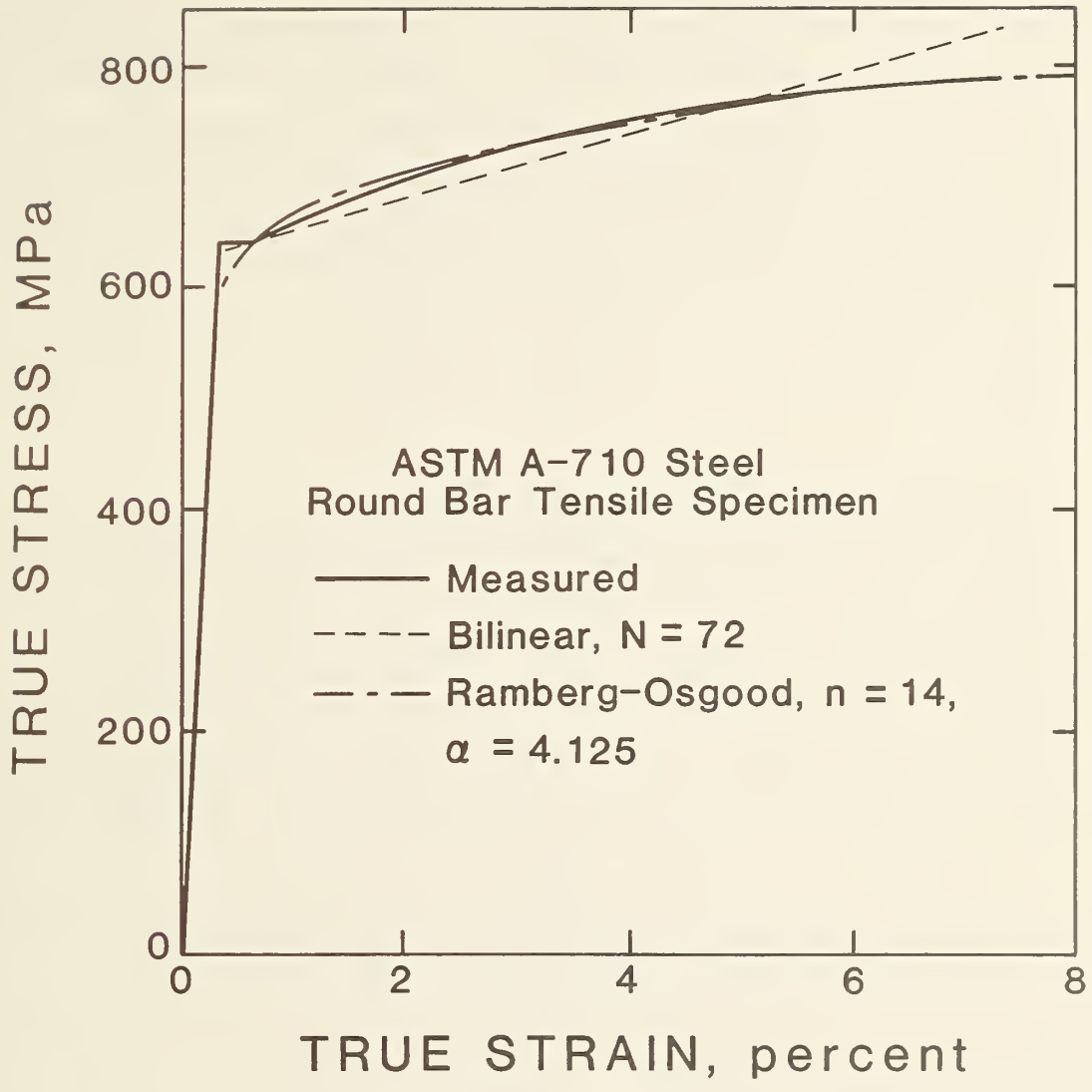

Figure 2. Engineering stress/strain curve for longitudinal and transverse round-bar tensile specimens of the ASTM Grade A Class 3 alloy steel specimen material used in the present study.

The difference between the Shih et al. curve and the others in Figure 1 is that only it was derived for a specific finite crack size, namely, $a/W = 1/8$. The others all refer to small or infinitesimal cracks compared to the plate width. The difference between the behavior of small cracks and cracks of relative size $a/W \geq 1/8$ has been confirmed experimentally and related to plate deformation patterns elsewhere [13-15]. Previous experimental results [13-15] indicated that the J-integral for small cracks in a high-strength quenched and tempered nickel steel fell between the two predictions by Wilson, closer to the upper curve.

4.4 Material

The specimen material used in this investigation was reported by the manufacturer to be ASTM A710 Grade A Class 3 alloy steel. It was received in the form of 19-mm- (0.75-in-) thick plate. The chemistry, as supplied by a commercial source, is listed in Table 1. This chemical analysis indicates less than 0.01 weight per cent of Nb, which violates the specification for A710 Grade A Class 3 steel. Some unusual behavior of this alloy under heat treatment, which may be related to its chemistry, have been noted [16]. The

TABLE 1-Chemical composition, in weight per cent, of the ASTM A710 Grade A Class 3 alloy steel specimen material used in the present study.

Carbon	Manganese	Nickel	Chromium	Silicon	Copper	Sulfur
0.042	0.54	0.85	0.65	0.34	1.2	0.010

Phosphorous	Niobium	Aluminum	Iron
less than 0.005	less than 0.010	less than 0.020	balance

tensile properties of the specimen material, obtained using replicate round bar tensile specimens 6.4 mm (0.25 in) in diameter, are listed in Table 2. The engineering stress-strain curve contains a slight yield point, some Lüders extension, and strain hardening. The tensile properties of the specimen material at room temperature were essentially the same in the transverse and longitudinal directions, except for the elongation, as can be seen from Table 2. The Lüders strain after the yield point was present in both longitudinal and transverse orientations. After its maximum, the load decreased more rapidly with extension in the longitudinal specimens than in the transverse ones, leading to the lower elongation values for the longitudinal specimens.

TABLE 2-Tensile properties, at room temperature, of the ASTM Grade A Class 3 alloy steel specimen material used in the present study.

Longitudinal		
Yield Strength, 0.2 percent offset	637	92.4 ksi
Ultimate tensile strength	732 MPa	106.2 ksi
Elongation	12.0 percent	
Reduction of Area	75.5 percent	
Transverse		
Yield Strength, 0.2 percent offset	634	93.2 ksi
Ultimate tensile strength	727 MPa	105.5 ksi
Elongation	17 percent	
Reduction of Area	71 percent	

The fracture toughness of this specimen material at room temperature was investigated using three-point-bend specimens in the LT and TL orientations. The in-plane dimensions were nominally 50 by 220 mm (2 by 9 in). Thicknesses of 14 and 19 mm (0.55 and 0.75 in) were used as noted. Half of the specimens (as noted) were side-grooved 12.5 percent on each side after fatigue pre-cracking. The tests were performed according to ASTM Standard Test Method E-813. The J_{Ic} and J-R results are listed in Table 3. Items of non-compliance with the standard were the differences between compliance-measured and physical

TABLE 3-Toughness and tearing resistance, in terms of the J-integral, of the ASTM Grade A Class 3 alloy steel specimen material used in the present study.

Orientation	Side-grooved			Non-side-grooved		
	J_{Ic} N/mm	J_{Ic} lb/in	T_{mat}	J_{Ic} N/mm	J_{Ic} lb/in	T_{mat}
TL	118	674	53	183	1046	73
	120	686	49	117	669	84
	145	829	41	___	_____	__
Average	128	731	48	150	857	78
LT	234	1337	103	371*	2120*	168*
				377*	2154*	186*
Average				374	2137	177

*19 mm thick specimen.

crack extension values, Δa_c and Δa_p, noted below, and the specimen dimensions. The higher values of J used to obtain the material tearing modulus failed to meet the specimen size requirement. The results of the J-integral tests indicate that the specimen material is quite tough at room temperature, and that non-side-grooved specimens in the LT orientation (crack grows across the rolling direction) are the toughest (J_{Ic} = 374 N/mm, T_{mat} = 177), while side-grooved specimens in the TL orientation (crack grows along the rolling direction) are the least tough (J_{Ic} = 128 N/mm, T_{mat} = 48). These values were calculated using $T = E \cdot (dJ/da)/\sigma_y^2$, where E is Young's modulus. In the TL orientation, the side-grooved and non-grooved specimens had similar J_{Ic} values. However in the LT orientation, the one side-grooved specimen had lower J_{Ic} and T_{mat} values that the two non-grooved specimens.

The compliance-measured crack extension values, Δa_c, differed from the respective physical crack extension values, Δa_p, by more than 15 percent. This is attributed to friction in the conventional three-point-bend fixture used and to crack front curvature. The Δa_c values were corrected by linear scaling before data reduction. No pop-ins or other signs of rapid crack advance were observed in these room temperature tests.

In the TL orientation, the side-grooved and non-side-grooved specimens had similar J_{Ic} values. However in the LT orientation, the one side-grooved specimen had lower J_{Ic} and T_{mat} values than the two non-side-grooved specimens.

4.5 Specimens, Apparatus, Instrumentation, and Techniques

Tensile and four-point-bending panel specimens of the specimen material were machined with gauge sections measuring 82 mm (3.22 in) wide by 14 mm (0.55 in) thick by 250 mm (10 in) long. The total specimen lengths were 584 mm (23 in) for the transverse specimens and 850 mm (33 in) for the longitudinal specimens. The transverse specimens were made shorter because of the size of the plate of specimen material available. The grip sections at each end of the specimen were 108 mm (4.25 in) wide to confine plastic strain to the gauge section. Table 4 gives the details of the crack geometries tested. Figure 3 shows the loading methods used for the tension and bending tests. For the tensile tests, mechanical wedge-grips clamped the specimen grip sec-

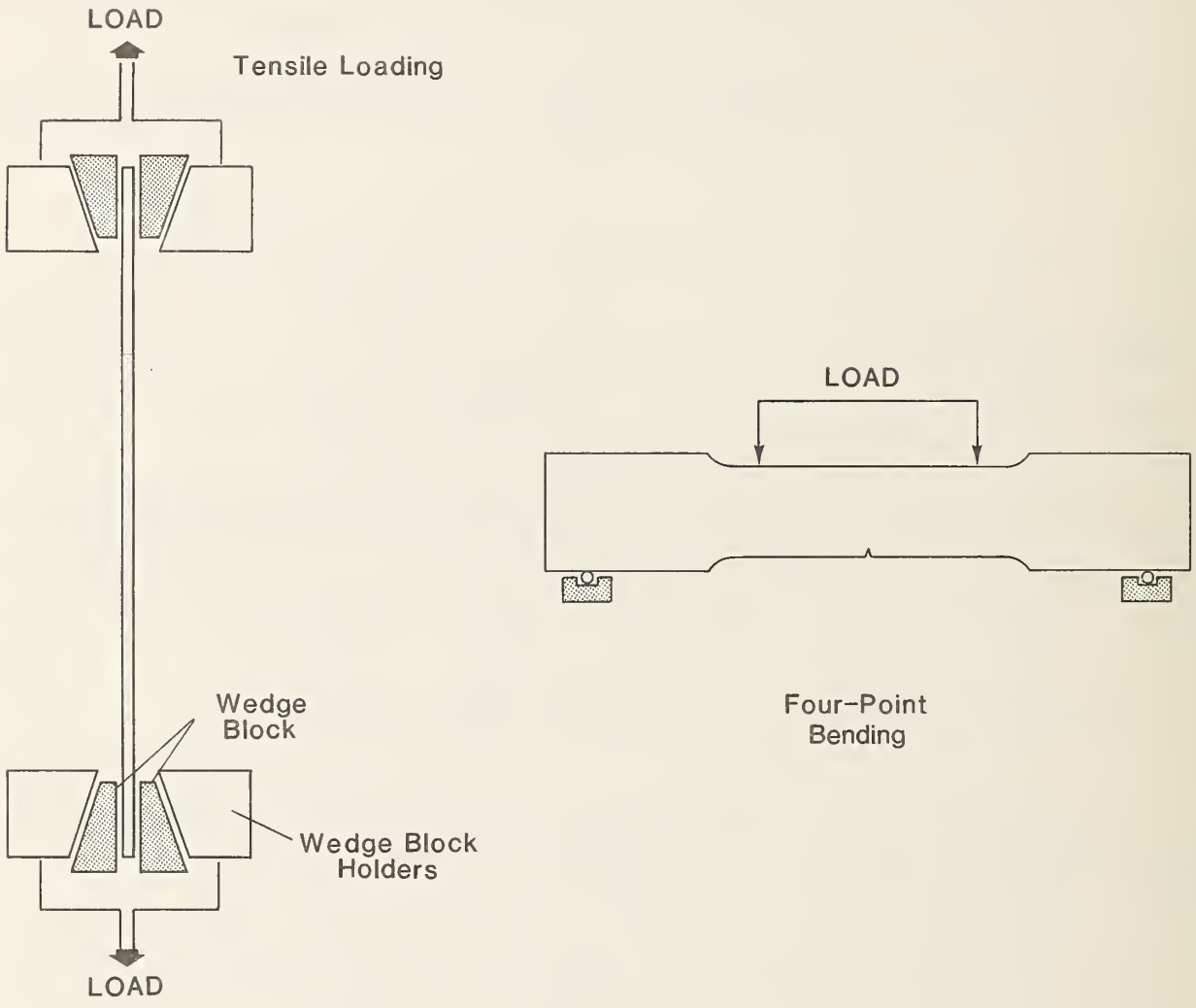

Figure 3. Loading methods used for tensile and four-point-bend tests.

TABLE 4-Specimen and test types and for the specimens used on the present study.

Abbreviation	Orientation	Crack Geometry	Loading Mode	Crack Length mm	Relative Crack Size
DECT (saw-cut crack tips)	LT	Double-Edge	Tension	1.1	0.014
SECT	LT	Single-Edge	Tension	1.9	0.023
SECT (prestrained)	LT	Single-Edge	Tension	2.3	0.028
SECT	LT	Single-Edge	Bending	1.4	0.017
SECT	TL	Single-Edge	Tension	1.5	0.018
PTST	TL	Part-Through Surface	Tension	3.7 x 13	0.034
SECT	TL	Single-Edge	Bending	1.2	0.015
SECT (-30 C)	TL	Single-Edge	Tension	1.2	0.015

DECT = Double-edge-cracked tensile.

SECT = Single-edge-cracked tensile.

SECB = Single-edge cracked bend.

PTST = Part-through-surface tensile.

tions; for the bend tests, four-point loading was used. The outer bending points were 560 mm (22 in) apart for the transverse specimens and 810 mm (32 in) apart for the longitudinal specimens. The inner bending points were 250 mm (10 in) apart for the transverse specimens and 300 mm (12 in) apart for the longitudinal specimens. The bending points were 25 mm (1 in) diameter steel rollers on flat steel holders. The rollers were free to rock as the specimen bent. Loads were supplied by a displacement-controlled servo-hydraulic testing machine with a capacity of 1 MN (225,000 lbs).

Instrumentation as developed previously [1] for direct measurement of the J-integral was used, including a load cell built into the testing machine, a crack mouth opening displacement (CMOD) gauge (ring-gauge), about 35 electrical resistance strain gauges, and up to 3 linear variable differential transformer (LVDT) gauges for displacement measurement. An array of 5 small strain gauges was located near the crack mouth to give the strain profile there, as shown in Figure 4. An additional high-strain-gradient location, such as the specimen back face opposite a surface flaw, could also be instrumented with a linear array of 5 closely-spaced small strain gauges. Some gauges were always located away from the crack, for measurement of remote strain.

The strain gauges, load cell,and crack mouth (CMOD) gauge were wired to conventional signal conditioning circuitry. The LVDTs contained signal conditioning circuits within their cases. The conditioned signals from all the gauges were introduced to the input of a commercially available sixteen-bit analog to digital (A/D) conversion system. The least significant bit in the load reading corresponded to a load of 30 N, and the least significant bit in the CMOD reading corresponded to a displacement of less than 1×10^{-4} mm. The least significant bit in the strain readings corresponded to a strain of about 3×10^{-5}. The A/D system was linked to a commercially available microcomputer system for converting voltage readings to physical quantity values and storing these on floppy discs. The specimens were tested under displacement control. Increments of displacement were imposed. At each increment, the gauges were scanned and the readings were recorded, printed, and used to calculate a preliminary J-integral which was plotted along with the strain gauge strains. Slight relaxations of the load, on the order of 1 percent, were observed after displacement increments imposed at high strains. These occurred over a period of up to 2 minutes after the displacement increment.

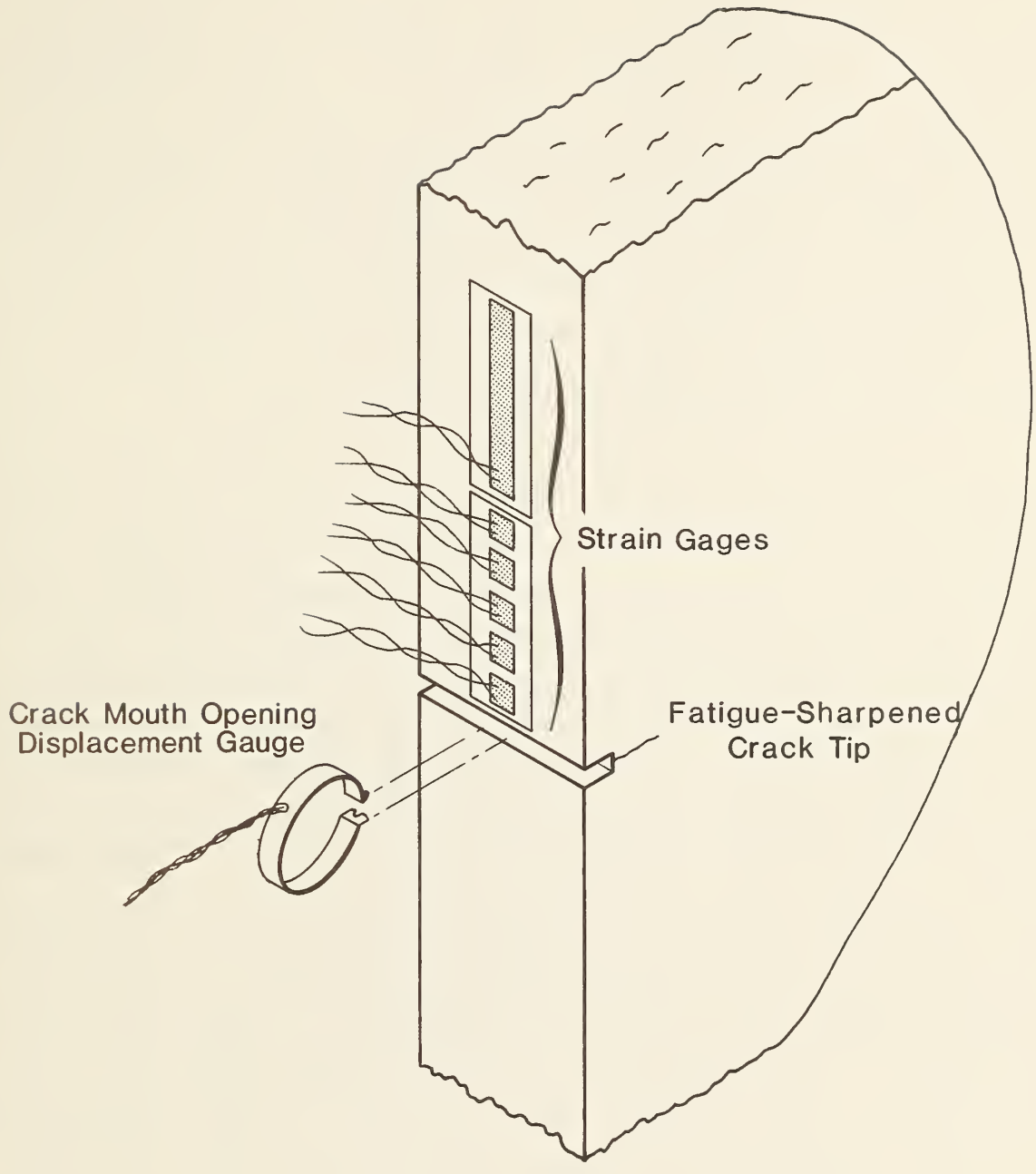

Figure 4. Crack mouth instrumentation, including an array of small strain gauges and a crack mouth opening displacement gauge.

The usual procedure was to impose the displacement increment, wait 2 minutes for the load to become constant, and then scan all instruments. The scanning itself took about 10 seconds. After the instrumentation readings had been recorded, the unloading compliance, CMOD per unit load, was measured during an unloading of 10 to 20 percent of the load. An approximate crack length was obtained. These values were corrected by linear scaling after the test to give the correct initial and final crack depths. These crack depths were used to detect the initiation of tearing and in the calculation of the tearing modulus. In a typical test, on the order of 100 displacement increments would be used. At some stage, the strain gauges would begin to fail because of high imposed strains of the order of 2 to 3 percent. From this point on a different data analysis method had to be used.

In the post-test data analysis, all the measured strain and displacement quantities were zero-corrected by fitting the linear part of the record for each quantity to a linear dependence on the stress, then forcing zero strain or displacement at zero stress by offsetting the measured strain or displacement. The J-integral was calculated using the trapezoidal rule for displacement and stress-work integrals along both sides of the contour. Because the contours were chosen along specimen edges so that the stresses at the contour were uniaxial, an elastic-perfectly-plastic approximation of the simple round-bar stress-strain curve was used for calculating stress-work integral. Integration of strain gauge strains to obtain the displacements needed for calculation of the traction-bending term of the J-integral gave some error cancellation, which would not have been obtained had the LVDT displacements been used. The LVDT displacements were used to check the integrated strain values and for gauge length strain measurement after strain gauge failure. Good correlations were obtained experimentally between J-integral and 1.0 x σy x CMOD. This correlation is expected because of low geometrical constraint of the simple tension and very-short-crack bend geometries used here. After strain gauge failure, this correlation was used to obtain J-integral values.

Photoelastic coatings were bonded to the surfaces of the specimens to allow photographic recording of the strain patterns in the specimens. The coatings were observed through a polarizing sheet using white light. Colored fringes corresponding to the difference between longitudinal and transverse

principal strains were observed. This allowed observation of the Lüders bands.

4.6 Results and Discussion

Results on remote strain, gauge length strain, stress, crack mouth opening displacement, J-integral, and strain as a function of distance from the crack plane on the cracked and uncracked specimen edges were obtained over the whole course of all the tests. A complete presentation of these results is too lengthy for this publication, and is found elsewhere [17]. The key results are the plots of J-integral against remote strain. All the other results, though interesting and important in themselves, are supportive of the J-integral results.

Figure 5 shows the measured J-integral as a function of strain for four-point-bending with crack length 1.4 mm for a single-edge-cracked longitudinal specimen. This figure shows the usual parabolic dependence at low strains followed by an approximately linear dependence above yield. The deviation of the post-yield dependence from true linearity is believed to be an artifact of the experimental arrangement; perhaps it is a result of the significant curvature induced in the specimen by bending by the end of the test. The important point is the gradual rate of rise of J-integral with imposed strain above yield. This result is qualitatively similar to the Wilson results in Figure 1.

Figure 6 shows the behavior of J-integral as a function of strain for all the specimens tested. Six of these are tensile panels, two are four-point-bending panels. This plot shows a feature of the tensile tests not present in the bend results of Figure 5, namely, the step in J-integral at a fixed value of strain near yield. From the photoelasticity results, this step in J-integral is associated with an area of high strain that first extends at an angle from the crack tip to the opposite edge of the specimen, and then spreads along the specimen gauge section. This behavior is the same as the Lüders band phenomenon in tensile tests, and is associated with the Lüders extension found in the tensile bar stress/strain curves for this material. This step in the J-integral vs strain behavior was not present in the bend tests; the photoelastic results for bending confirmed that no

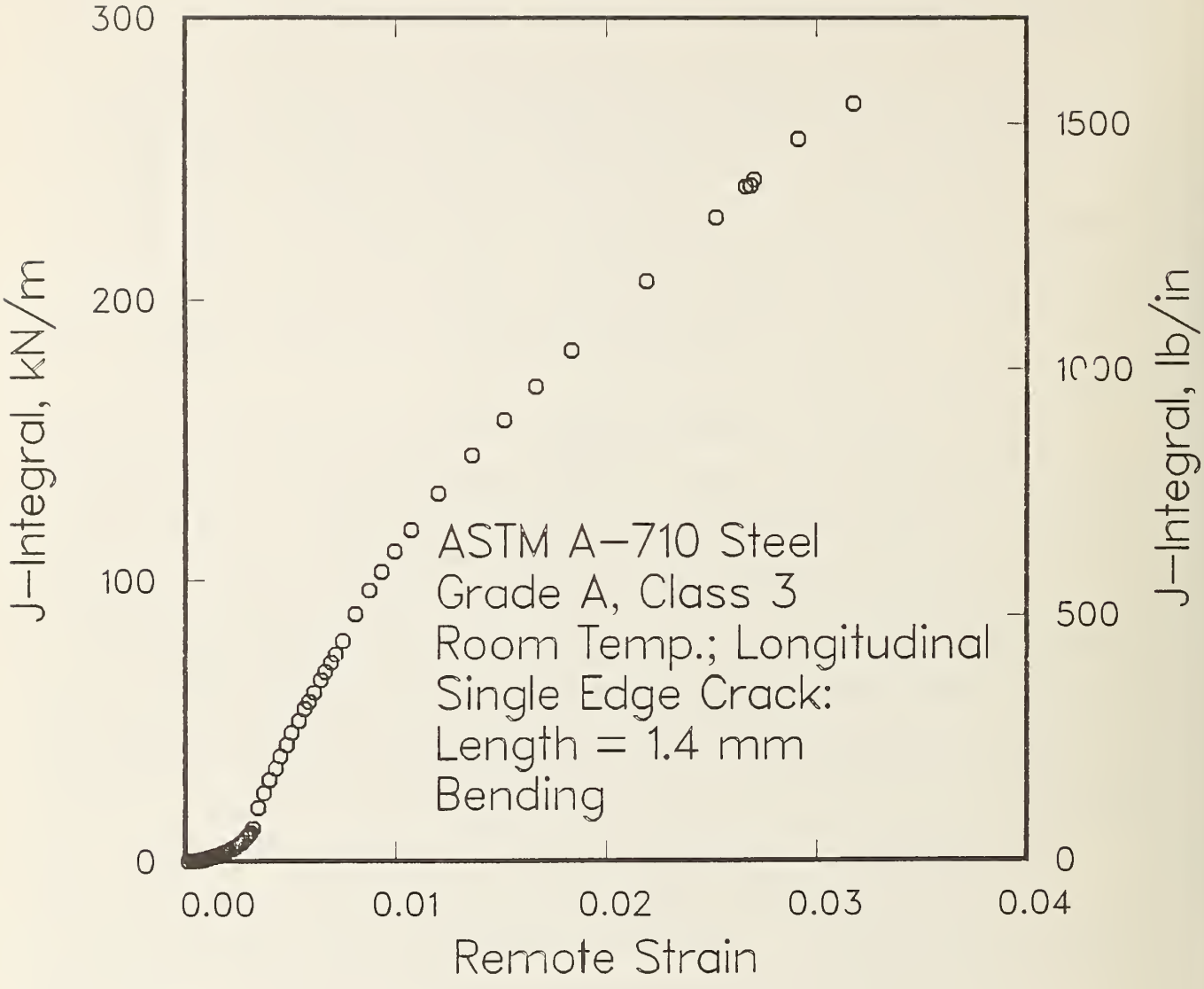

Figure 5. Experimentally measured J-integral as a function of applied strain for a four-point-bend specimen with crack length of 1.4 mm.

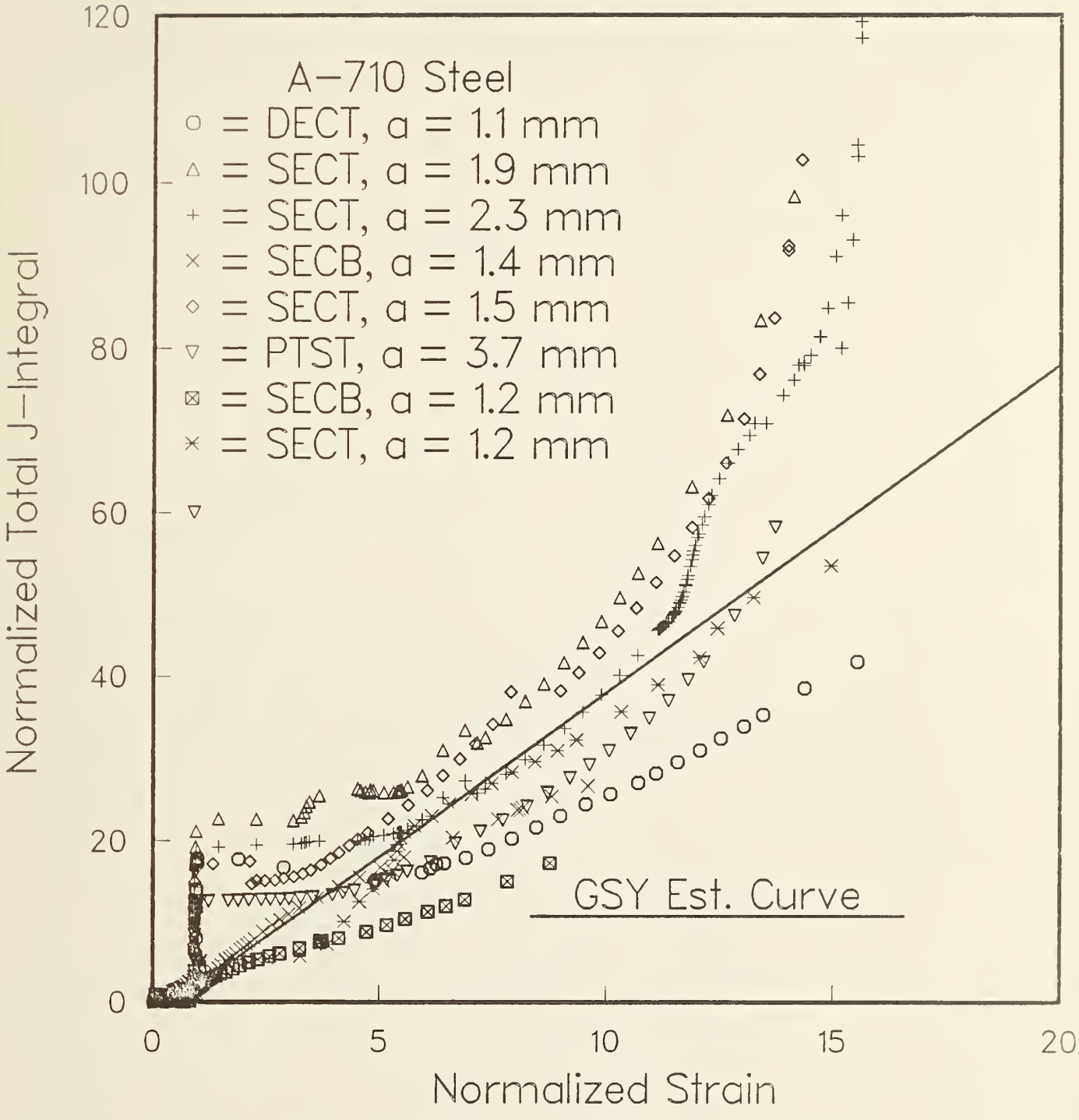

Figure 6. Experimentally measured total J-integral as a function of applied strain for the eight specimens of this study.

Lüders-type strains occurred in the bend tests; the measured J-integral values agree roughly with the Ramberg-Osgood curve shown in Figure 1. This agreement is believed to be accidental. The agreement with the previous experimental estimate confirms that behavior of the applied J-integral is the same for different specimen materials.

The results from the tensile specimens with unusual features, one with sawcut notches, one prestrained, and one tested −30°C, are indistinguishable from the rest in Figure 6. This is as expected for applied J-integral. The −30°C specimen had a low value of J_c, (Table 5); this is consistent with expectation.

The bend test results end at strains lower than the tensile test results because the specimens buckled after strains of several times yield and could not be strained further. At high strains on the order of 10 times yield, tearing initiated in the tensile tests, as shown by the unloading compliance data. Because of the buckling, the bend panels could not be strained enough to initiate tearing. Tearing produces the upturn in the J-integral data of Figure 6 at strains of about 10 times yield.

Figure 7 interprets the behavior of the J-integral as a function of strain for small cracks in tension and bending specimens. Both types have a parabolic region below yield. The tension specimens show a step-like increase near yield because of Lüders strain, while the J-integral in the bending specimens increases gradually. The tensile and bending results converge after the Lüders strain region ends, and both show gradual increases of J-integral with strain. At some J-integral level, tearing begins, increasing the rate of rise of J-integral with strain.

An attempt was made to correct the data of Figure 6 to reflect the behavior of flaws in infinitely wide plates. The correction procedure extracted only that part of the J-integral that resulted from gross section yielding. All net section yielding effects were excluded. The justification for this procedure is that through cracks in structures would be relatively much smaller than 1 to 3 percent of the structural element width; therefore net section yielding effects that may be present in these specimens would be absent in a real structure. The specific assumption used in the correction procedure was that contributions to the J-integral from strains on the specimen edge opposite the crack would not be present in a structural element with

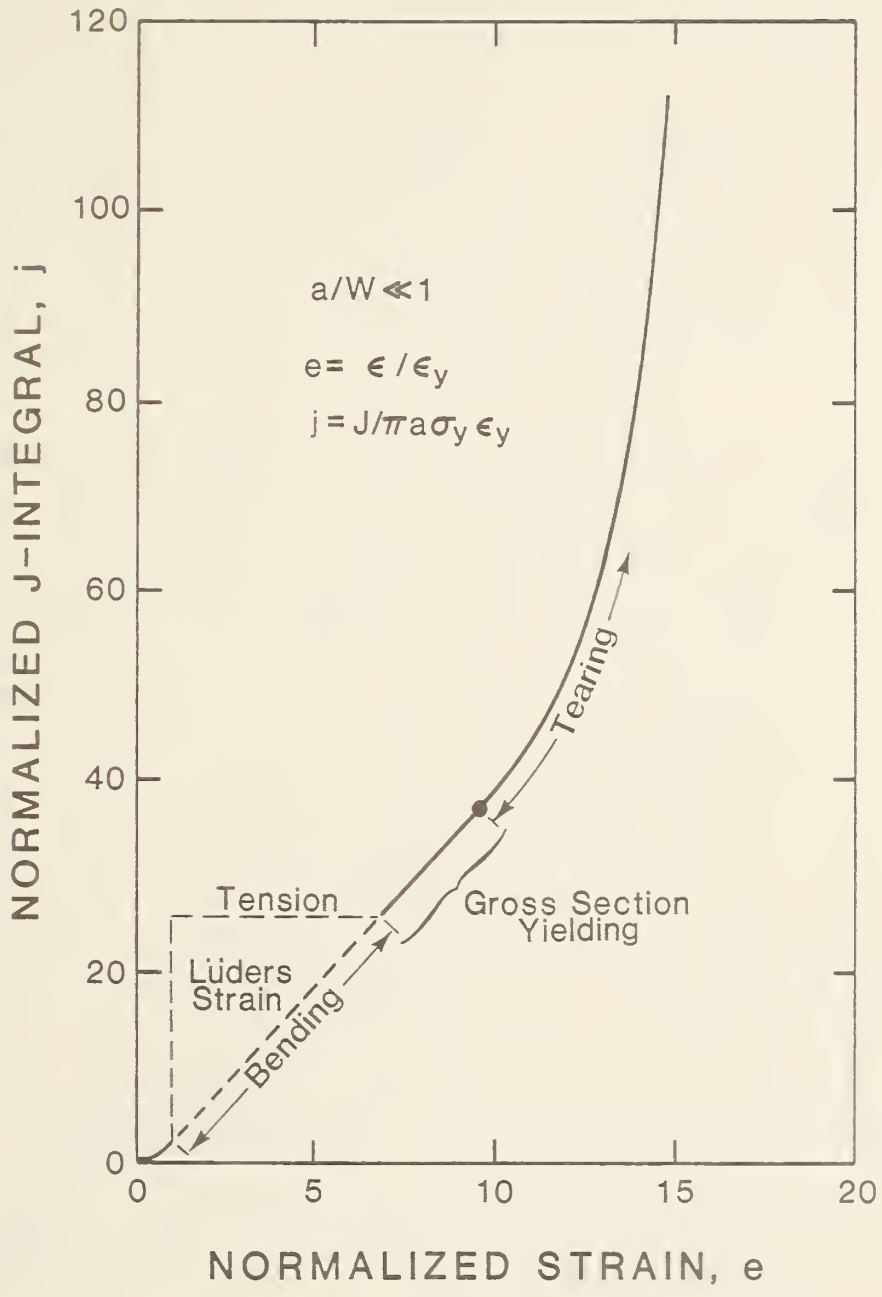

Figure 7. Schematic interpretation of the behavior of J-integral as a function of strain for small cracks in tensile and bending specimens.

a small crack. Therefore only the strain profile in the neighborhood of the crack mouth was considered in the calculation of the corrected J-integral. The strains on the specimen edge opposite the crack were assumed to be equal to the remote strain on the cracked edge. The J-integral values resulting from this correction were termed gross section yielding (GSY) J-integral values and are plotted in Figure 8. This plot, when compared to the total J-integral values of Figure 6, indicates that the GSY part was only about half the total J-integral value. Although data from a surface-cracked specimen are included in Figure 8, a more complex correction procedure is probably needed for this crack geometry because of the presence of ligament yielding.

It is the GSY J-integral values that are appropriate for comparison with the theoretical predictions discussed above for small cracks in infinite plates. The data are compared to the Wilson bilinear result in for interior cracks in plane stress Figure 8. This figure shows good agreement between experiment and theory. As a result of this comparison it is concluded that the relationship given by Wilson [10] for a bilinear material, which is similar to expressions given earlier by Begley, Landes, and Wilson [6] and by Merkle [7], is the correct expression of the dependence of J-integral on flaw size and applied strain for small through cracks in infinitely wide plates.

The J-integral values at the initiation of tearing in the tensile panels were considerably higher than those in the side-grooved three-point-bend fracture toughness specimens, as can be seen from a comparison of Table 3 and Table 5. The initiation J_c values in the tensile panels were slightly above those in the non-grooved, three-point-bend toughness specimens. The cause of this discrepancy is believed to be the low geometrical constraint in the shallow-cracked tensile and bending panels as compared to the deeply cracked three-point-bend fracture toughness specimens [18]. The effect of specimen geometry on crack tip strain fields has been pointed out by McMeeking and Parks [19]. The present results indicate that the use of toughness values from three-point-bend specimens for predictions of crack initiation in elements with small cracks is conservative and may be excessively conservative for certain cases.

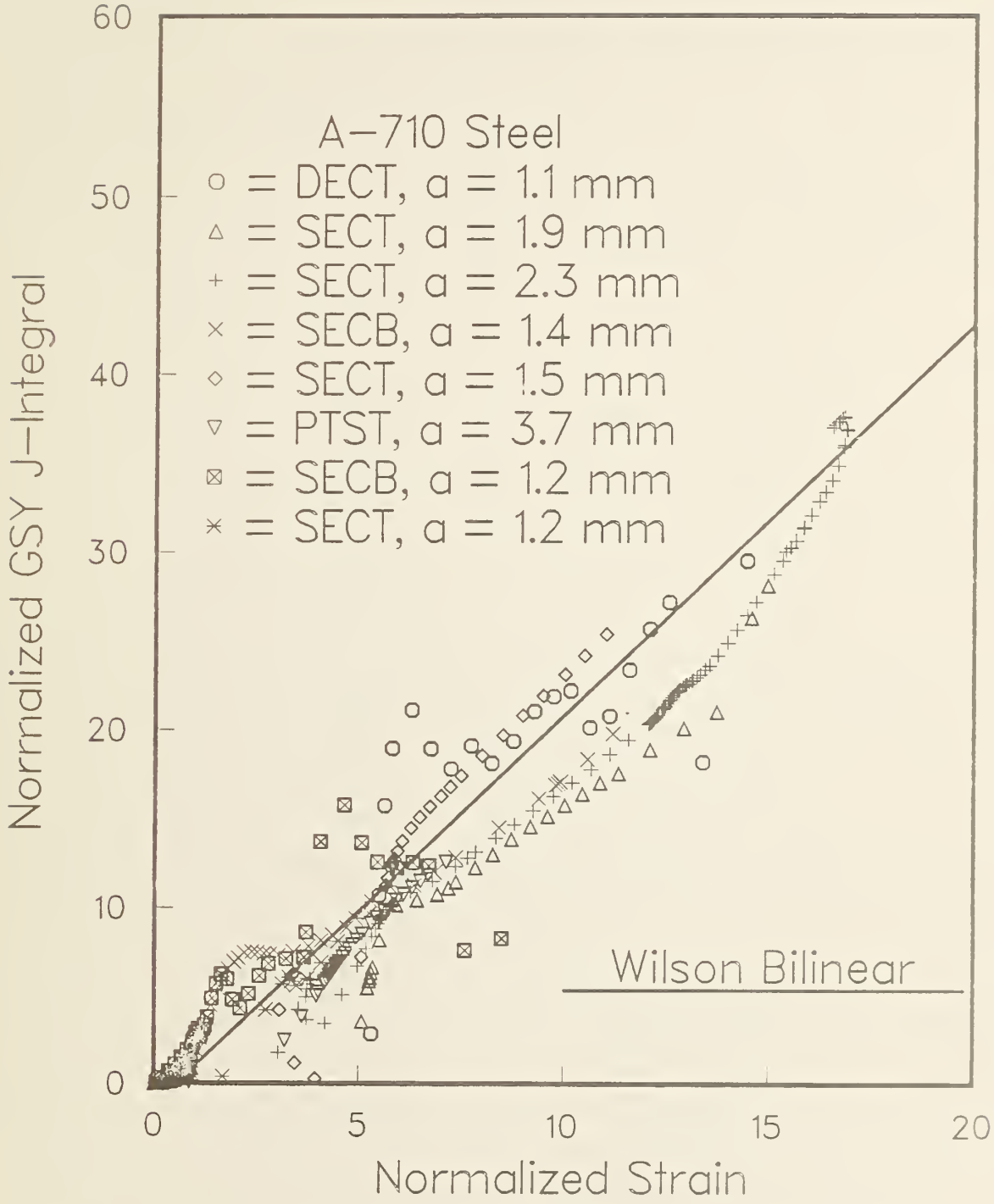

Figure 8. Data points: experimentally measured J-integral values corrected to eliminate all except the gross section yielding contribution; solid curve: theoretical prediction made using Wilson's equations for a bilinear material.

TABLE 5-Toughness and tearing resistance, in terms of the J-integral, of tensile and bend specimens with short cracks.

Tensile and bending panel tests

Specimen Type	Orientation	Side-Grooves ?	a/W	J_c, initiation	T_{mat}
DECT (saw-cut cracks)	LT	no	0.014	NA	NA
SECT	LT	no	0.023	438	400
SECT (prestrained)	LT	no	0.028	NA	66
SECB	LT	no	0.017	NA	NA
SECT	TL	no	0.018	338	319
PTST	TL	no	0.036	382	187
SECB	TL	no	0.015	NA	NA
SECT*	TL	no	0.014	225	119

*-30°C

DECT = Double-edge-cracked tensile

SECT = Single-edge-cracked tensile

SECB = Single-edge-cracked bend

PTST = Part-through-surface tensile

LT = Longitudinal orientation

TL = Transverse orientation

NA = Not available

4.7 Conclusions

Experimental results on direct measurement of the J-integral in alloy steel panels with small relative crack sizes loaded in tension and bending allow the following conclusions to be drawn:

1. Loading in bending suppresses Lüders band effects that influence J-integral values measured on ASTM A-710 Grade A Class 3 alloy steel specimens loaded in tension.
2. When remote strain in tension is equated with remote outer fiber strain in bending, the behavior of the J-integral as a function of remote strain for panels containing small cracks is the same in bending as in tension, except for the step associated with Lüders strains in the tensile results. Comparisons of tensile results for two alloys, including a result at −30°C and results for transverse- and longitudinal-oriented specimens, confirm the theoretically predicted commonality of behavior of the normalized J-integral for specimens with small relative crack sizes.
3. The total J-integral measured in panels with relative crack sizes of 1 to 3 percent followed roughly a theoretical prediction made using formulas given by Wilson [10] for a Ramberg-Osgood material in plane stress, however this agreement is believed to be accidental.
4. Correction of the J-integral results to include only the gross-section-yielding contribution reduced the J-integral values by about a factor of 2. The corrected values agreed approximately with predictions made using formulas given by Wilson [10] for a bilinear material in plane stress. The corrected J-integral values are believed to be more accurate than the uncorrected values for cracks in infinite panels.
5. The toughness and tearing resistance, as measured by the J-integral, of panels with small relative crack sizes were found to be significantly higher than the toughness and tearing resistance of side-grooved standard three-point-bend test specimens, and slightly higher than values for non-side-grooved specimens.

4.8 Acknowledgments

This work was supported by the Naval Sea Systems Command under project SEA 05 R 25, and monitored by J. P. Gudas of the David Taylor Naval Ship Research and Development Center, Annapolis, Maryland. The experimental assistance of J. D. McColskey and helpful discussions with H. I. McHenry and J. P. Gudas are appreciated.

4.9 References

[1] Read, D. T., "Experimental Method for Direct Evaluation of the J-Contour Integral," Fracture Mechanics: Fourteenth Symposium--Volume II: Testing and Applications, ASTM STP 791, J. C. Lewis and G. Sines, Eds., American Society for Testing and Materials, 1983, pp. II-199-II-213.

[2] Rice, J. R., "A Path Independent Integral and the Approximate Analysis of Strain Concentrations by Notches and Cracks," Journal of Applied Mechanics, Vol. 35, No., June 1968, pp. 379-386.

[3] Hutchinson, J. W., "Singular Behavior at the End of a Tensile Crack in a Hardening Material," Journal of the Mechanics and Physics of Solids, Vol. 16, No., 1968, pp. 13-31.

[4] Rice, J. R. and Rosengren, G. F.,"Plane Strain Deformation Near a Crack Tip in a Power-Law Hardening Material," Journal of the Mechanics and Physics of Solids, Vol. 16, No. , 1968, pp. 1-12.

[5] Ernst, H. A., "Material Resistance and Instability Beyond J-Controlled Crack Growth," Elastic-Plastic Fracture: Second Symposium, Volume I--In Elastic Crack Analysis, ASTM STP 803, C. F. Shih and J. P. Gudas, Eds., American Society for Testing and Materials, 1983, pp. I-191-I-213.

[6] Begely, J. A., Landes, J. D., and Wilson, W. K., "An Estimation Model for the Application of the J-Integral," Fracture Analysis, ASTM STP 560, American Society for Testing and Materials, 1974, pp. 155-169.

[7] Merkle, J. G., "Analytical Relations Between Elastic-Plastic Fracture Criteria," Technical Report ORNL/NUREG/TM-27, Oak Ridge National Laboratory, Oak Ridge, Tennessee, 1976.

[8] Turner, C. E., "Elastic-plastic aspects of fracture stress analysis: methods for other than standardized test conditions, in Fracture

Mechanics in Design and Service, Philosophical Transactions of the Rural Society of London, Vol. A299, 1981, pp. 73-92.

[9] Dawes, M. G., "Welding Journal Research Supplement, Vol. 53, 1974, pp. 369s-379s.

[10] Wilson, W. K., "J-Integral Estimate for Small Edge and Interior Cracks," Engineering Fracture Mechanics, Vol. 20, No. 4, 1984, pp. 655-665.

[11] Shih, C. F., German, M. D., and Kumar, V., "An Engineering Approach for Examining Crack Growth and Stability in Flawed Structures," Technical Report SRD-80-94, General Electric Company, Schenectady, New York, 1980, pp. A1-A47.

[12] He, M. Y. and Hutchinson, J. W., "Bounds for Fully Plastic Crack Problems for Infinite Bodies," Elastic-Plastic Fracture," Volume I--Inelastic Crack Analysis, ASTM STP 803, C. F. Shih and J. P. Gudas, Eds., American Society for Testing and Materials, 1083, pp. I-277-I-290.

[13] Read, D. T. and McHenry, H. I., "Interim Progress Report: J-Integral Method for Fitness-for-Service Assessment," Technical Report NBSIR 81-1648, National Bureau of Standards, Boulder, Colorado, May 1981.

[14] Read, D. T., "Applied J-Integral in HY130 Tensile Panels and Implications for Fitness for Service Assessment," Technical Report NBSIR 82-1670, National Bureau of Standards, Boulder, Colorado, July, 1982.

[15] Read, D. T., "Experimental Results for Fitness-for-Service Assessment of HY130 Weldments," Technical Report NBSIR 84-1699, National Bureau of Standards, Boulder, Colorado, March, 1984.

[16] Fields, R. J., private communication.

[17] Appendix of this section.

[18] Li, Q.-F., "A Study About Ji and detail in Three-Point Bend Specimens with Deep and Shallow Notches," Engineering Fracture Mechanics Vol. 22, No. 1, 1985, pp. 9-15.

[19] McMeeking, R. M. and Parks, D. M., "On Criteria for J-Dominance of Crack-Tip Fields in Large-Scale Yielding," Elastic-Plastic Fracture, ASTM STP 668, J. D. Landes, J. A. Begley, and G. A. Clarke, Eds., American Society for Testing and Materials, 1979, pp. 175-194.

4.10 Appendix.

AUXILIARY RESULTS FROM DIRECT MEASUREMENT OF APPLIED J-INTEGRAL IN ASTM A-710 STEEL PANELS

Results on the complex relationships among remote strain, gauge length strain, stress, crack mouth opening displacement, and J-integral are given in this Appendix. Also included are typical measured strain distributions at three stages of tension and bend tests. These results were obtained as part of the direct measurement of the applied J-integral. They are included here because they are useful in understanding the behavior of the applied J-integral.

Figure A1a-g. Dependence of J-integral, stress, and crack mouth opening displacement on strain for double-edge-notched tensile panel with crack length of 1.1 mm.

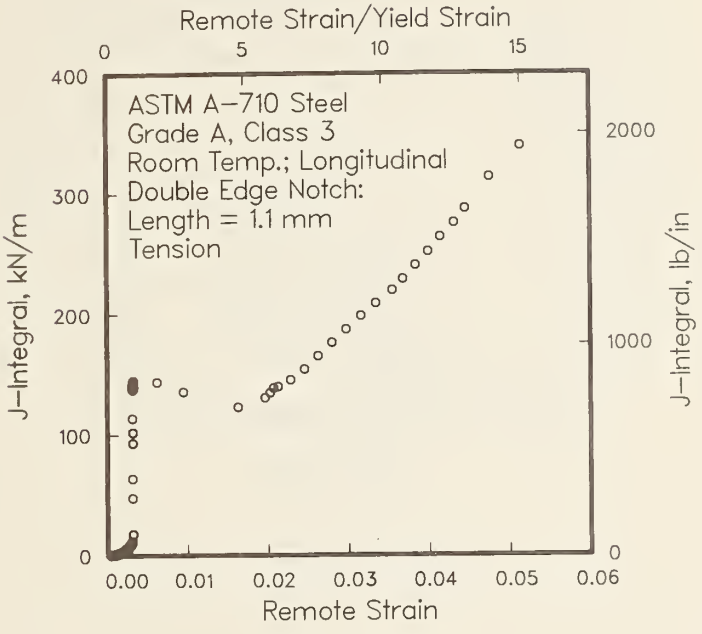

Figure A1a.

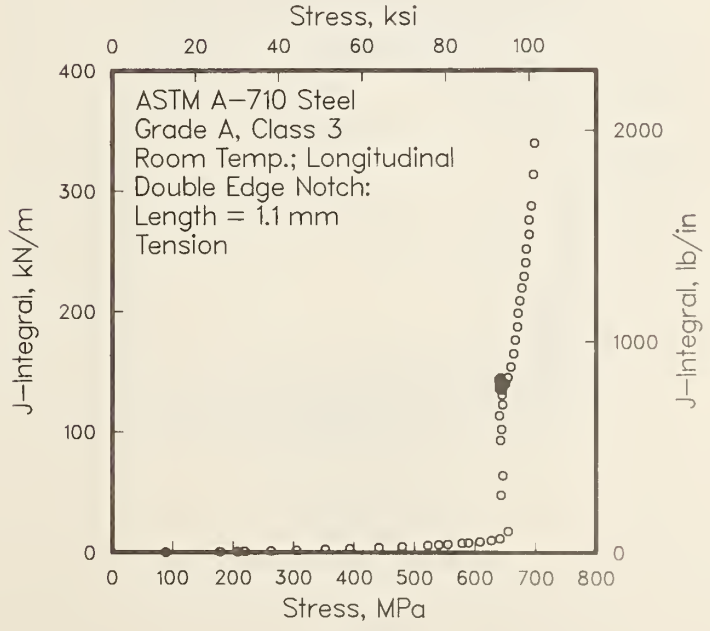

Figure A1b.

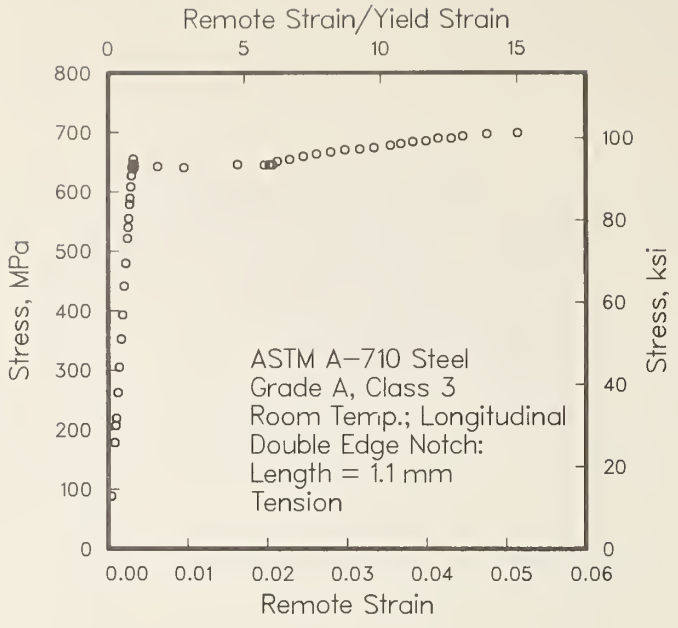

Figure A1c.

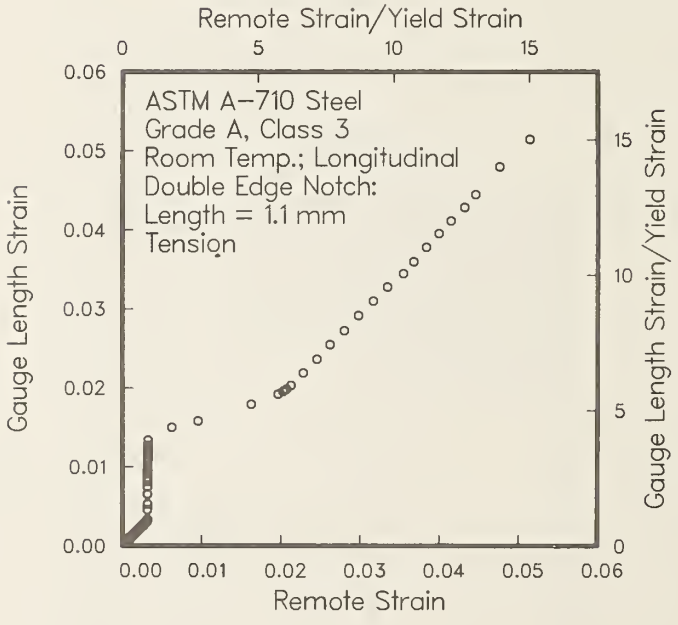

Figure A1d.

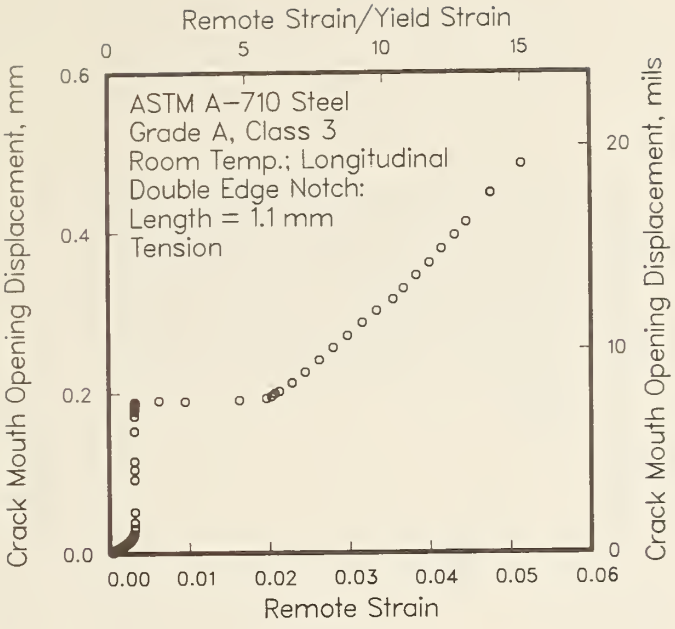

Figure A1e.

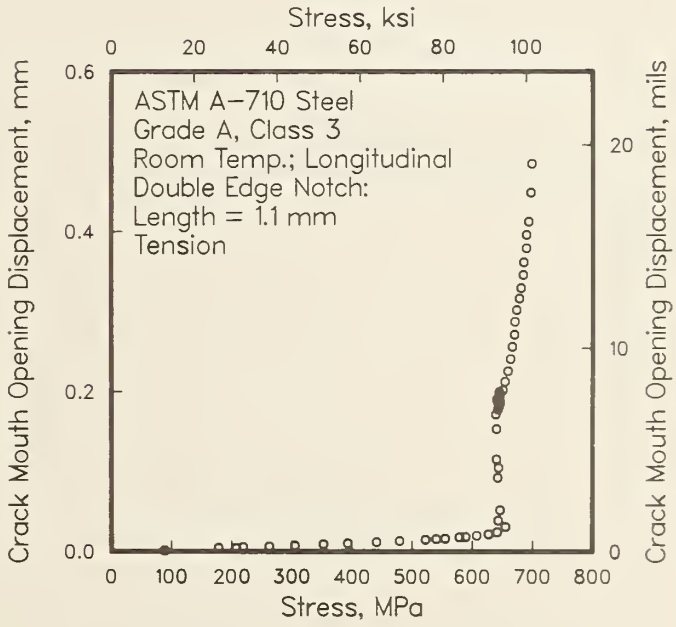

Figure A1f.

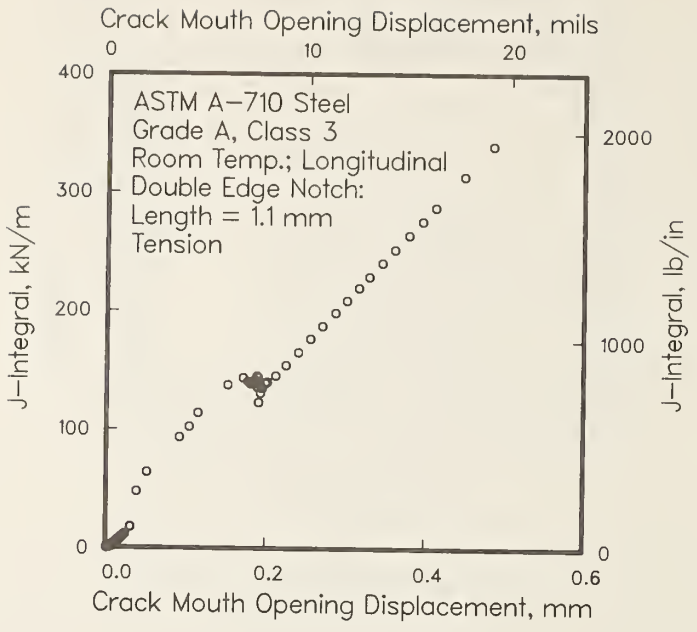
Crack Mouth Opening Displacement, mils
0
10
20
ASTM A-710 Steel
Grade A, Class 3
Room Temp.; Longitudinal
Double Edge Notch:
Length = 1.1 mm
Tension
J-Integral, kN/m
400
300
200
100
0
J-Integral, lb/in
2000
1000
0
0.0
0.2
0.4
0.6
Crack Mouth Opening Displacement, mm

Figure A1g.

Figure A2a-h. Dependence of J-integral, stress, and crack mouth opening displacement on strain, and J-R curve, for single-cracked longitudinal tensile panel at room temperature crack length of 1.9 mm.

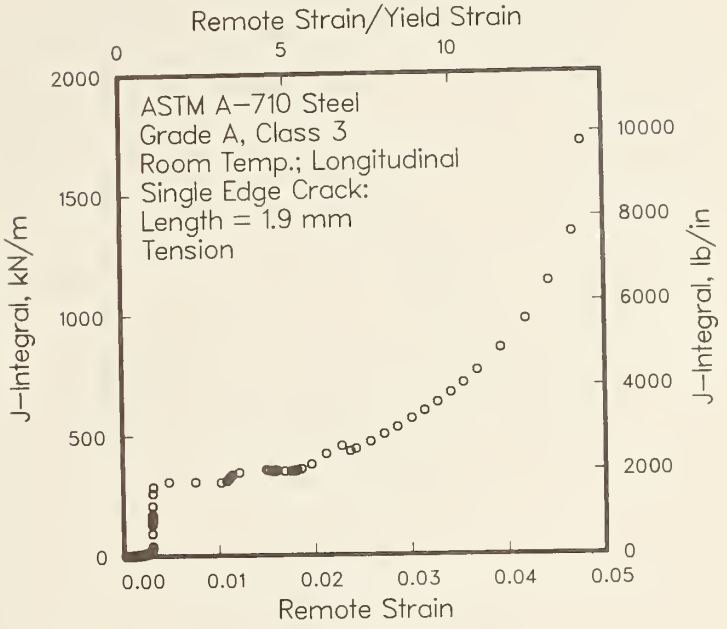

Figure A2a.

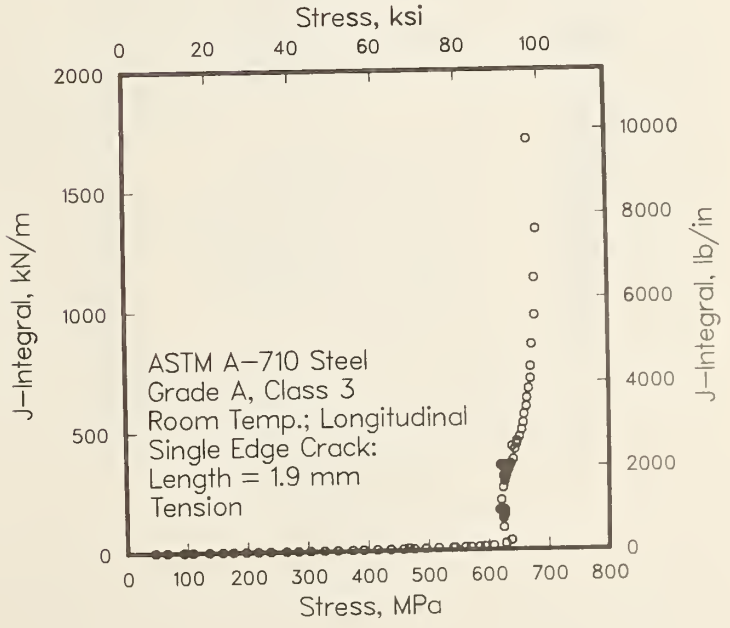

Figure A2b.

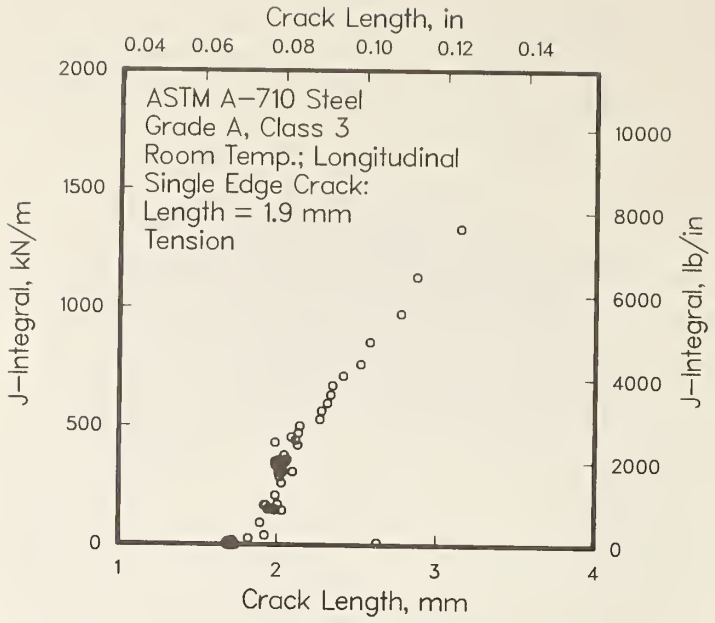

Figure A2c.

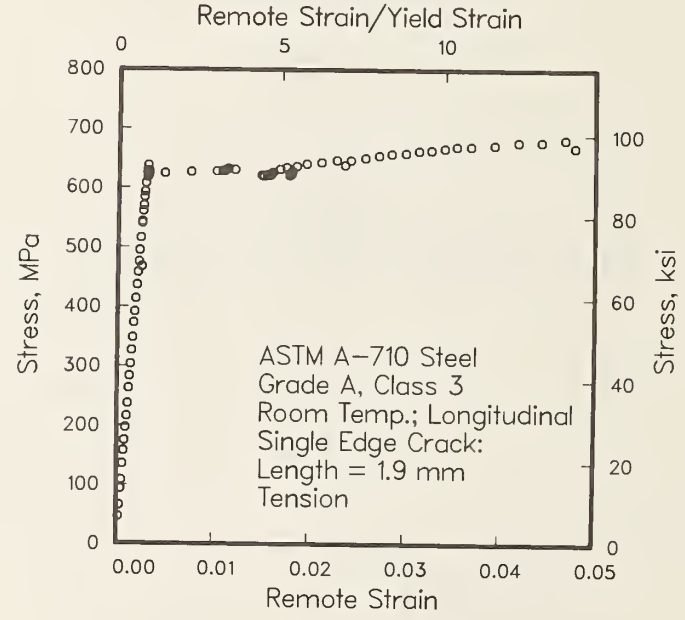

Figure A2d.

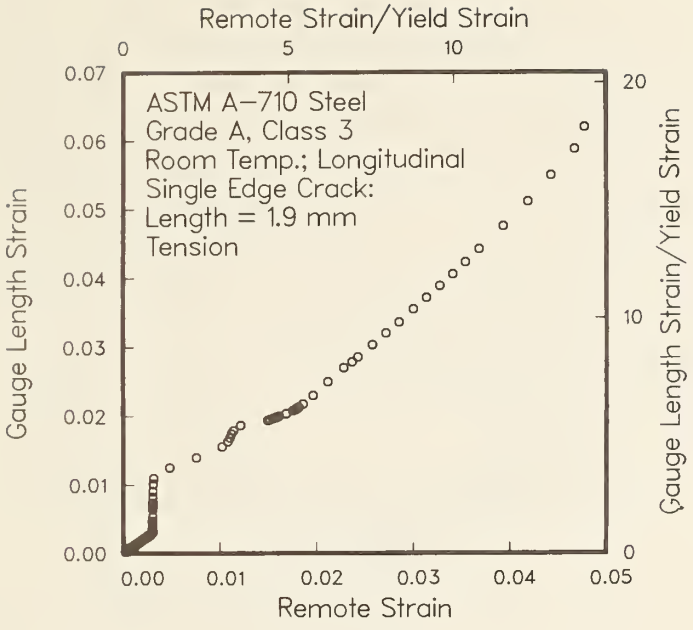

Figure A2e.

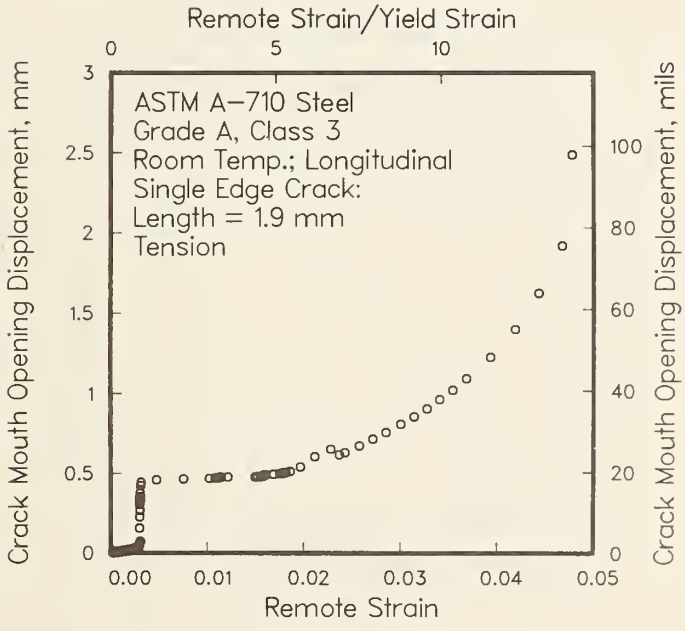

Figure A2f.

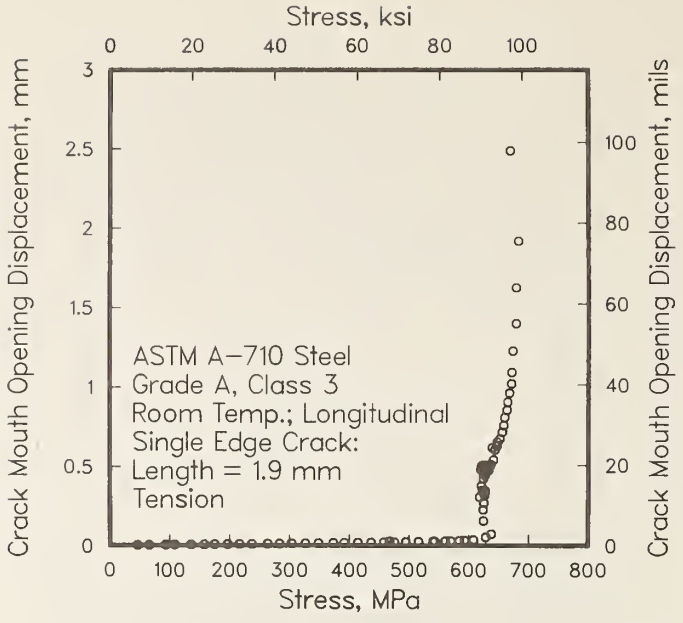

Figure A2g.

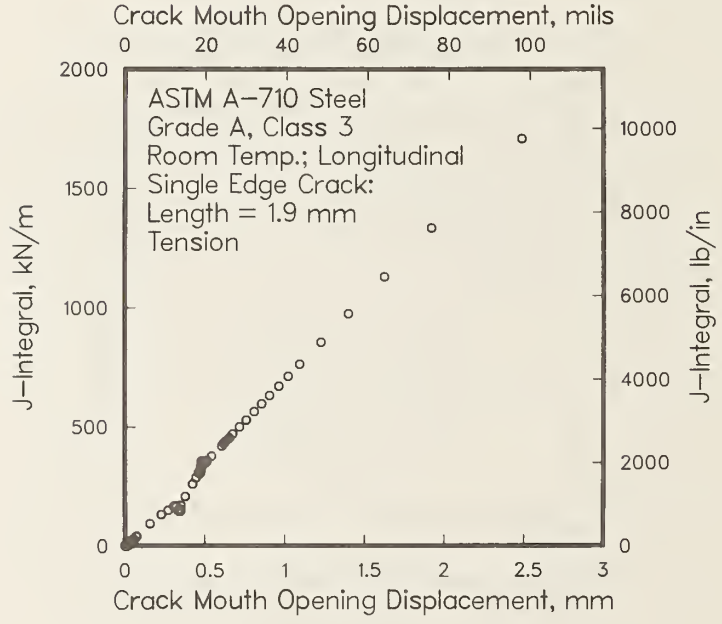

Figure A2h.

Figure A3a-h. Dependence of J-integral, stress, and crack mouth opening displacement on strain, and J-R curve, for pre-strained single-edge-cracked longitudinal tensile panel at room temperature with crack length 2.3 mm.

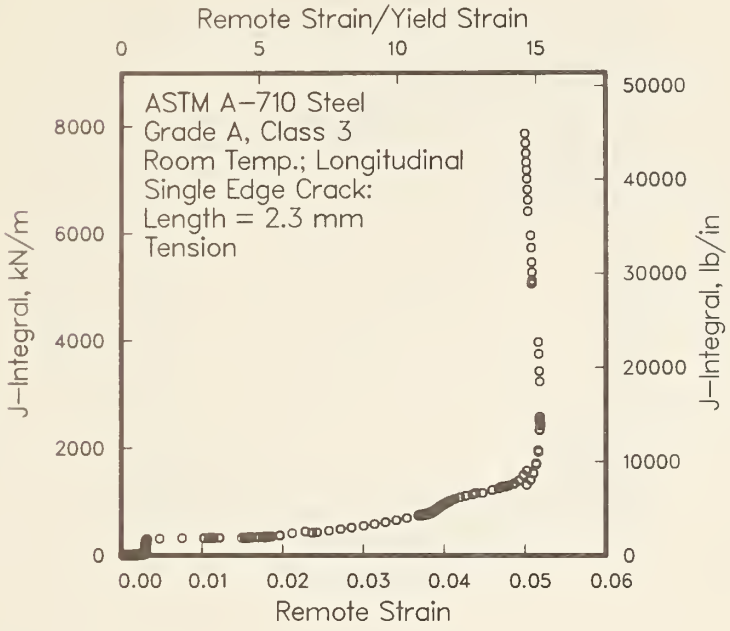

Figure A3a.

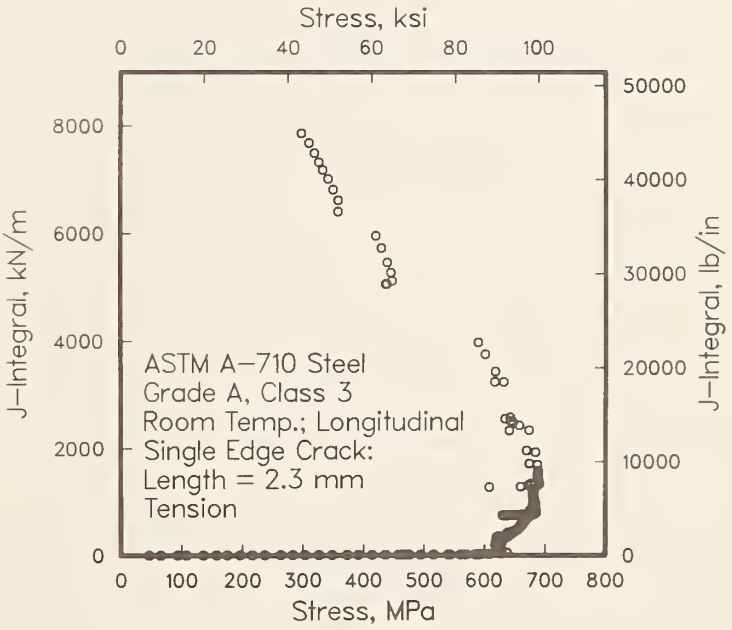

Figure A3b.

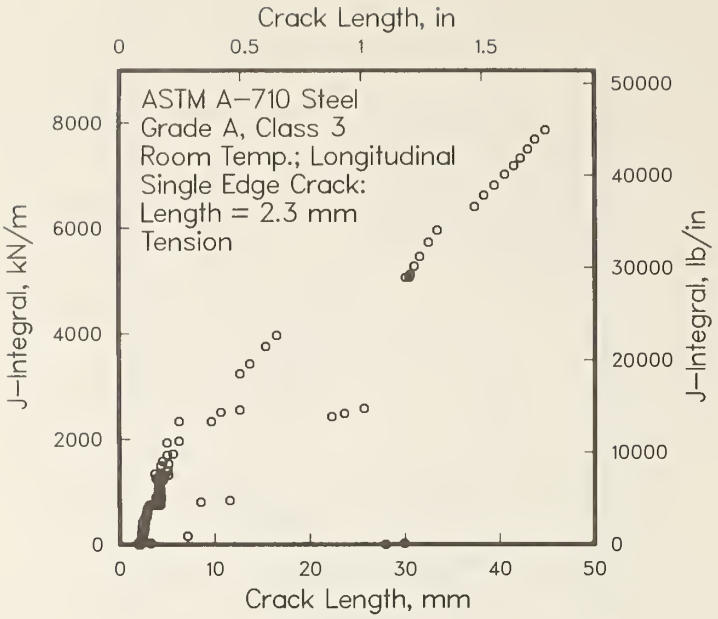

Figure A3c.

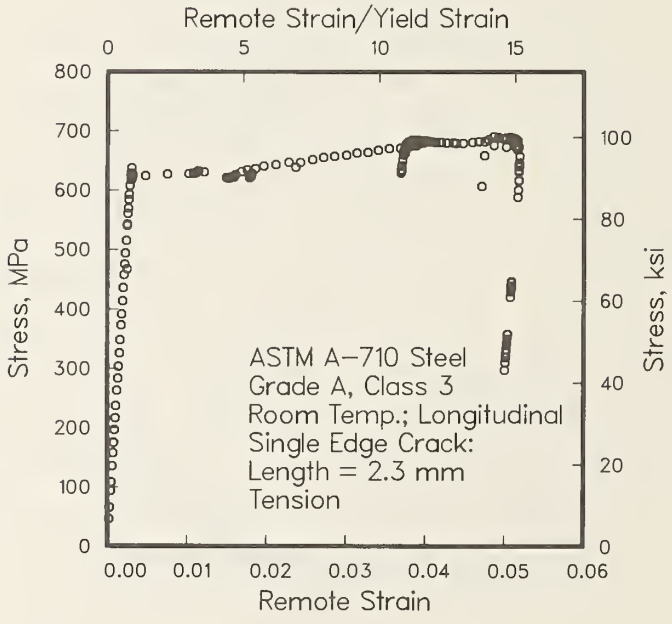

Figure A3d.

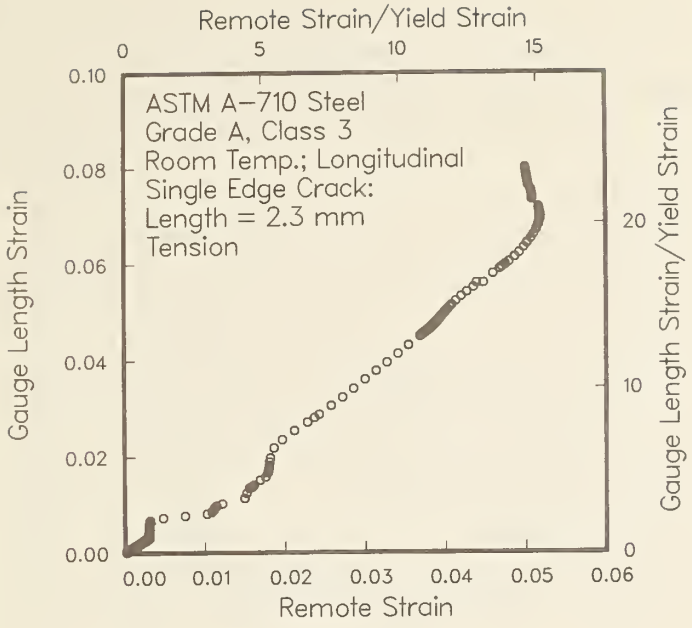

Figure A3e.

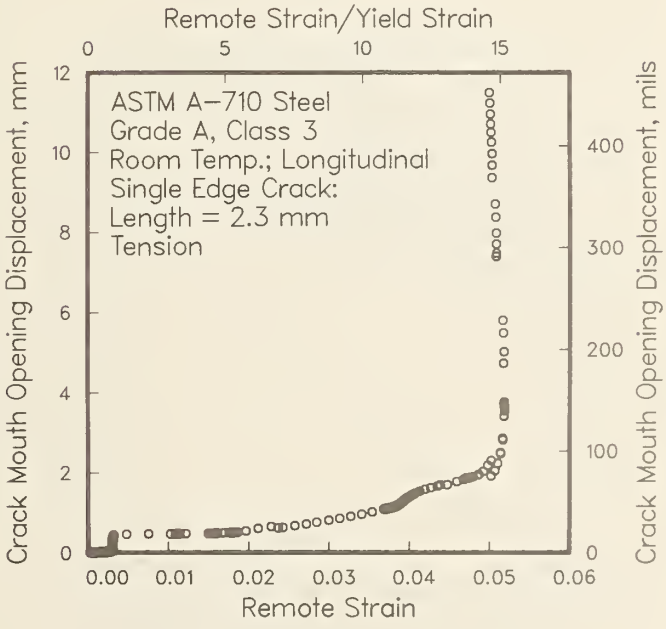

Figure A3f.

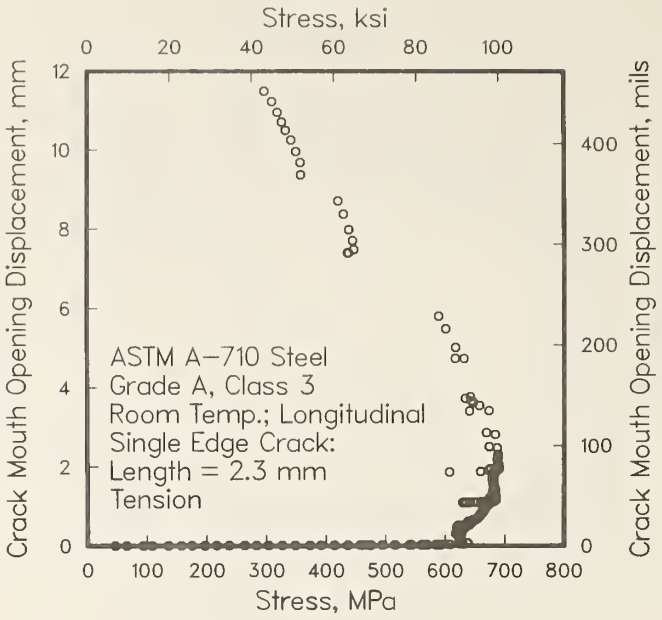

Figure A3g.

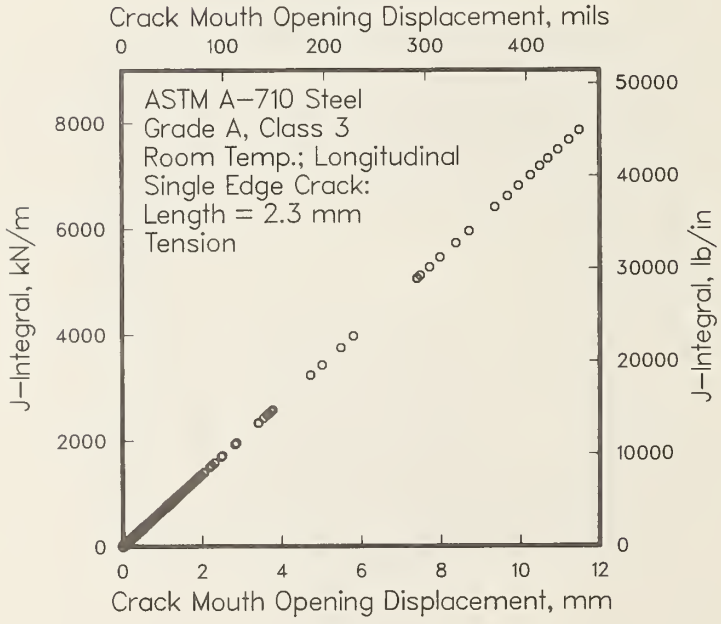

Figure A3h.

Figure A4a-g. Dependence of J-integral, stress, and crack mouth displacement on strain, and J-R curves, for single cracked longitudinal bending panel at room tempera crack length 1.4 mm.

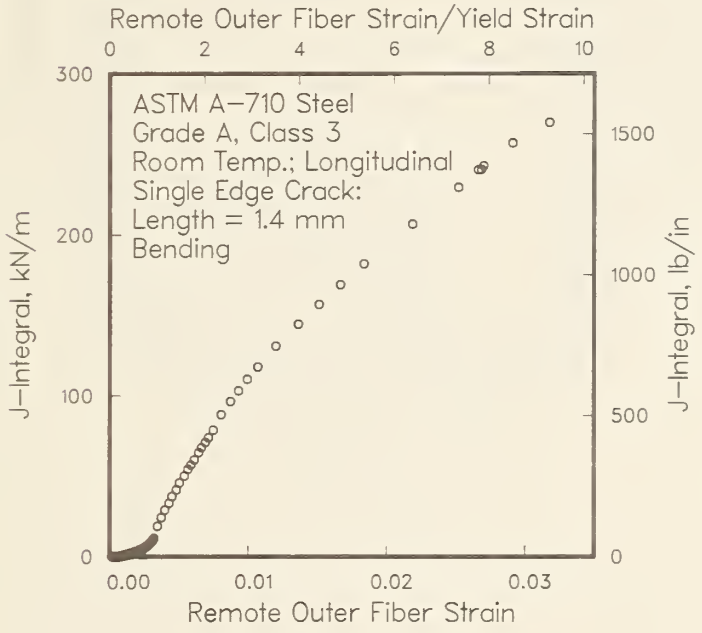

Figure A4a.

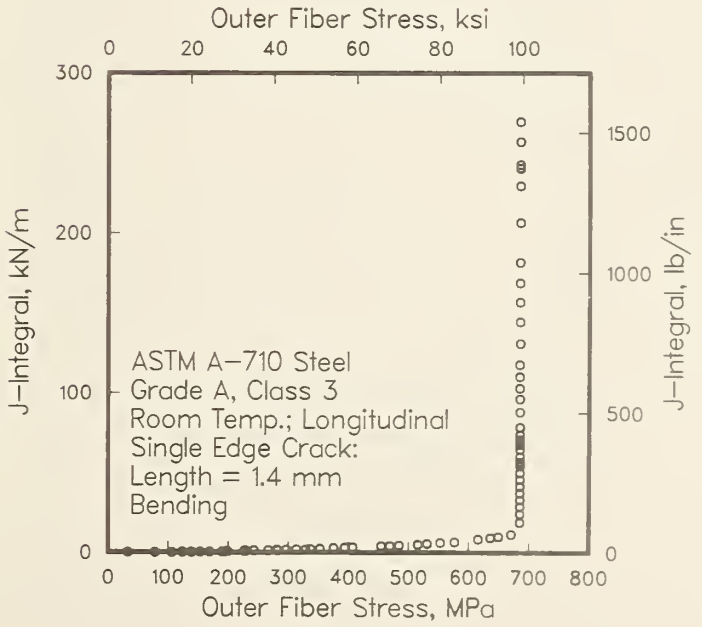

Figure A4b.

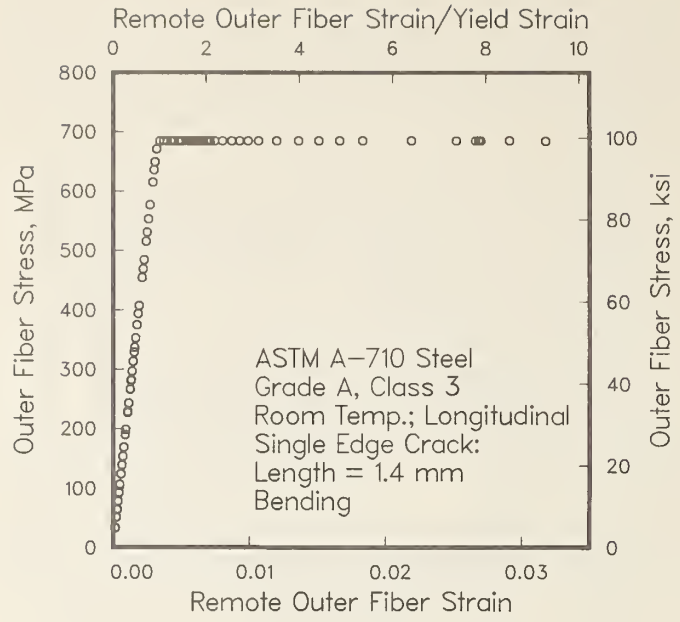

Figure A4c.

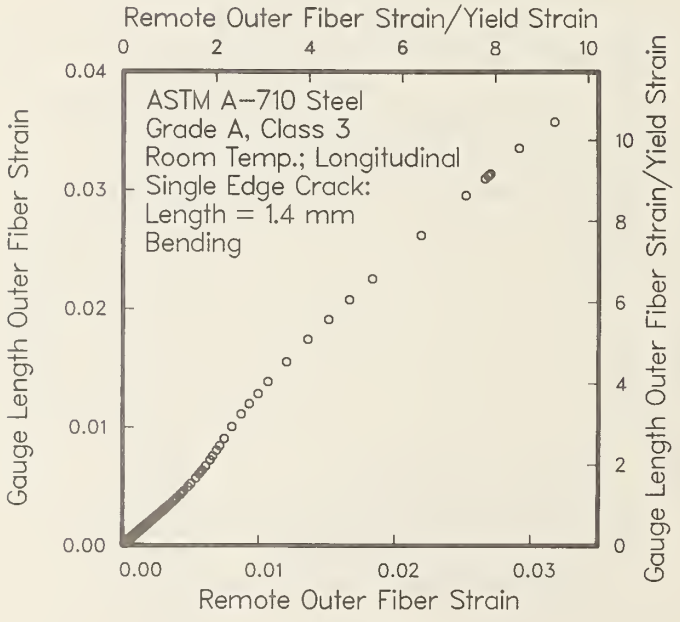

Figure A4d.

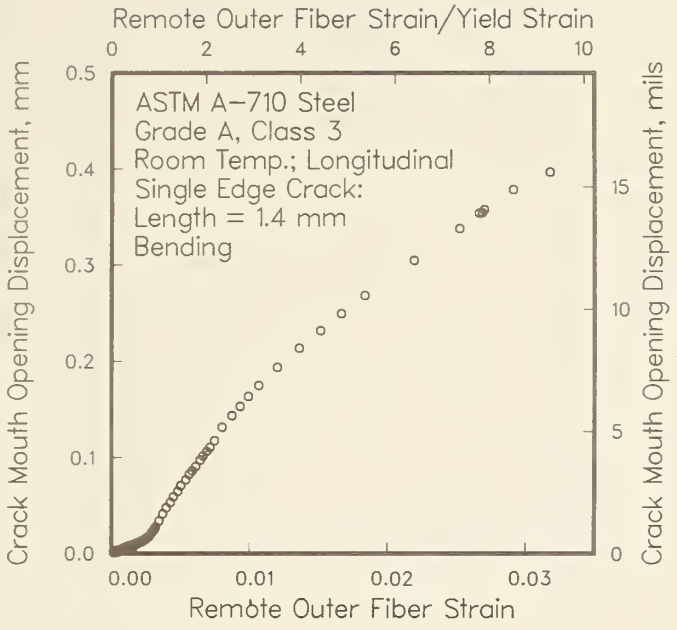

Figure A4e.

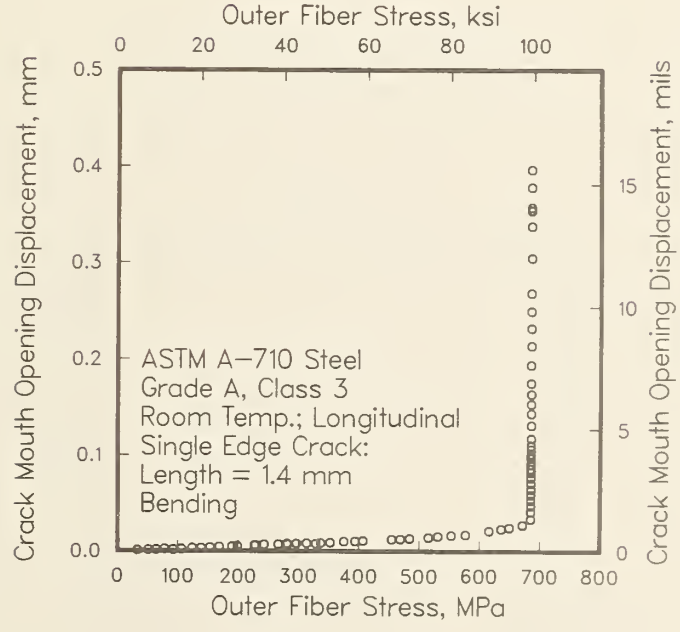

Figure A4f.

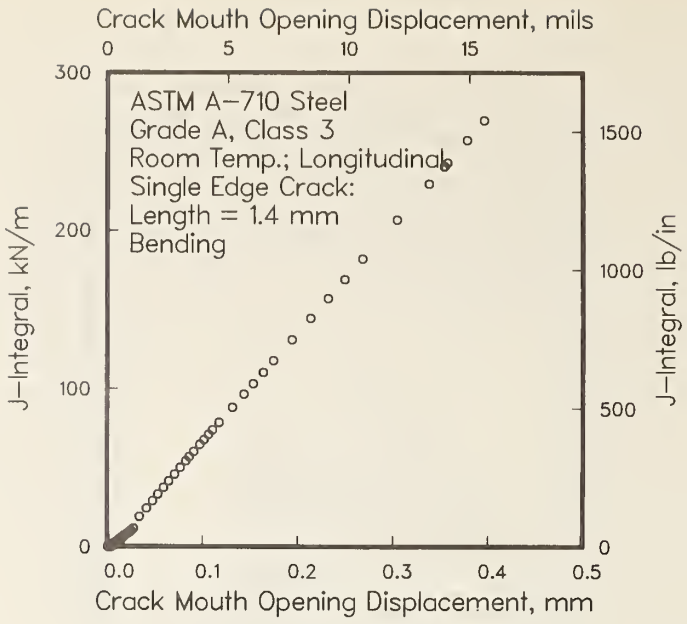
Crack Mouth Opening Displacement, mils
0
5
10
15
300
200
100
0
ASTM A-710 Steel
Grade A, Class 3
Room Temp.; Longitudinal
Single Edge Crack:
Length = 1.4 mm
Bending
J-Integral, kN/m
1500
1000
500
0
J-Integral, lb/in
0.0
0.1
0.2
0.3
0.4
0.5
Crack Mouth Opening Displacement, mm

Figure A4g.

Figure A5a-h. Dependence of J-integral, stress, and crack mouth opening displacement on strain, and J-R curve for single-edge-crack transverse tensile panel at room temperature with crack length 1.5 mm.

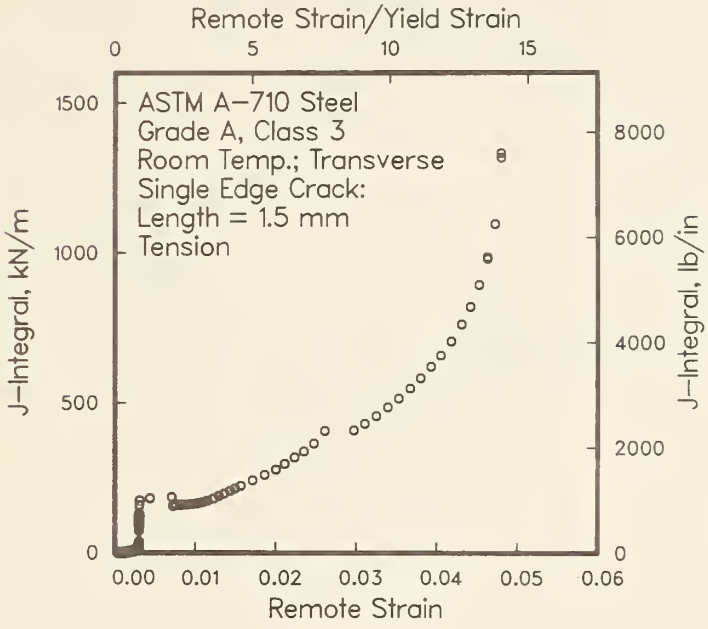

Figure A5a.

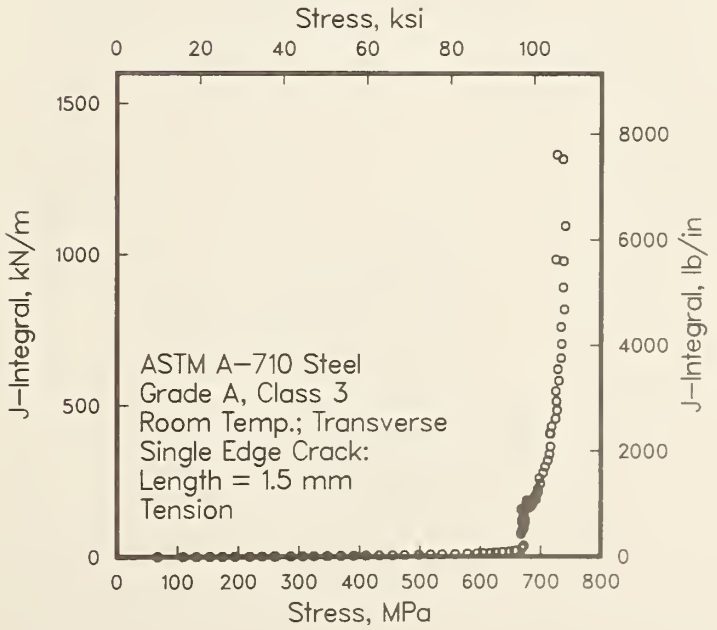

Figure A5b.

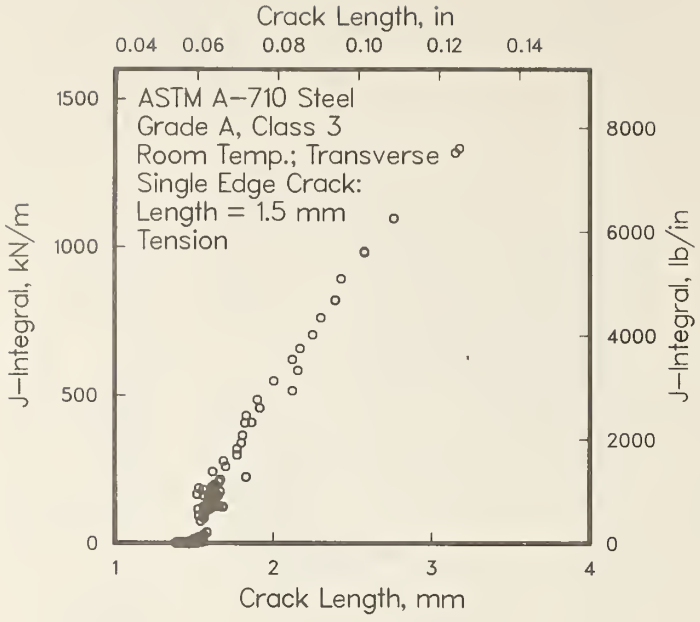

Figure A5c.

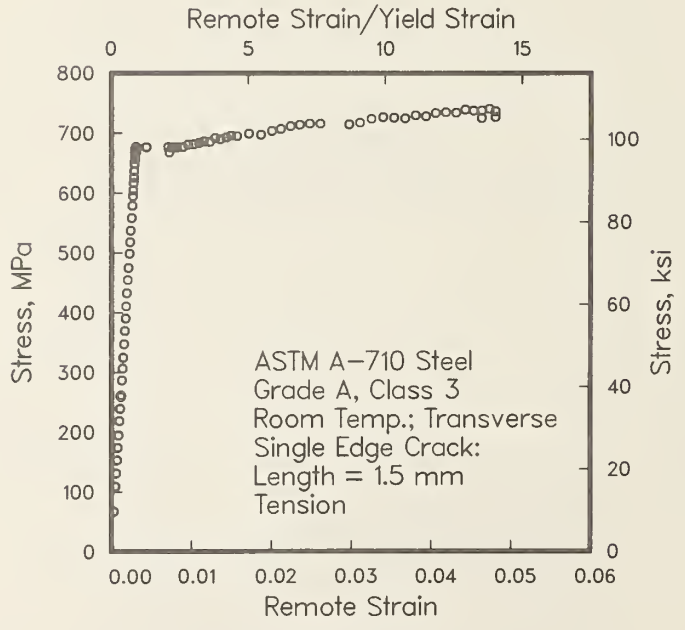

Figure A5d.

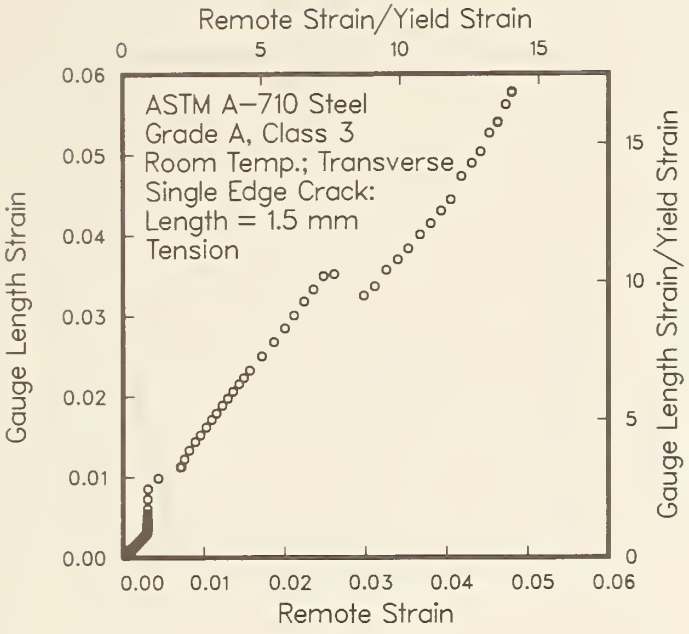

Figure A5e.

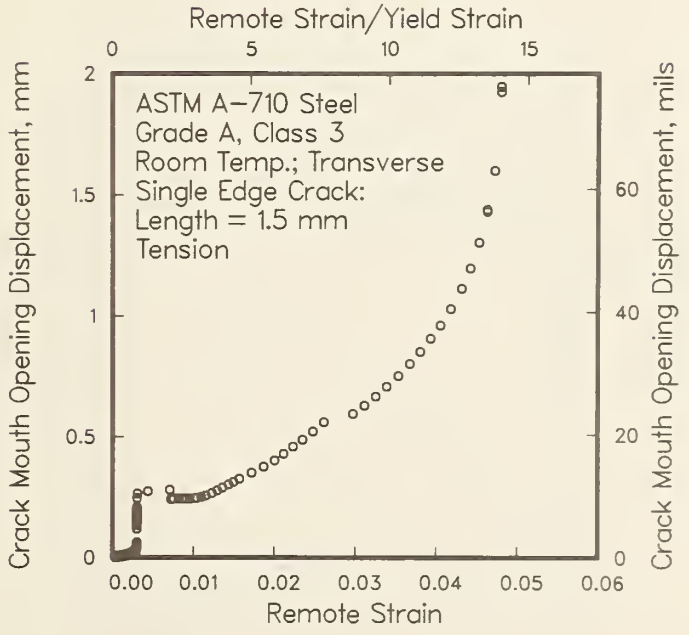

Figure A5f.

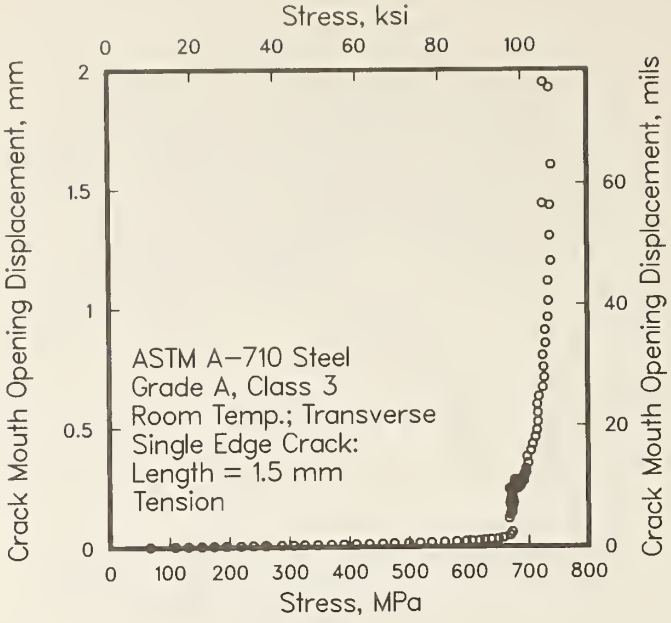

Figure A5g.

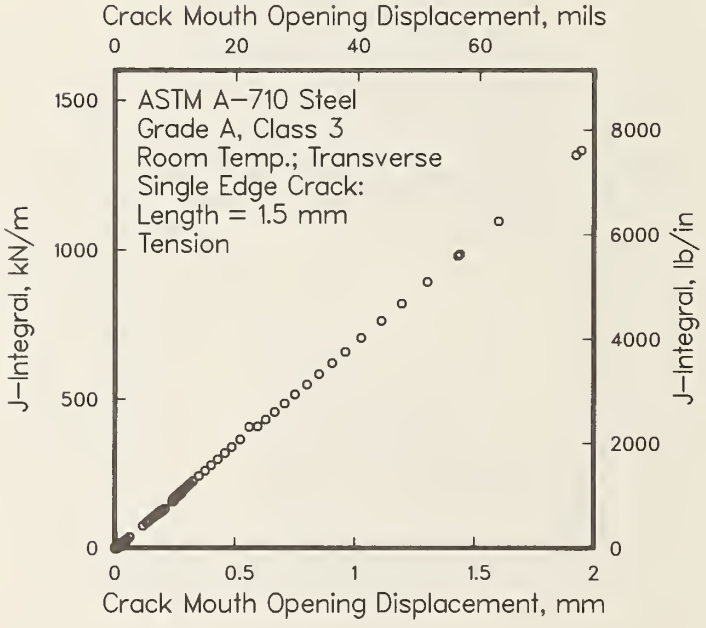

Figure A5h.

Figure A6a-h. Dependence of J-integral, stress, and crack mouth opening displacement on strain, and J-R curve, for part-through-surface-cracked transverse tensile panel at room temperature, with crack depth 3.9 mm and total crack length 13.3 mm.

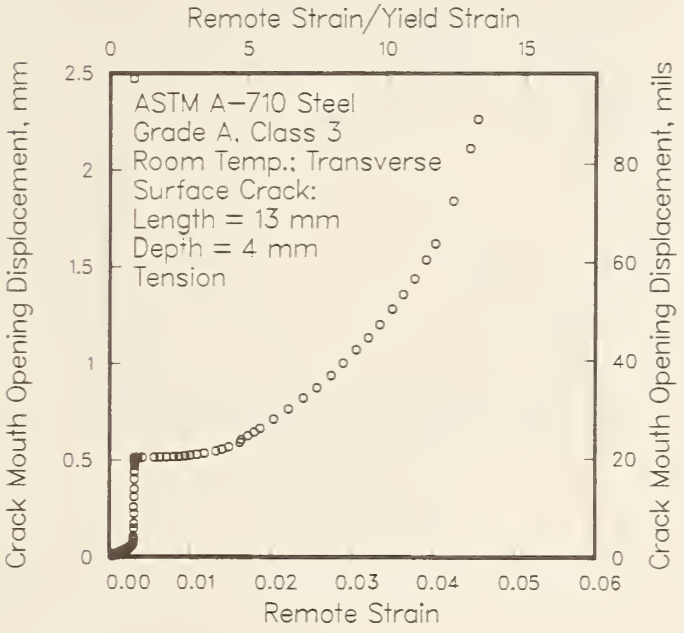

Figure A6a.

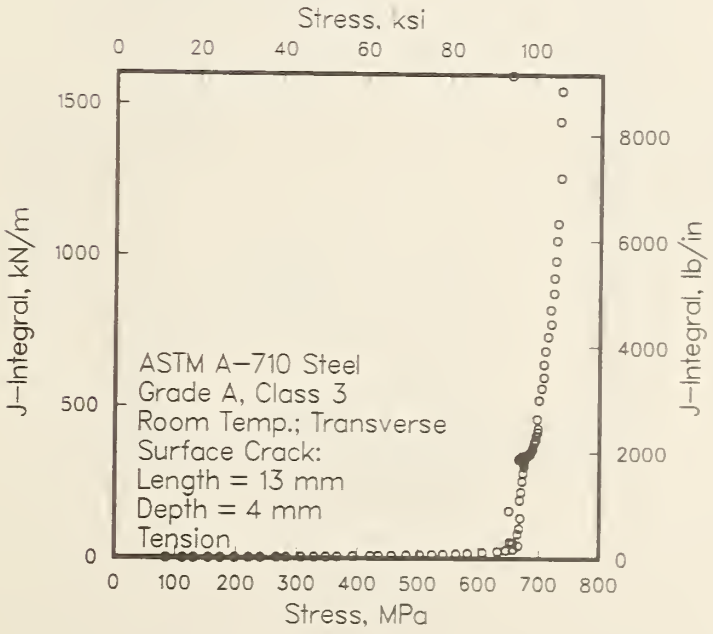

Figure A6b.

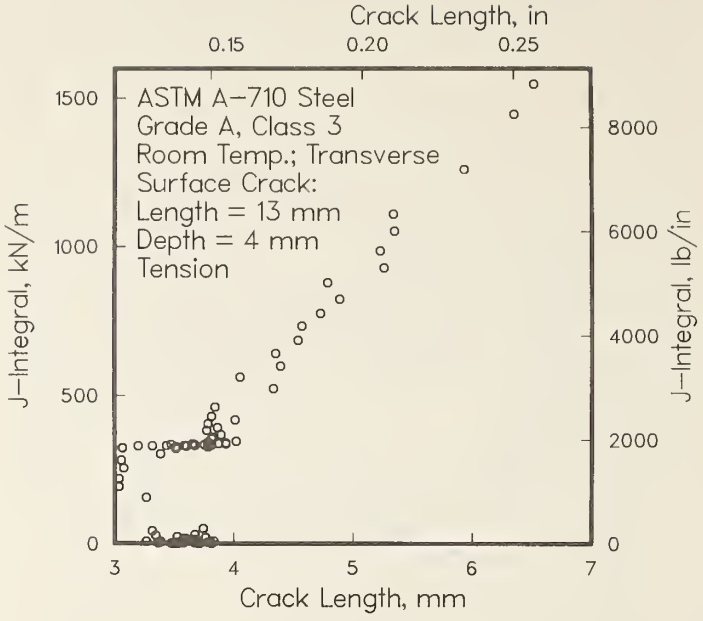

Figure A6c.

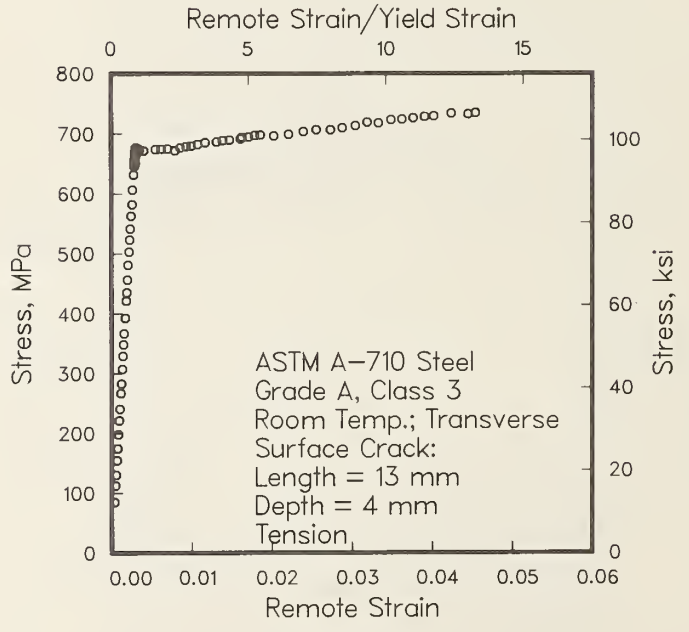

Figure A6d.

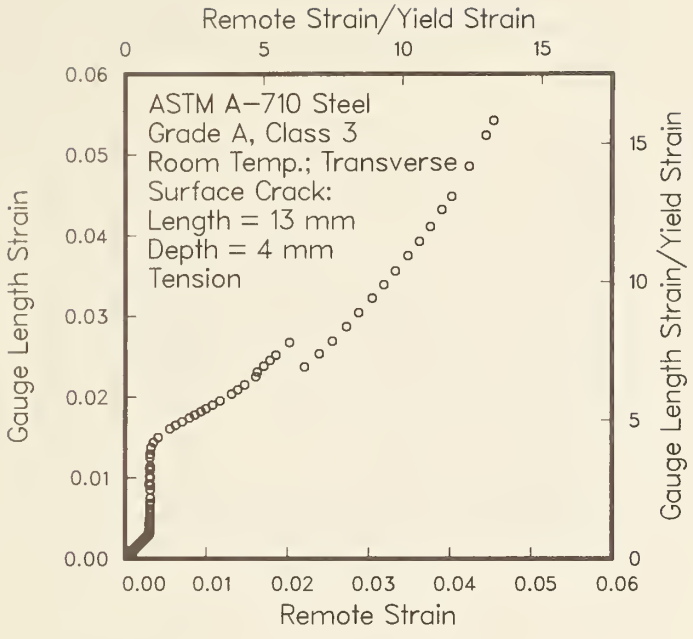

Figure A6e.

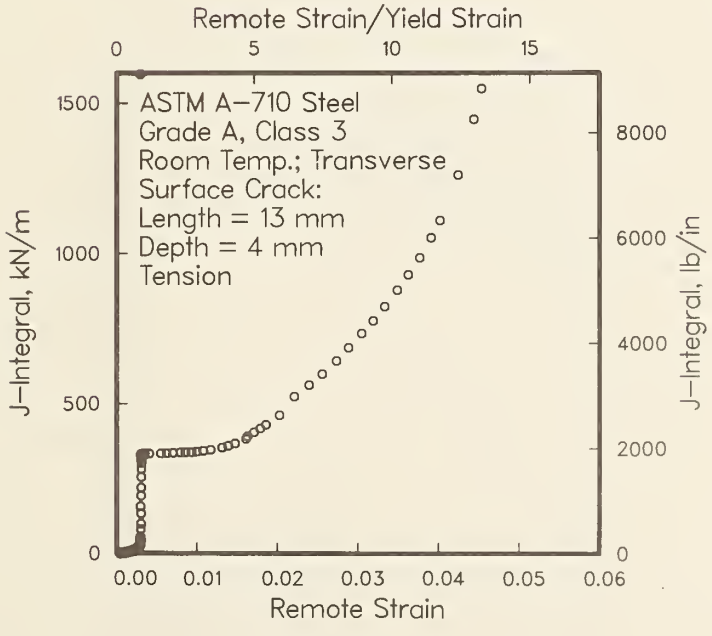

Figure A6f.

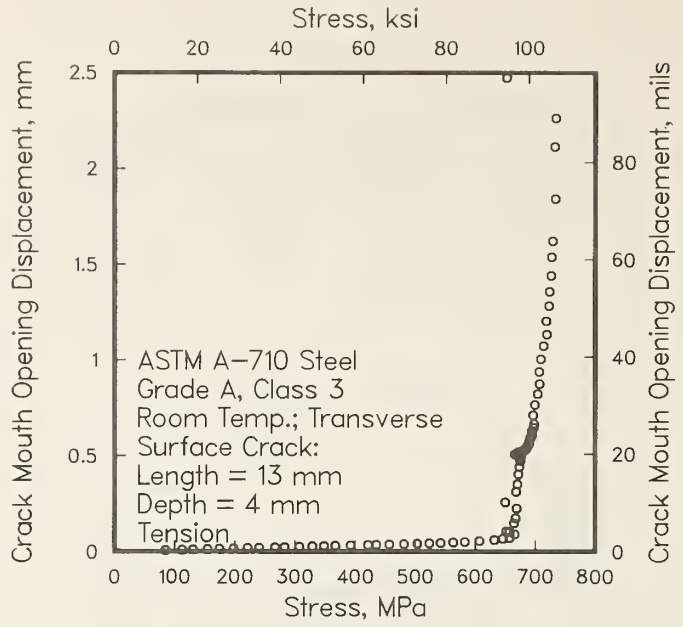

Figure A6g.

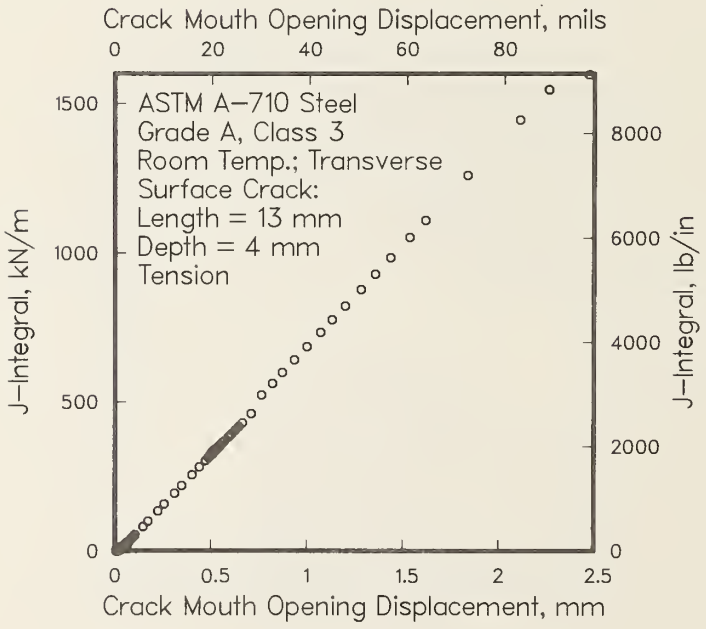

Figure A6h.

Figure A7a-h. Dependence of J-integral, stress, and crack mouth opening displacement on strain, for single-edge-cracked transverse bending panel at room temperature with crack length 1.2 mm.

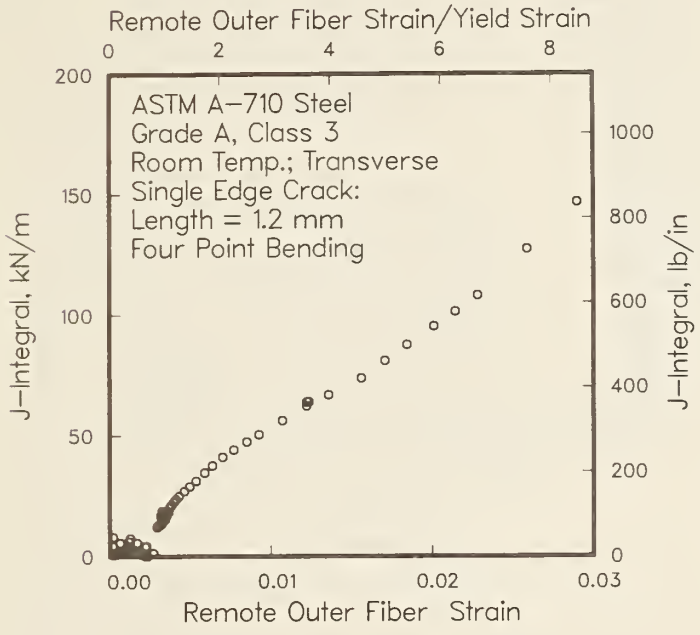

Figure A7a.

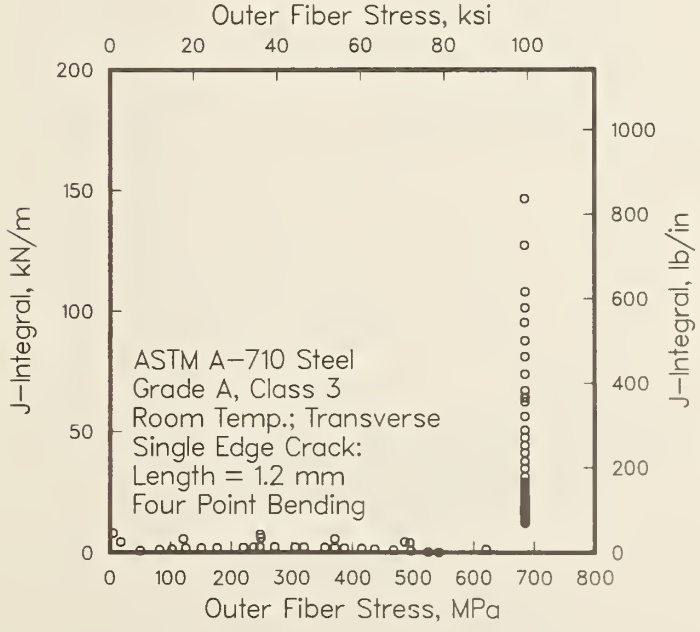

Figure A7b.

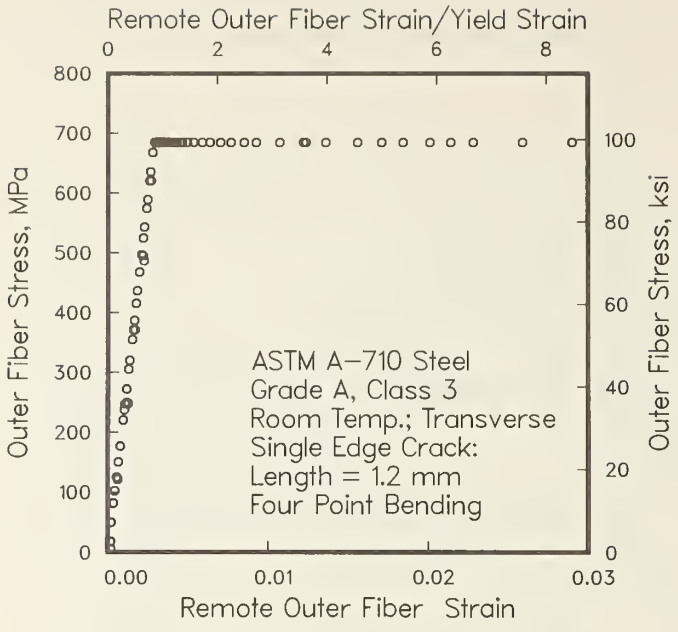

Figure A7c.

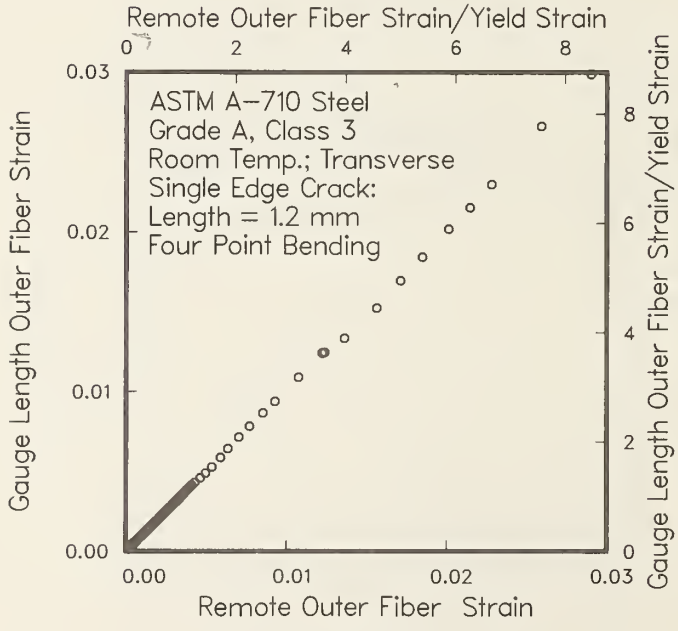

Figure A7d.

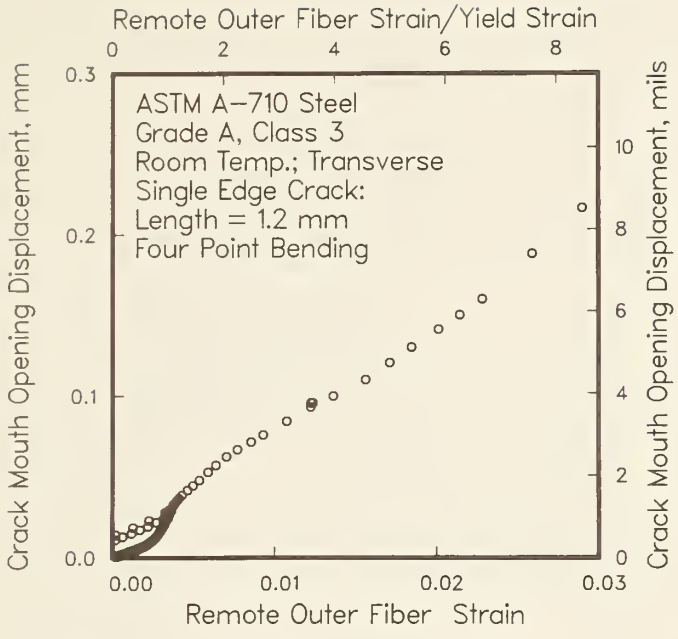

Figure A7e.

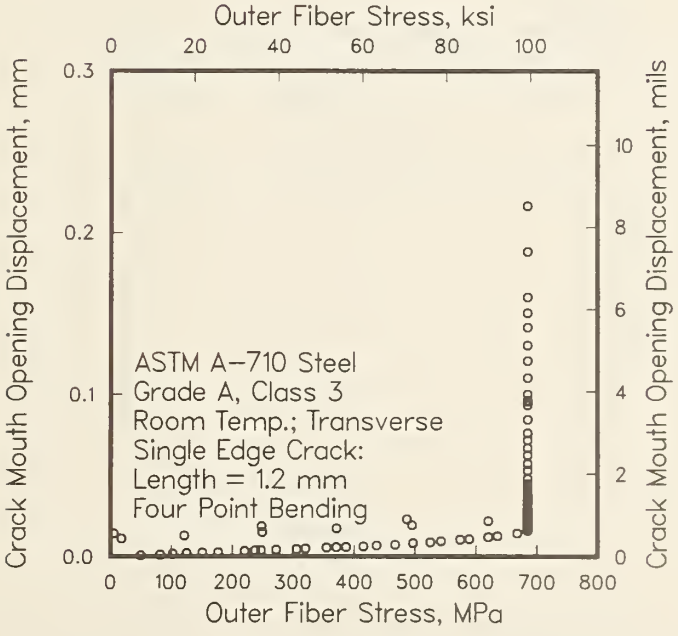

Figure A7f.

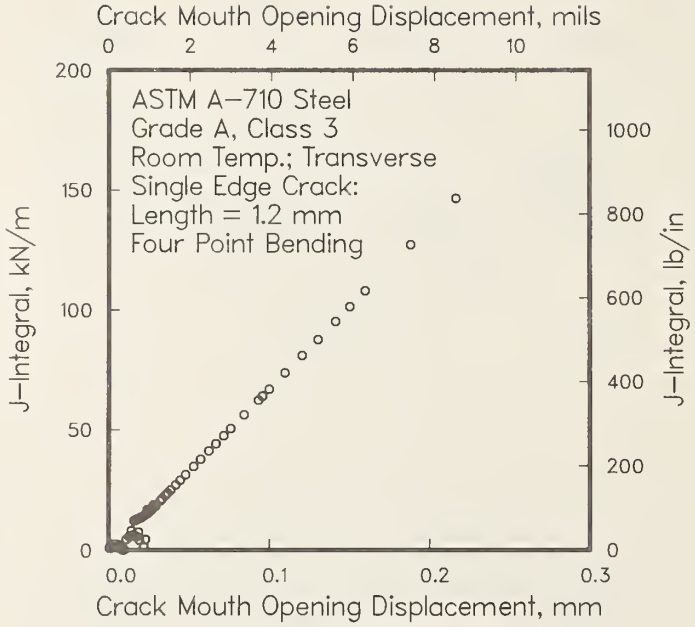
Crack Mouth Opening Displacement, mils
0
2
4
6
8
10
200
150
100
50
0
ASTM A-710 Steel
Grade A, Class 3
Room Temp.; Transverse
Single Edge Crack:
Length = 1.2 mm
Four Point Bending
J-Integral, kN/m
1000
800
600
400
200
0
J-Integral, lb/in
0.0
0.1
0.2
0.3
Crack Mouth Opening Displacement, mm

Figure A7g.

Figure A8a-h. Dependence of J-integral, stress, and crack mouth opening displacement on strain, and J-R curve, for single-edge-cracked transverse tensile panel at −30°C with crack length 1.2 mm.

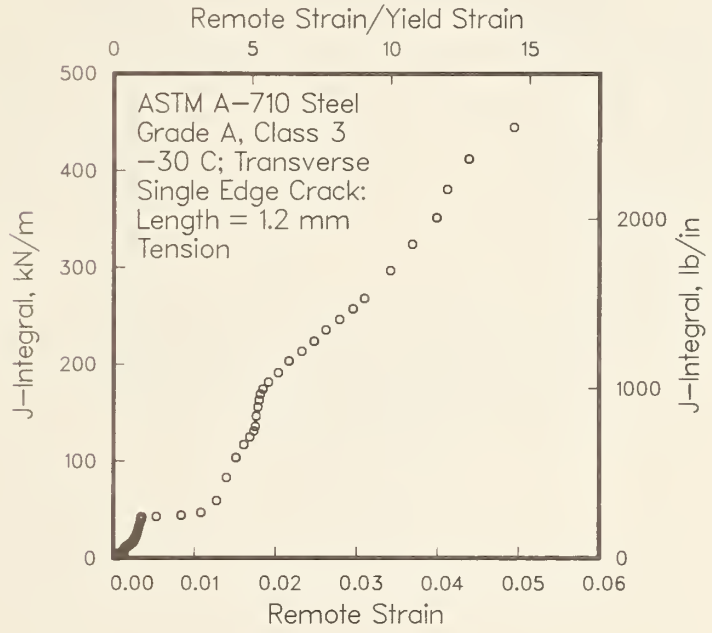

Figure A8a.

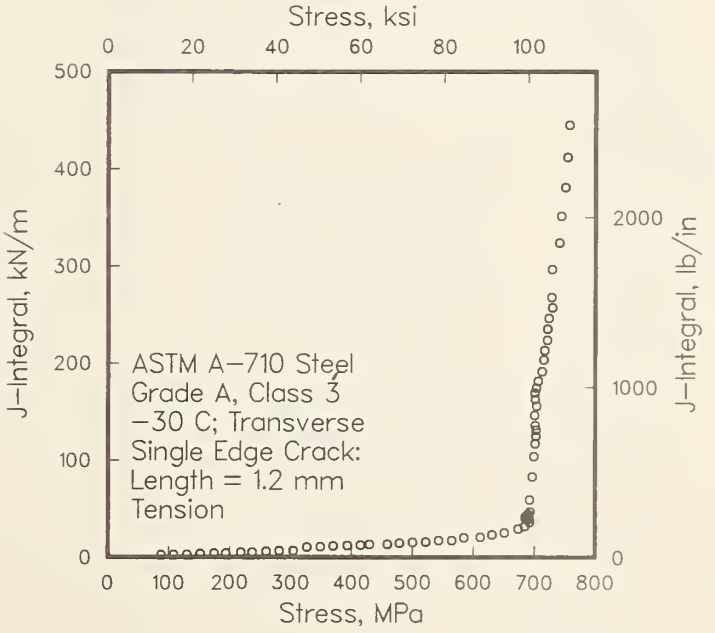

Figure A8b.

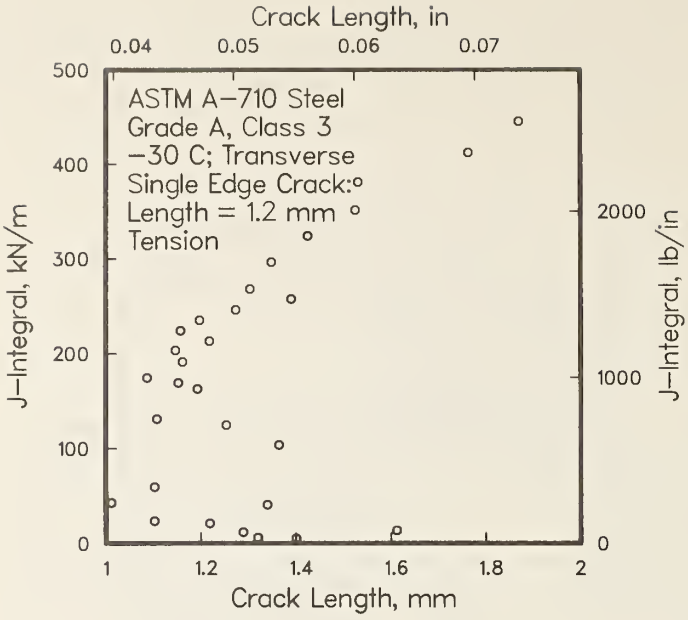

Figure A8c.

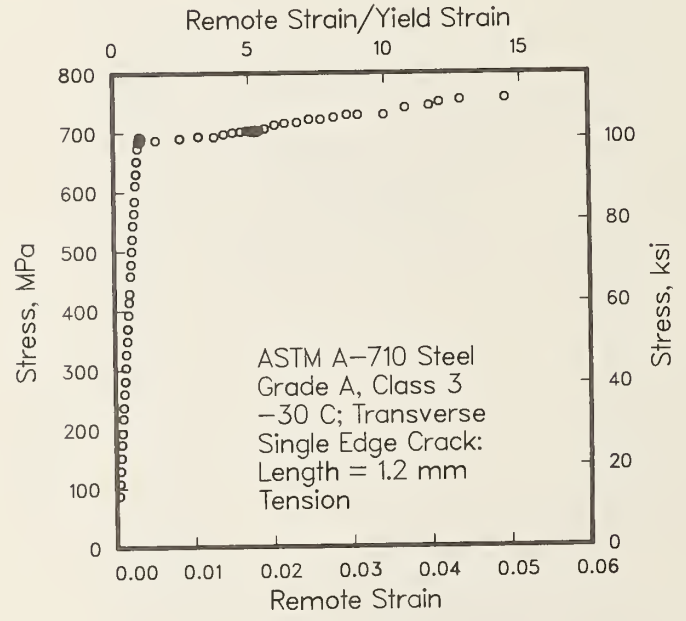

Figure A8d.

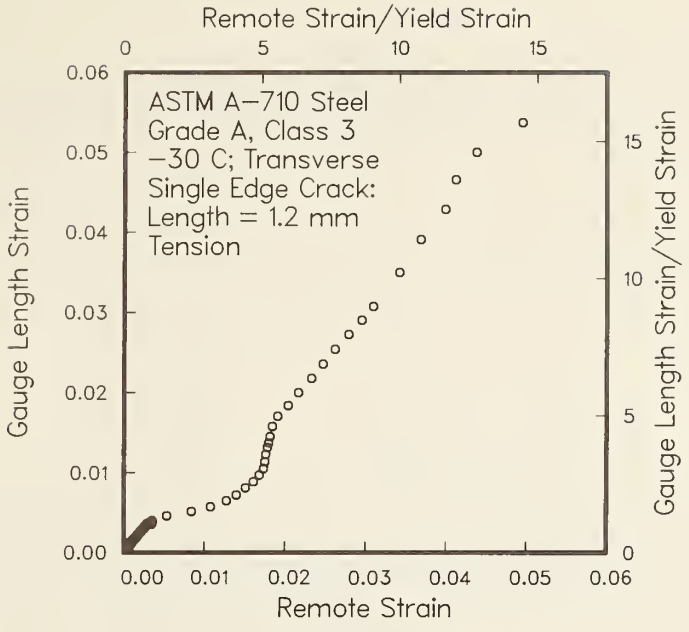

Figure A8e.

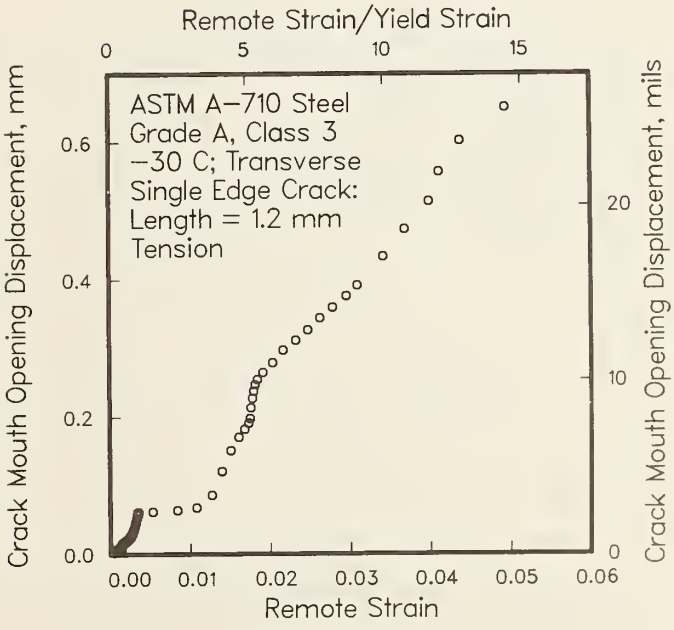

Figure A8f.

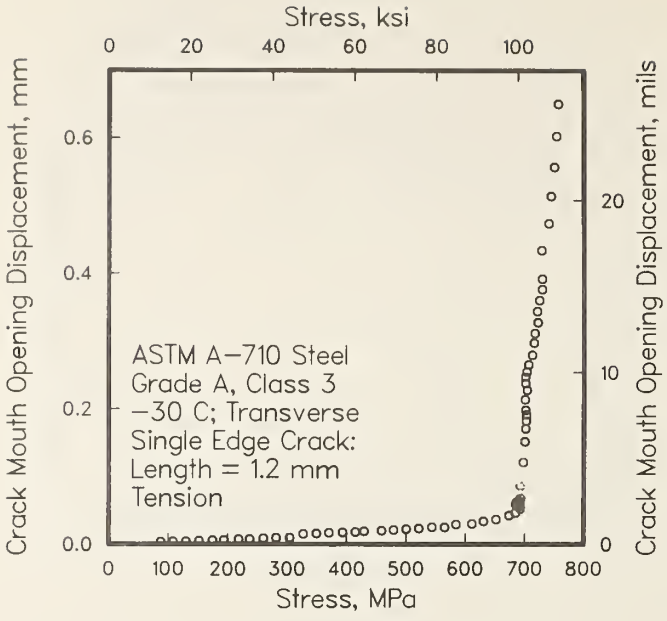

Figure A8g.

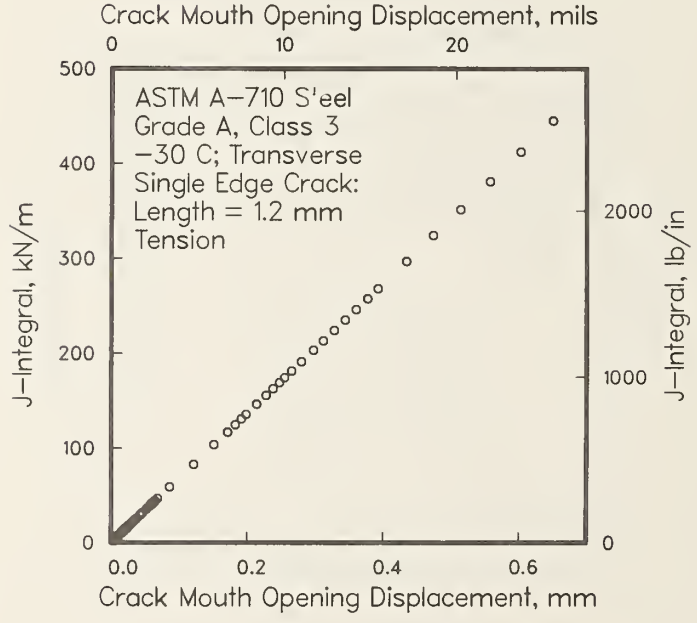

Figure A8h.

International Journal of Fracture 31 (1986) 161–171

5.

Essential work of fracture (w_e) versus energy dissipation rate (J_c) in plane stress ductile fracture

M.P. WNUK * and D.T. READ

Fracture and Deformation Division, National Bureau of Standards, Boulder, CO 80303, USA

(Received 24 July 1984; in revised form 20 February 1986)

Abstract.

Two measures of fracture toughness have been investigated. The first is the Cotterell's essential work of fracture (w_e) which reflects the energy absorbed in the process of localized necking and decohesion occurring within the crack tip region. The second is the familiar critical energy dissipation rate associated with the onset of crack extension and commonly designated by J_c. Total of 48 fracture tests have been performed on thin aluminum double-edge-notched panels and thin compact tension specimens with varying crack size-to-ligament ratios. In a simple experimental procedure it has been established that both measures are equivalent, at least under the plane stress conditions, and that they both represent the fraction of energy which is transmitted through the plastic deformation field into the crack tip region. The ratio "essential work of fracture/total work of fracture" has been suggested as a quantitative measure of the energy transmission process. Certain predictions are made concerning variations of the energy transmission factor (ETF) during the stable phase of ductile fracture propagation.

Introduction

Energy release rates have been considered fundamental to fracture mechanics since Griffith's original work in the field. In elastic materials, whether linear or non-linear, there is no history dependence associated with the deformation process, and the energy released when a crack grows from length a to $a + \Delta a$ is equal to the difference between the elastic energies stored in the specimen containing crack of length a and the same specimen with crack of length $a + \Delta a$; all at constant imposed displacement. Real materials, however, are irreversible. They store some amount of strain energy but they absorb much more energy as work. By analogy to the reversible deformation field generated within a cracked body, the critical rate of energy absorption serves as a measure of fracture toughness. As we intend to show, the critical J-integral and the Cotterell's essential work of fracture may be used interchangeably, as the equivalent measures of specific work absorption associated with the initiation of fracture in real materials. Final results of this investigation are in qualitative agreement with the theoretical considerations of Turner [10,11] and Paris et al. [12] which focus on applications of J-integral in the description of ductile failure. More detailed discussion of the "ubiquitous η factor", cf. [10], or the I-term (our w_0) which represents the true energy release rate for irreversible solids, cf. [11], are beyond the scope of this research.

In recent times, R-curves have been plotted for elasto-plastic materials to describe changes in apparent fracture toughness or energy dissipation rate with crack growth.

* On leave from The University of Wisconsin-Milwaukee.

Attempts have been made to analyze the fracture process by breaking it up into parts that are the same in all specimen geometries and those that depend on specimen geometry. The former are usually associated with certain *local* fracture features while the latter encompass fracture parameters of *global* nature. For example, theoretical predictions of the geometry dependence of R-curves (global entities) would be of practical significance in describing failure under various loading conditions. On the other hand, the concept of the essential work of fracture, which is obviously a local quantity, has been proposed as a geometry-independent and crack-extension-invariant feature of the fracture process. In 1977 Cotterell [1] reported experimental measurements concerned with plane stress situations and intended to differentiate between essential work of fracture and work done in the outer plastic region, which shields the crack tip region.

Since the concept of "essential work of fracture" w_e, is not widely known, and since we consider the quantity w_e a potentially useful parameter for assessment of material toughness against ductile failure, we have set up a simple experimental program with an intention (a) to verify the existence of the essential work of fracture, w_e, and (b) to find a relationship between the quantity w_e and other well established parameters characterizing occurrence of ductile fracture, such as the critical J-integral value, J_c.

2. Specimens and experimental procedures

Cotterell's experiment has been repeated on thin (3.2 mm thick) sheets of a ductile aluminum alloy, 5052-H32. This alloy had a yield strength of 179 MPa and an ultimate strength of 245 MPa, uniform elongation of 10 percent, and reduction of area of 57 percent. It contained 2.5 percent magnesium and 0.25 percent chromium by weight. Deep double-edge notches were cut into tensile panels 560 mm long and 82 mm wide, Fig. 1a. The panels were instrumented with an extensometer of gage length 80 mm spanning the plane of the notches. The specimens were strained to failure in a servo-controlled hydraulic testing machine under displacement control. Load was plotted continuously against extension during the test. The same test procedure was repeated using specimens of the ITCT compact specimen geometry, Fig. 1b. Anti-buckling guides were used to prevent out-of-plane deformation, resulting in some uncertainty in the load.

Compact tensile specimens of the same alloy were used to obtain a J_R curve. The notch preparation was the same as in the notched tensile panels. The in-plane specimen dimensions were as usual for ITCT specimens, but the thickness was 3.2 mm, as it was for the tensile specimens. The J_R curve data for three specimens, Fig. 2, had the usual shape, with a critical value of J, of (0.170 ± 0.025) J/mm^2 and a slope, $\mathrm{d}J/\mathrm{d}a$, of $50 \pm 8\text{N}/\text{mm}^2$. The slight negative values of crack extension, Δa, in Fig. 2, are not real, but are an artifact of the test procedure.

3. Results

According to Cotterell's procedure, the recorded load-displacement curves were integrated to give work done to failure. The work for each specimen was divided by specimen thickness and initial ligament length to give the work done per unit area of fracture surface. These work density values were plotted against ligament length, Fig. 3a and 3b. Best-fit straight lines were drawn through the data. The zero-ligament intercepts, which according to Cotterell represent the specific essential work of fracture, were 0.20 ± 0.026 J/mm^2, for the DEN specimens, and 0.20 ± 0.05 J/mm^2 for the compact specimens.

For the compact specimens, the data were subject to a large uncertainty, as indicated in Fig. 3b. The uncertainties arose mainly from friction between the specimens and the

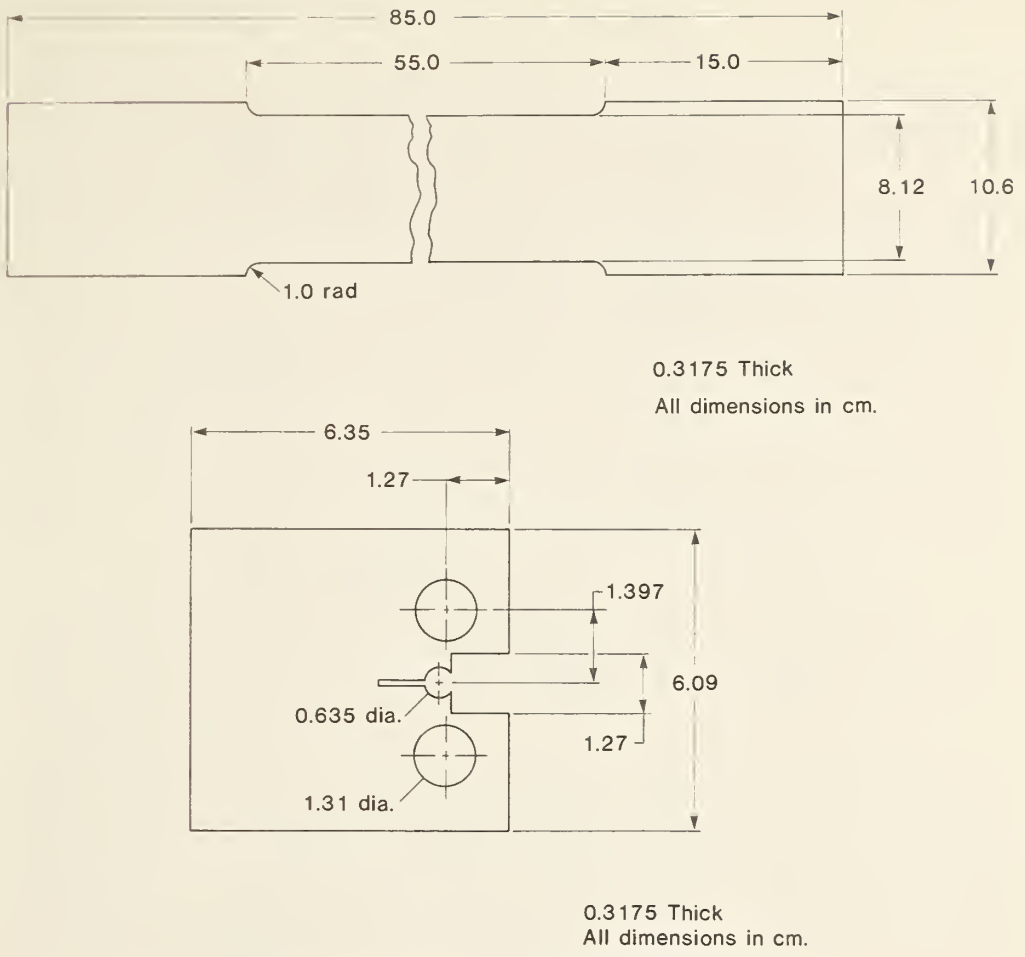

Figure 1. Tensile panel (a) and compact (b) specimens used in the present study.

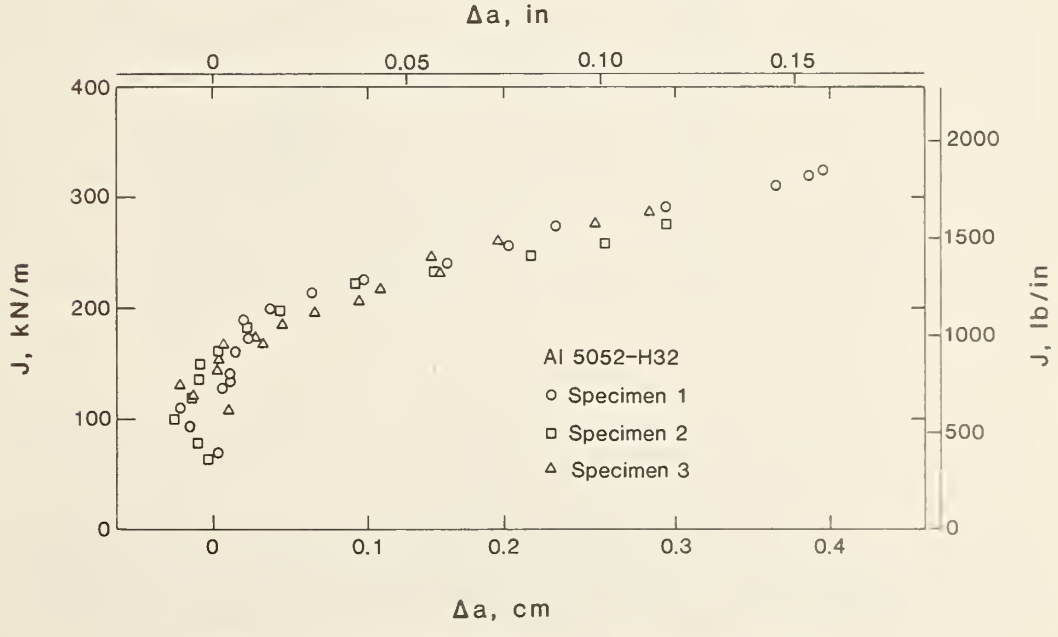

Figure 2. *J-R* curve data for aluminum 5052-H32 specimen material.

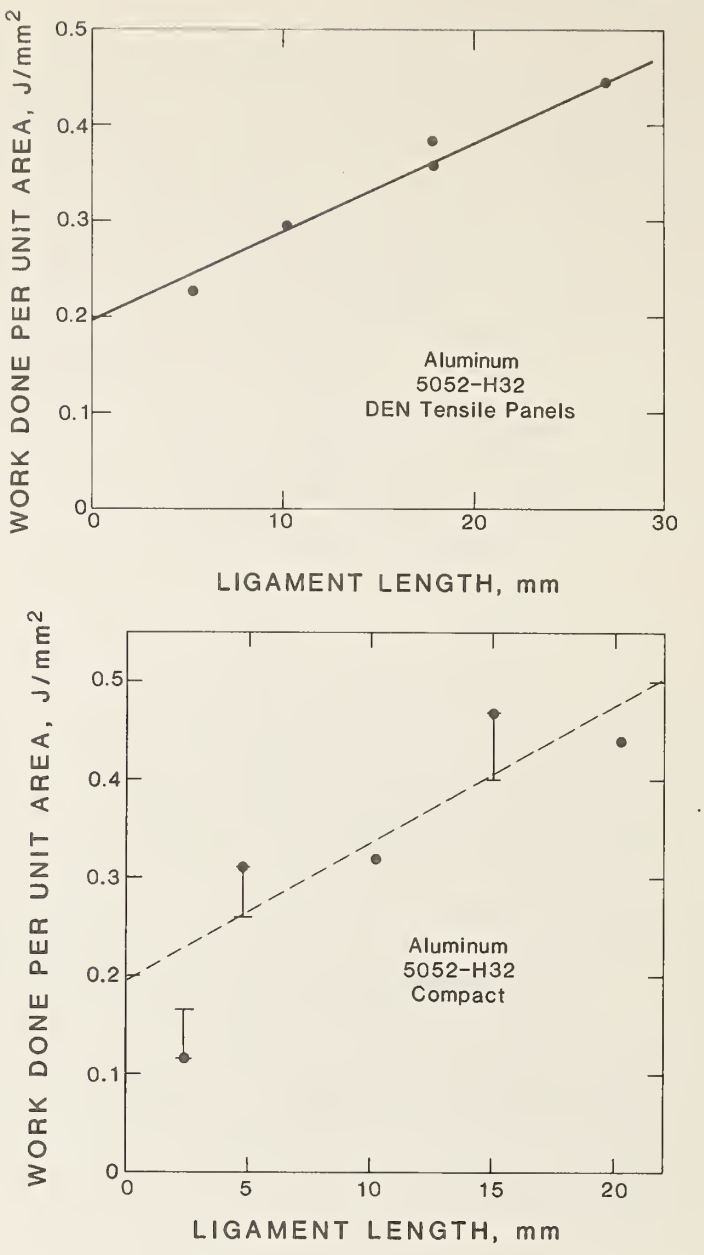

Figure 3. Specific work to fracture plotted against ligament length for DEN tensile panels (a) and compact specimens (b).

anti-buckling guide. Loading due to friction was estimated, and was eliminated from the work calculation. The data point with the smallest ligament was not considered in drawing a straight line through the data points.

The specific essential work of fracture for the CT specimens was consistent with that for the DEN specimens, within experimental uncertainty. More precise experiments are needed to determine the difference, if any, between the specific essential work of fracture for these two specimen geometries.

4. Discussion

The significance of these test results lies in the equality, within experimental error, of the critical J value and the specific essential work of fracture. This agreement is not considered coincidental. This result is interpreted to mean that both the critical J-integral for initiation of tearing and the specific work to fracture measure the work done in local straining, necking and material separation near the plane of the propagating crack. *

A relation between fracture toughness and absorbed energy has been suggested previously for side-grooved steel bend specimens with shallower cracks than those of the present study [2]. This work proposed a functional relationship between work of fracture and toughness, but the function included arbitrary constants which were calculated from the experimental data.

The agreement between critical J value and specific essential work of fracture could be further interpreted as support for the conclusion of Willoughby, Pratt, and Turner [3] that R-curves reflect work done remotely from the crack. Even though the work done during failure of the tensile panels included contributions from the whole R-curve (whatever the R-curve may have been for such specimens), the work done locally near the crack plane corresponded to the critical J value for initiation of tearing. Figure 5 shows the entire plastic strain field, and the local plastic strain field within it. The local field is within a distance of approximately t, the specimen thickness, of the fracture surface, and its thickness reduction, by necking, is more severe than the remote thickness reduction within the uniform plastic strain field.

Considerations of local vs. remote straining bring up another interesting feature of ductile fracture. Work done by the loading system in deforming the specimen must be stored as strain work density. Consider the plastic part of this work, which is permanently absorbed as strain work density. The strain work density is increased both locally, near the fracture plane, and remotely, away from the fracture plane. The work absorbed locally contributes directly to the fracture process. Load is transmitted from the specimen grips to the local crack tip region by remote regions of the specimen. Because this load does

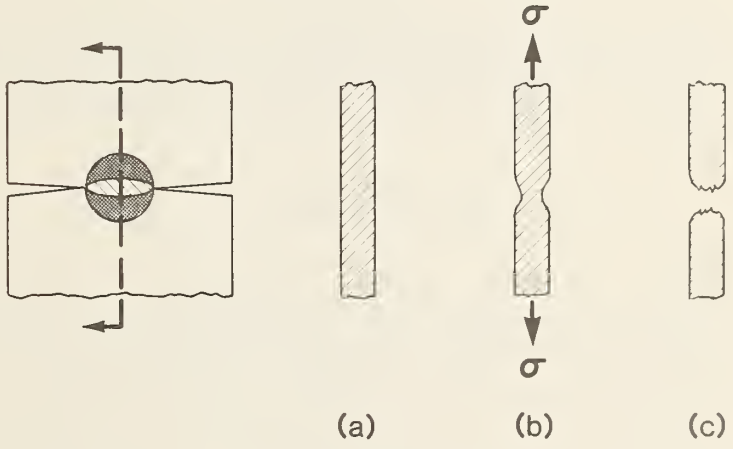

Figure 4. Side view of three stages in failure of tensile panel: (a) unstrained; (b) strained and necked; (c) fractured.

* Figure 4 shows a side view of three stages in the failure process of the tensile panels used here. The agreement between J_c and w_e implies that the measured work density gives the work needed to go from stage (a) to stage (c). If the energy needed to go from stage (b) to stage (c) were sought, more sensitive experimental techniques than those used here would be needed.

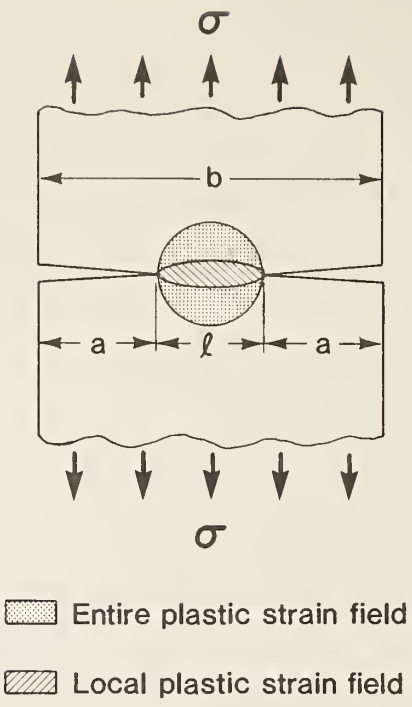

Figure 5. Entire and local plastic strain fields in double-edge-notched tensile panel.

work, one can view the remote regions of the specimen as conduits of work from the grips toward the local fracture region. Any work absorbed in remote regions is not available to the crack tip region. The remote energy absorption process can be viewed as a screening action that prevents some work from reaching the crack tip region where it can contribute to fracture. This screening action of the plastic deformation field has been considered a primary reason for the existence of the slow stable cracking occurring during the early stages of ductile fracture, cf. Broberg [4].

This effect can be described using the final stretch model of a slowly growing crack, Wnuk [5]. If we agree to define the so-called "energy transmission factor" (ETF for short) as the ratio

$$\mathrm{ETF} = \frac{w_e}{w_f} = \frac{\text{essential work of fracture}}{\text{total work of fracture}} \tag{1}$$

where w_e, the essential work of fracture, is the specific essential work of fracture multiplied by the ligament area, and w_f is the total work done on the fractured specimen, then we may indeed assign a quantitative measure to the screening phenomenon. It is noted that high screening corresponds to lower transmission, and vice versa.

We proceed to show that the quotient ETF is always less than or equal to one, and that it decreases from its initial value as the stable crack propagates (a decrease in ETF signifies a more intensive screening action). To demonstrate these effects let us first calculate the ETF at the onset of crack extension. We use only the DEN panel data because it has less scatter. Dividing the value of the fracture energy obtained at the zero-ligament intercept by the density of the total work of fracture, as given by the experimental points in Fig. 3a, we obtain estimates of the ETF at the onset of crack extension for various ligament lengths. These numbers are listed in the third column of Table 1. For the deeply notched tensile specimens used in our experiment, the ligament l

Table 1. Screening of fracture energy by the field of plastic deformation generated around the leading edges of deep notches in a tensile specimen. The quantity "ETF" represents the "damping effect" of the plastic zone developed around the notches prior to fracture. ETF is defined as the ratio of the essential (or local) energy expended in the fracture process to the total (or global) work done in the entire volume of the specimen

Ligament l(mm)	(R/a) ini	ETF_{exp}	ETF (6)	Error
5	0.065	0.870	0.959	10%
10	0.139	0.678	0.916	35%
18	0.281	0.556	0.846	52%
27.5	0.505	0.449	0.756	68%

was fully yielded prior to fracture, thus $l \simeq 2R$. Here, the factor 2 is added because of the symmetry of the double edge notch specimen, while R denotes the plastic zone radius associated with a single crack tip. For a stationary crack the ratio R/a, where crack length $a = (b - l)/2$, with b the full specimen width, is calculated as follows

$$\frac{R}{a} = \frac{l/2}{(b-l)/2} = \frac{l}{b-l}. \tag{2}$$

The R/a ratios obtained from each data point of Fig. 3a, are shown in the second column of Table 1. The fourth column provides the ETF values calculated from the line plasticity model of ductile fracture [6,7], applied to an infinite width center crack panel. Identifying the essential work of fracture, w_e, per unit area, with the energy absorption rate J_c, and then dividing J_c by the total specific work of fracture, w_f, (which consists of the specific elastic strain energy, w_0, and the plastic energy dissipation per unit area, w_p) we obtain the theoretical energy transmission factor

$$\text{ETF} = \frac{J}{w_0 + w_p} \tag{3}$$

The numerator of this expression represents energy dissipation rate measured by the J-integral which for the D-BCS [6,7] model of a stationary crack can be readily obtained from the known crack tip opening displacement, δ_t. We have

$$J = \sigma_y \delta_t = \frac{8a\sigma_y^2}{\pi E_1} \begin{cases} \ln(\sec \beta), & \text{or} \\ \ln\left(1 + \dfrac{R}{a}\right). \end{cases} \tag{4}$$

The symbol β denotes the nondimensional loading parameter, $\beta = \pi\sigma/2\sigma_y$. As usual, σ indicates applied stress, σ_y indicates flow strength, and E_1 is the effective modulus for plane stress or plain strain, as is appropriate. Here we use the plane stress value. In numerous instances it is convenient to use the extent of the plastic zone R as a measure of the external field intensity. In such a case the loading parameter β should be replaced by $\cos^{-1}[a/(a+R)]$ according to the Dugdale equation. The denominator of the expression (3) has been evaluated by Wnuk [8], and for the configuration considered here it reads

$$w_f = w_0 + w_p = \frac{8a\sigma_y^2}{\pi E_1} \begin{cases} \beta \tan \beta + \ln(\cos \beta), & \text{or} \\ \sqrt{2\dfrac{R}{a} + \left(\dfrac{R}{a}\right)^2}\ \cos^{-1}\left(\dfrac{a}{a+R}\right) + \ln\left(\dfrac{a}{a+R}\right). \end{cases}$$

When we divide (4) by (5), the following theoretical estimate of the energy transmission factor follows

$$\mathrm{ETF} = \begin{cases} \dfrac{\ln \sec \beta}{\beta \tan \beta + \ln \cos \beta}, & \text{or} \\ \dfrac{\ln(1 + R/a)}{\left\{2(R/a) + (R/a)^2\right\}^{1/2} \cos^{-1}\left(\dfrac{a}{a+R}\right) + \ln\left(\dfrac{a}{a+R}\right)} \end{cases}$$

These two expressions can be used to obtain quantitative predictions for the ETF both for a stationary and a quasi-static crack. The important difference in application of (6) to a quasi-static crack case consists in the evaluation of the quantity "R" which for a stationary crack is given by the well-known Dugdale expression, so that the ratio R/a ($= \sec \beta - 1$) does not depend on the crack length (at least for an infinite width CCP geometry), while for a moving crack the extent of plastic zone R must be treated as an R-curve quantity, i.e. it has to be thought of as a certain function of the current crack length, $R = R(a)$. This function may be determined through one of Wnuk's equations derived from the final stretch model of a quasi-static crack [5,9]

$$\frac{\mathrm{d}R}{\mathrm{d}a} = \begin{cases} M - \tfrac{1}{2} - \tfrac{1}{2} \log(4R/\rho), & R \ll a \quad (7a) \\ \dfrac{R}{a}\left[M + \tfrac{1}{2} - \tfrac{1}{2} \log(2R^2/a\rho)\right], & R \gg a. \quad (7b) \end{cases}$$

Here, M denotes Wnuk's tearing modulus, directly proportional to the ratio of the final stretch $\hat{\rho}$ and the process zone size ρ. M differs from Shih's modulus based on the CTOA model of quasi-static mode I crack T_ρ by a constant factor of $\pi/8$, i.e. $M = (\pi/8)T_\rho$. Equation (7a) applies to the small scale yielding case regardless of crack configuration, while the expression (7b) is valid * for the large scale yielding situation encountered in an infinite width center cracked panel (CCP). In both instances the state of plane stress is presumed. For an intermediate range of the R/a ratios the following equation should be used, cf. [9]

$$\mathrm{d}R/\mathrm{d}a = \frac{a+R}{a}\left\{M - \tfrac{1}{2} \log\left[\frac{2\mathrm{e}R(2a+R)}{a\rho}\right]\right\} + \frac{R}{a}. \quad (7c)$$

It is readily seen that both (7a) and (7b) result as limiting cases from the expression (7c).

When R exceeds the initiation threshold, R_{ini}, the function $R = R(a)$ must be obtained by numerical integration of (7). Finally, when these results are substituted for R in the second expression in (6), it yields the three steeper curves for the ETF vs. R/a shown in Fig. 6 as curves 1, 2 and 3.

As expected, the expressions in (6) approach one for the case of brittle fracture when the effects of ductile screening disappear ($\beta \to 0$, $R \to 0$), while in the other extreme case of material behavior under the large scale yielding situation ($R \gg a$), the ETF predicted by (6) drops to zero. Of course, before this may happen the crack opens up. The ensuing stable growth and the associated energy transmission factor are governed by the equations pertaining to a quasi-static, rather than stationary, crack.

---

* Note that (7b) may be written in an alternative form

$$\frac{\mathrm{d}J}{\mathrm{d}a} = \left(\frac{8\sigma_y^2}{\pi E}\right) M - \frac{4\sigma_y^2}{\pi E} \lim\left[\frac{2\mathrm{e}}{\rho}(\Delta a + a_0)\right] \quad (7d)$$

which for small increments of crack extension, $\Delta a/a_0 \ll 1$ agrees with the well known result of Paris, $\mathrm{d}J/\mathrm{d}a = \text{constant}$, suggested for metallic alloys of significant ductility. The "constant" becomes then $(\sigma_y^2/E)T_J$ or simply $T_\delta (= \hat{\delta}/\epsilon_y \rho)$, in which ϵ_y denotes strain at the onset of yield.

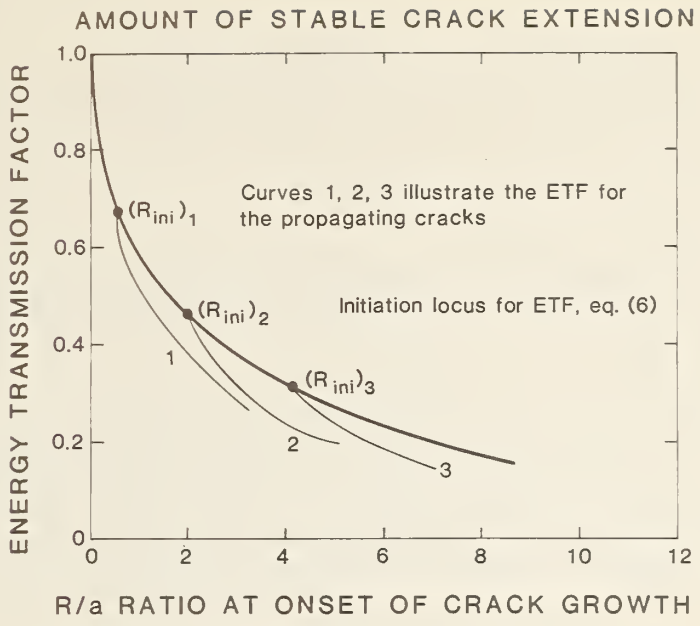

Figure 6. Initiation locus and the variation of the energy transmission factor due to stable crack extension. Note that both an increasing ductility and the subsequent stable crack growth tend to intensify the screening action of the plastic deformation field, which is represented by a lower ETF. Two horizontal scales are used: R/a for the upper curve valid for a stationary crack; and $\Delta a/R_{ini}$ for the three curves concerning a growing quasi-static crack in an infinite width center crack panel curves 1–3. The R-curves used to draw curves 1–3 were obtained from the final stretch model [9].

Variation of the theoretical ETF with the extent of yielding preceding fracture, as measured by the ratio R/a, is depicted in Fig. 7. The experimental values of the ETF are also shown for comparison. Only a qualitative agreement is to be expected because different configurations were used, double edge notch for the experiment, and CCP of infinite width for the theory. Another source of error is lack of strain hardening in the

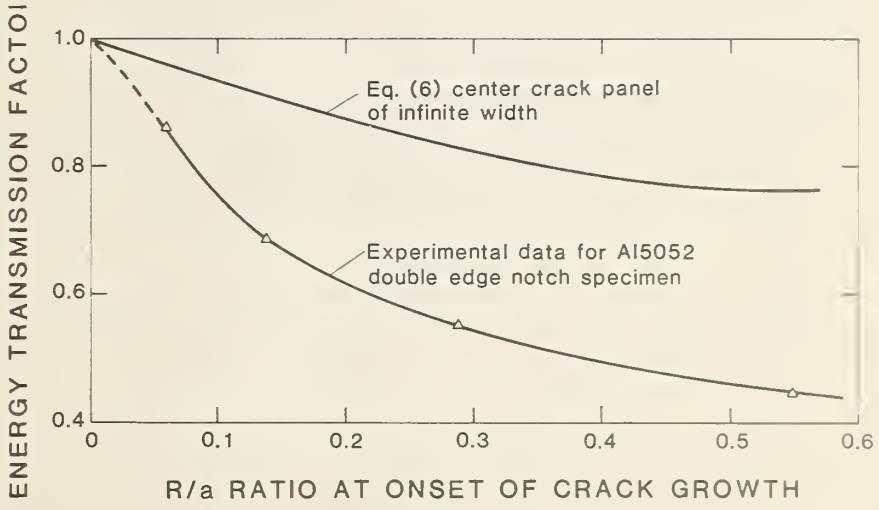

Figure 7. Comparison of experimental and theoretical variations of the energy transmission factor (w_e - w_f) with the ductility of fracture specimen.

theoretical model, which in its present form describes only the behavior of an ideally elastic-plastic material. Thus the plastic energy dissipation, w_p in (3), is underestimated. Despite all the differences in the conditions of the test and the assumptions underlying the mathematical model, both curves shown in Fig. 7 exhibit the same trend. The screening action of the plastic deformation field increases with higher ductility, while it vanishes in the limit of brittle fracture.

It should be noted that at a certain threshold value of the plastic zone size R, say $R = R_{ini}$, the crack enters into the propagation phase. Description of the variations of the ETF vs. the amount of crack growth, Δa, is still possible through the use of (6), but now the entire R-curve has to be substituted for the symbol "R" appearing in (6). Since in the course of stable cracking the ratio R/a tends to increase from its initial value of R_{ini}/a_0, we observe a more pronounced drop in the energy transmission factor as depicted in Fig. 6. The R-curves employed in drafting Fig. 6 obey the differential equation derived by one of the authors (MPW) from his final stretch model of a quasi-static crack propagating in a ductile material. It is noteworthy that one of those equations, namely (7a) valid for a small scale yielding plane stress situation is virtually identical to (6.9) in [13] derived more recently through an entirely different approach for the case of small scale yielding in plane strain.

5. Conclusions

Our conclusions are drawn from the total of 48 data points, in which 20 points were obtained in testing five DEN specimens of varying ligament size, 25 points were derived from tests performed on five CT specimens with various a/w ratios, while additional 3 CT specimens were used to determine the critical value of J-integral by the conventional ASTM-approved, experimental procedure as specified by the Standard E813-81. The essential findings are as follows.

1. The critical J-integral for initiation of tearing and the specific work of fracture as defined by Cotterell both measure work done in *local* straining, necking, and material separation near the plane of the propagating crack.
2. An energy transmission factor (ETF), which is the ratio of the essential work of fracture (that is, the strain work absorbed in regions near the plane of crack propagation) to the total work of fracture, has been defined.
3. The ETF was shown to decrease during stable crack propagation based on the final stretch model of quasi-static crack propagation applied to an *infinitely wide* center-cracked-panel. This trend is confirmed by the data points derived from the set of experiments performed on the *finite-width* double-edge panel. Obviously, the intention is to compare only the gross features in the ETF variations during the stable crack growth phase, see Fig. 7 and Table 1. The ETF found experimentally was shown to decrease with decreasing initial crack size. In other words, small initial cracks tend to enhance the screening effect of the plastic deformation field.
4. It is noted that while the *slopes* of lines shown in Figs. 3a and 3b differ, reflecting the geometry dependence of the global fracture characteristic such as total work done per unit area (w_f) for DEN and CT specimens respectively, the *intercept* points of these two lines are identical. They both converge on the value of 0.2 J/mm^2 for the essential work of fracture, or the critical J-integral. This agreement is a manifestation of an important property of the tested fracture parameters (w_e and J_c), namely, their geometry-invariance.
5. The simple test procedures presented here should perhaps be extended so that they include plane strain situations. If proven successful, they would offer a novel and

unique method of determining J_{IC} without a measurement of Δa during the test. This would allow one to avoid the difficult problem of judgment when the crack initiates, as the experimental technique described in this report would automatically yield J_{IC}.

Acknowledgements

This work was sponsored in part by the Naval Sea Systems Command (SEA 05R25). Experimental assistance was provided by J.D. McColskey.

References

[1] B. Cotterell, in *Fracture Mechanics and Technology*, Vol. 2, Ed. G.C. Sih and C.L. Chow, Sijthoff and Noordhoff International Publishers (1977) 785–795.
[2] V.L. Gel'miza and D.M. Shur, *Problemy Prochnosti*, No. 5 (1974) 85–87 (in Russian).
[3] A.A. Willoughby, P.L. Pratt and C.E. Turner, *International Journal of Fracture* 17 (1981) 449–465.
[4] K.B. Broberg, ibid (1977) 837–859.
[5] M.P. Wnuk, in *Proceedings of International Conference on Dynamic Crack Propagation* Ed. G.C. Sih, Noordhoff, Leyden, The Netherlands (1972) 273–280.
[6] D.S. Dugdale, *Journal of the Mechanics and Physics of Solids* 8 (1960) 100–104.
[7] B.A. Bilby, A.H. Cotterell, K.H. Swinden, *Proceedings Royal Society*, A., 279 (1963) 1–9.
[8] M.P. Wnuk, *International Journal of Fracture Mechanics* 7 (1971) 383–407.
[9] M.P. Wnuk, *International Journal of Fracture Mechanics* 19 (1979) 553–581.
[10] C.E. Turner, in *Fracture Mechanics: Twelfth Conference*, ASTM STP 700 (1980) 314–337.
[11] C.E. Turner, in *Fracture Mechanics*, ASTM STP 677 (1979) 614–628.
[12] P.C. Paris, H. Ernst and C.E. Turner, in *Fracture Mechanics: Twelfth Conference*, ASTM STP 700 (1980) 338–351.
[13] W.J. Drugan, J.R. Rice and T.L. Sham, *Journal of the Mechanics and Physics of Solids* 30 (1982) 447–473.

Résumé

On étudie deux mesures de la ténacité à la rupture. La première est le travail essentiel de rupture de Cotterell (w_e) qui représente l'énergie absorbée au cours du processus de striction et de décohésion localisées qui se produit dans la région de l'extrémité d'une fissure. La deuxième est la notion familière de vitesse critique de dissipation d'énergie associée au démarrage de l'extension d'une fissure, qui est couramment représentée par J_c. On a procédé à un total de 48 essais de rupture sur des panneaux minces d'aluminium présentant une double entaille de bord, et sur des éprouvettes minces de traction compactes présentant divers rapport de longueur de fissure sur longueurs de ligaments. Par une procédure expérimentale simple, on a établi que les deux mesures de la ténacité sont équivalentes, du moins en état plan de tension, et qu'elles représentent toutes deux la fraction d'énergie qui est transmise au travers du champ de déformation plastique dans la zone de l'extrémité de la fissure. On suggère comme mesure quantitative du processus de transmission d'énergie d'utiliser le rapport "travail essentiel de rupture/travail total de rupture". Diverses prédictions sont faites en ce qui concerne les variations du facteur de transmission d'énergie au cours de la phase stable de propagation d'une rupture ductile.

6. POTENTIAL DROP MEASUREMENTS OF CRACK LENGTH IN TENSILE PANELS

Several authors have investigated the use of measurement of electrical potential difference (PD) as an indirect measurement of crack length [1,2]. The PD technique was investigated for this study. A calibration function for the double-edge-notched (DEN) tensile panel for one pair of pickup leads was derived and tested. With only one PD value, no information about differences in crack length between the two cracks in a DEN specimen can be obtained. Therefore a four-PD technique, involving PD measured at four locations across the specimen was tried. A calibration function was derived and checked briefly. This method was found to be potentially useful. However, because PD for the thin aluminum 5052 H-32 sheets used appeared to be sensitive to local necking in the crack plane as well as to tearing, the technique was not used in experiments on tearing in this material. It may prove useful on thicker steel specimens, which should have a smaller relative thickness reduction in the crack plane.

6.1 Calibration Formulae

Standard textbooks on electrostatics should be consulted for the methods of deriving relationships between conductor geometry and the electric field within the conductor. Here only results will be presented. From now on, calculated and measured PD values will be referred to as voltages.

6.1.1 Single Pair of Pickups

For a DEN specimen with two coplanar slit-like edge cracks of equal length, with pickups located symmetrically about the crack plane on the specimen centerline, the calculated voltage V is:

$$V = V_o \text{ arc sinh } (\sinh(\pi y/2W)/\cos(\pi a/2W) \qquad (1)$$

where V is voltage, V_o is a constant to be determined, y is distance of pickup above crack plane, W is specimen half width, and a is crack length. The constant V_o can be determined experimentally, by measuring V for a known crack length a.

6.1.2 Four Pairs of Pickups

Because the situation for four pairs of pickups is more complex, an intermediate step will be given. The pickup locations are shown in figure 1. In the theory of complex potentials, each location on the specimen is associated with a complex number $z = x + iy$, where (x,y) is the position in the usual Cartesian coordinates with the origin at the intersection of the specimen centerline with the crack plane. A complex set of voltages V exists, such that $V = V_r + iV_i$, where V_r is the real part of V and V_i is its imaginary part. The component sought in the following is V_i.

The following expression was derived:

$$V = V_o \text{ arc sin } (\sin(\pi/2W - \Delta B)/B) \qquad (2)$$

where V_o is a real constant, $B = 0.5\ (\sin(\pi b_1/2W) + \sin(\pi b_2/2W))$, $\Delta B = 0.5\ (\sin(\pi b_1/2W) - \sin(\pi b_2/2W))$, $b_1 = W - a_1$, $b_2 = W - a_2$, and a_1 and a_2 are the lengths of the two edge cracks. If we let $x = \pi x/2W$, and $y = \pi y/2W$, the equation above has the solution

$$B^2 + \Delta B(2 \sin x \cosh y/\cosh^2 V_i) - (\Delta B)^2/\cosh^2 V_i = \sin^2 x \cosh^2 y/\sinh^2 V_i + \cosh^2 x \sin^2 y/\sinh^2 V_i \qquad (3)$$

While this equation could be solved for V_i, the result would be complicated and would not be useful for calculating B and $B\Delta$ from four measured values of V_i at four (x,y) locations. The present form is more useful for this purpose. Equation 3 can be rewritten in the form

$$a + bX_i + cY_i = Z_i \qquad (4)$$

where a, b, and c correspond to the unknowns B^2, ΔB and ΔB^2, and the X_i, Y_i and Z_i are known functions of the pickup coordinates and the measured values of V_i, taken term by term from Equation (3), and the index i ranges from 1 to 4 when four pickup-pairs are used to obtain values of V_i at four locations (x,y). This is simply a system of four linear equations with three unknown constants, which can be solved by regression techniques. Or, nonlinear least squares methods can be used. The constant V_o can be evaluated from a specimen with a known average crack length, so that B is known, and both crack lengths the same, so that ΔB is 0.

Both of the equations given above assume that the cracks are infinitely narrow, like slits, that the specimen thickness and resistivity are independent of position, and that "far away" from the crack tip the current flowing along the specimen length is uniform across the specimen width. In order to use either of these equations, further understanding of the effects of necking and crack tip blunting on measured PD would be needed.

6.2 Experimental Techniques

Direct current, magnitude 40 amp, was passed through the aluminum tensile panel specimen described in Chapter 3. Potential drop was measured across a high-current-capacity resistor in series with the specimen, to verify that the current remained constant. The current was introduced into the specimen near the gripped ends, using heavy brass electrodes clamped with springs across the full width of the specimen. The voltage was monitored at one location (one-pair) in some tests and at four locations (four-pair) in others. In all cases, terminals were attached to the specimen with small screws. Each terminal therefore covered an area several millimeters square. These terminal contacts should be made smaller in future tests. The terminals were located opposite one another along the axial centerline of the specimen 3 cm from the transverse centerline, for the one-pair case, and opposite one another at distances of 0.8 and 2.4 cm on both sides of the axial centerline (Fig. 1), for the four-pair case. The specimen terminals were connected through shielded cables to the input terminals of differential-input analog-to-digital converters with a resolution of 1 part in 65536 over a range of ± 80 mv. Therefore, the least--

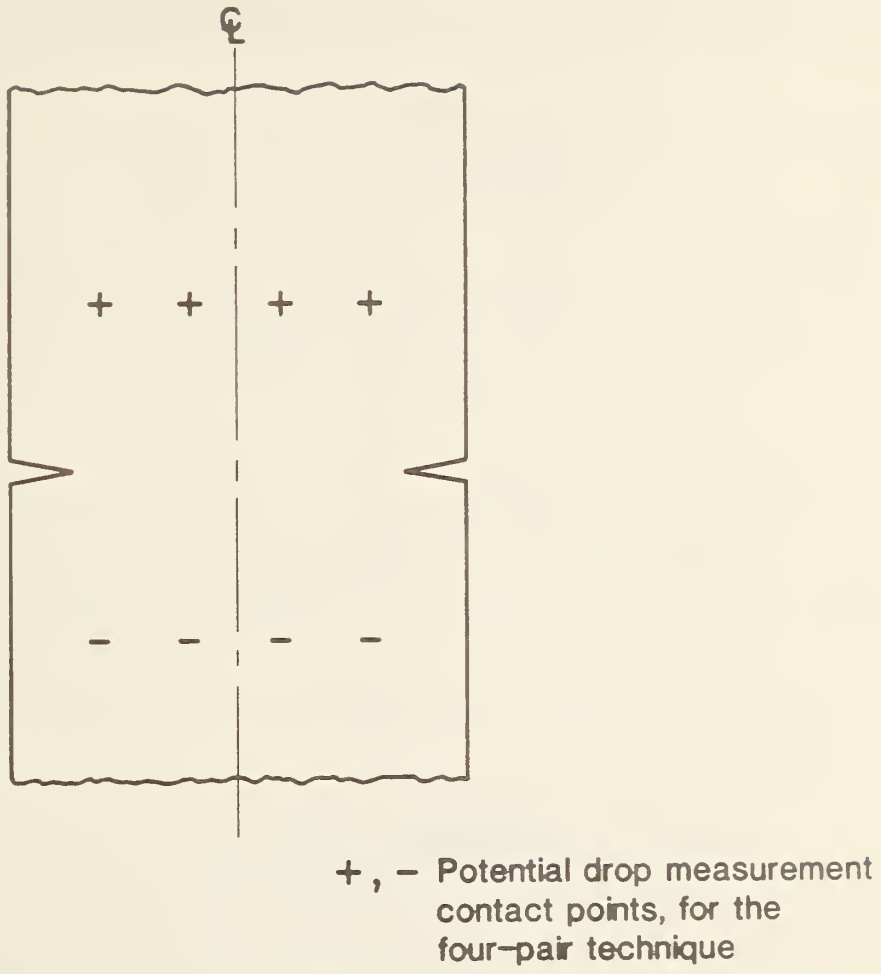

Figure 1. Location of voltage probes for four-pair measurement of crack length in a double-edge-notched tensile panel.

significant bit represented a change of about 2.5 μV. All instrumentation could be sampled about twice per second throughout the course of the test, with all results stored on floppy disk for later analysis and plotting.

6.3 Results

Results: Single-Pair

Figure 2 shows measured and calculated values of V for a series of saw-cut notches in a DEN tensile panel. The agreement between calculated and measured values is quite adequate.

Results: Four-Pair

Good results were found in a check at a single crack length, before straining. However, because of the previously mentioned problems with necking and tearing, this method was not tested thoroughly, and was not used in actual tearing studies.

6.4 References

[1] H. Tada, P. Paris, G. Irwin, The Stress Analysis of Cracks Handbook, Del Research, Providence, RI, 1973, p. 2.35.

[2] C. J. Beevers, ed., The Measurement of Crack Length and Shape During Fracture and Fatigue, Engineering Materials Advisory Services, London, 1980, pp. 85-272.

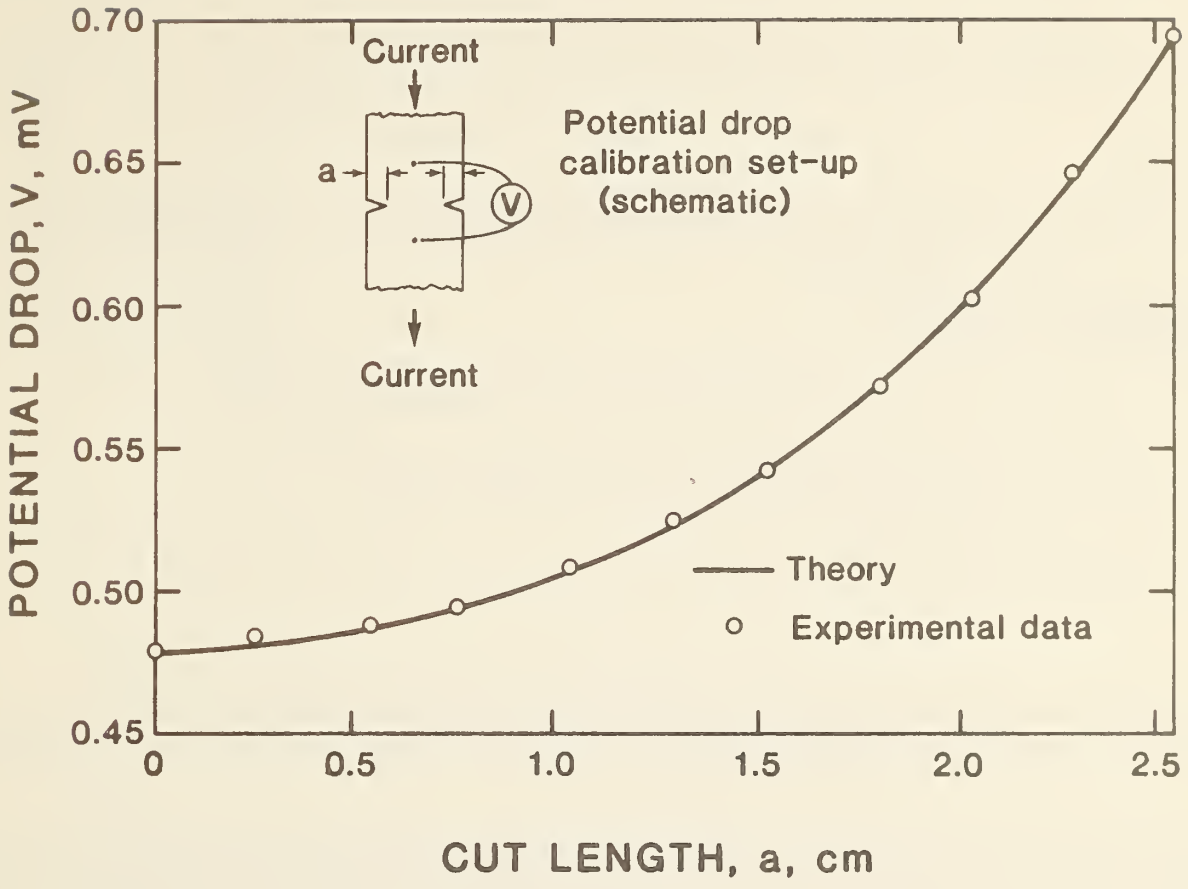

Figure 2. Measured and calculated value of single-pair pickup voltage as a function of crack length produced by saw-cutting in a double-edge notched panel.

NBS-114A (REV. 2-8C)

U.S. DEPT. OF COMM. BIBLIOGRAPHIC DATA SHEET (See instructions)	1. PUBLICATION OR REPORT NO. NBSIR 86-3045	2. Performing Organ. Report No.	3. Publication Date May 1987

4. TITLE AND SUBTITLE

Strain Hardening and Stable Tearing Effects in Fitness-for-Service Assessment: Progress Report

5. AUTHOR(S)

D.T. Read

6. PERFORMING ORGANIZATION (If joint or other than NBS, see instructions)

NATIONAL BUREAU OF STANDARDS
DEPARTMENT OF COMMERCE
WASHINGTON, D.C. 20234

7. Contract/Grant No.

8. Type of Report & Period Covered

9. SPONSORING ORGANIZATION NAME AND COMPLETE ADDRESS (Street, City, State, ZIP)

David Taylor Naval Ship Research and Development Center
Annapolis, Maryland 21402

10. SUPPLEMENTARY NOTES

☐ Document describes a computer program; SF-185, FIPS Software Summary, is attached.

11. ABSTRACT (A 200-word or less factual summary of most significant information. If document includes a significant bibliography or literature survey, mention it here)

This report describes studies done to provide information on how to account for material strain-hardening and tearing in fitness-for-service assessment. Included are a literature review, a study of the strength and ductility of cracked tensile panels under compliant loading, a report on applied J-integral measurements in an HSLA steel, a study of the relationship of the essential work of fracture to the J-integral, and a description of potential drop techniques for crack length measurement in double-edge-notched tensile panels.

12. KEY WORDS (Six to twelve entries; alphabetical order; capitalize only proper names; and separate key words by semicolons)

assessment curve; ductility; fracture; J-integral; R-curve; toughness

13. AVAILABILITY

☒ Unlimited

☐ For Official Distribution. Do Not Release to NTIS

☐ Order From Superintendent of Documents, U.S. Government Printing Office, Washington, D.C. 20402.

☒ Order From National Technical Information Service (NTIS), Springfield, VA. 22161

14. NO. OF PRINTED PAGES

120

15. Price

USCOMM-DC 6043-P80

☆ U.S. GOVERNMENT PRINTING OFFICE: 1987—776-003/65,196 REGION NO. 8